Testing potential drivers of carbon isotopic signature of particulate organic carbon in the Southern Ocean

Zandria Jordaan

Supervisor: Dr. S. Fietz

Co-supervisor: Dr. W.R. Joubert

December 2020

Declaration

I, Zandria Jordaan, hereby declare that this thesis, completed at the Department of Earth Sciences, Stellenbosch University, South Africa, is my work and it was not previously been submitted at any other University. Correct references and acknowledgements can be seen in the text where the work of other researchers and previous work has been done.

Full name: Zandria Jordaan

Signature: ……

Signed on …….. Day of …….. 2020

Acknowledgements

To the greatest extent, I would like to thank my research supervisor, Dr. Susanne Fietz for giving me this opportunity to commence this research project and for seeing it through. Thank you for your guidance, patience and expertise whenever I needed it. To my co-supervisor, Dr. Warren Joubert, thank you for your patience, guidance, understanding and willingness to offer help where it was needed. It was a great pleasure to work with both of you.

My utmost gratitude to the National Research Foundation (NRF) for making this study possible through financial support. To the TracEx team at Stellenbosch University, thank you for answering endless questions and all the support.

To my grandparents, Audrey and Wynand Combrink, thank you for the endless support on so many levels, for never giving up on me and for showing me what hard work is all about. Thank you for staying on your knees, so that I can stay on my feet, without the love and support from you, this would never have been possible. To all my friends, thank you for the encouragement, continuous support and for always believing in me.

Abstract

The carbon cycle in the Southern Ocean (SO) plays a very important role for all life on earth as it regulates carbon fluxes, transport nutrients to marine organisms and it is linked to the amount of available oxygen in the atmosphere. The conditions driving the carbon cycle dramatically changed over the past few decades which directly effects marine phytoplankton. Phytoplankton are key role players in the marine food web as they utilize atmospheric carbon dioxide transported into the surface ocean through different chemical exchanges. Fractionation of stable carbon isotopes occurs during the biological uptake of inorganic carbon, although all the influential forces behind the fractionation are not yet fully understood. Here we examine the potential physical- and chemical driving factors for carbon isotopic signature of particulate organic carbon ($\delta^{13}C_{POC}$) in the surface water of the SO. Winter and summer results are compared along the Bonus Good Hope line as well as a section in the Indian Ocean. The aim is to determine potential influences of the physical- and chemical driving factors on phytoplankton $\delta^{13}C_{POC}$, because it is possible to measure $\delta^{13}C_{POC}$ directly from underlying sediments. Understanding the driving factors of $\delta^{13}C_{POC}$, will help the interpretation of sedimentary $\delta^{13}C_{POC}$ in paleo-reconstruction studies, such as reconstructing past atmospheric partial pressure of carbon dioxide (pCO_2 concentrations). Our results indicate that silicic acid and nitrate concentrations (µM), cyanobacteria and diatoms contributions to total chl-a (%) and temperature (ºC) could potentially be primary driving factors of $\delta^{13}C_{POC}$ during the summer along the Bonus Good Hope line, as all these factors are significantly correlated to $\delta^{13}C_{POC.}$ Winter results in the Atlantic sector of the SO (Winter Cruise 2015) did not show any potential driving factor. This is in contrast with results found in the Indian sector of the SO (Winter Cruise 2017), where all four investigated macronutrients (silicic acid, nitrate, nitrite and phosphate), chl-a, seven phytoplankton groups' contributions to total chl-a (%), temperature and salinity could potentially drive the carbon isotopic signature. In addition, available pCO_2 data was used to determine whether pCO_2 is related to $\delta^{13}C_{POC}$ in the upper layer of the Southern Ocean. The pCO_2 results obtained during the Winter Cruise 2017, in the Indian sector of the Southern Ocean, were the only cruise where pCO_2 had a significant (negative) correlation with $\delta^{13}C_{POC}$, indicating increased fractionation related to increasing pCO_2 concentrations. In conclusion, for both the Atlantic and Indian sector of the SO, possible drivers of $\delta^{13}C_{POC}$ were identified. It is important to take note of the different biological- and environmental factors co-influencing those potential driving factors. Correlations may have been identified where similar distributions of two studied parameters have been driven by a third, common factor. Hence, further studies should be made to confirm which parameter or parameters definitely drives $\delta^{13}C_{POC}$.

Opsomming

Die koolstofsiklus in die Suidelike Oseaan (SO) speel 'n baie belangrike rol vir alle lewe op aarde, aangesien dit koolstof-uitruiling reguleer, voedingstowwe na mariene organismes vervoer en dit is ook gekoppel aan die hoeveelheid beskikbare suurstof in die atmosfeer. Die toestande wat die koolstof siklus dryf, het dramaties verander oor die afgelope paar dekades wat ‘n direkte invloed op mariene fitoplankton het. Fitoplankton is sleutel rolspelers in die mariene voedselweb, aangesien hulle atmosferiese koolstofdioksied opneem wat deur verskillende chemiese uitruilingsprosesse in die boonste laag van die oseaan geplaas word. Fraksionering van stabiele koolstof isotope vind plaas tydens die biologiese opname van anorganiese koolstof, alhoewel al die invloedryke magte agter die fraksionering nie ten volle verstaan word nie. Hier ondersoek ons die potensiële fisiese - en chemiese dryffaktore vir koolstof isotopiese handtekening van spesifieke organiese koolstof ($\delta 13C_{POC}$) in die oppervlakwater van die SO. Winter en somer resultate word vergelyk langs die Goeie Hoop moniteringslyn sowel as 'n afdeling in die Indiese oseaan. Die doel is om potensiële invloede van die fisiese - en chemiese dryffaktore op fitoplankton $\delta 13C_{POC}$ te bepaal, omdat dit moontlik is om $\delta 13C_{POC}$ direk van onderliggende sedimente te meet. Daarom is dit belangrik om 'n dryffaktor te identifiseer waarin die verhouding gebruik kan word vir toekomstige paleo-rekonstruksiestudies, soos die rekonstruksie van voirige atmosferiese gedeeltelike druk van koolstofdioksied (pCO_2) konsentrasies. Ons resultate dui daarop dat silikasuur en nitraatkonsentrasies (µM), sianbakterie en diatome se bydraes tot totale chl-a (%) en temperatuur (ºC) moontlik primêre dryffaktore van $\delta 13C_{POC}$ gedurende die somer langs die Goeie Hoop moniteringslyn kan wees, aangesien al hierdie faktore beduidende korrelasie teenoor $\delta 13C_{POC}$ toon. Winterresultate in die Atlantiese sektor van die SO (Wintervaart 2015) het nie enige potensiële dryffaktore getoon nie. Dit is in teenstelling met die resultate wat gevind is in die Indiese sektor (Wintervaart 2017), waar al vier makrovoedingstowwe (silikasuur, nitraat, nitriet en fosfaat), chl-a, sewe fitoplankton groepe se bydraes tot totale chl-a (%), temperatuur en soutgehalte moontlik die koolstof isotopiese handtekening kan dryf. Daarbenewens is beskikbare pCO_2 data gebruik om te bepaal of pCO_2 in die boonste laag van die SO verband hou met $\delta 13C_{POC}$. Die pCO_2 resultate wat verkry is tydens die Wintervaart 2017, in die Indiese sektor van die SO, was die enigste vaart waar pCO_2 'n beduidende (negatiewe) korrelasie met $\delta 13C_{POC}$ toon, wat dui op verhoogde fraksionering wat verband hou met die verhoging van pCO_2 konsentrasies. Ten slotte, vir beide die Atlantiese en Indiese sektor van die SO, is moontlike dryffaktore van $\delta 13C_{POC}$ geïdentifiseer. Dit is belangrik om kennis te neem van die verskillende biologiese-en omgewingfaktore wat die potensiële dryffaktrore kan beïnvloed. Korrelasies kan geïdentifiseer word waar soortgelyke uitreikings van twee parameters wat hier

bestudeer is, deur 'n derde, algemene faktor gedryf word. Juis om hierdie rede moet verdere studies gedoen word om te bevestig watter parameter of parameters defnitief die $\delta 13C_{POC}$ dryf.

Table of Contents

List of Figures

List of Tables

List of Abbreviations

AAZ – Antarctic zone

ACC – Antarctic Circumpolar Current

ATP – Adenosine triphosphate

CA – Carbonic anhydrase

CAM – Crassulacean acid metabolism

CCM – Carbon Concentrating Mechanism

CDW – Circumpolar deep water

CIW – Central Intermediate Water

DIC – Dissolved Inorganic Carbon

DIW – Deionized Water

HNLC – High nutrient low chlorophyll

NADPH – Nicotidamide dinucleotide phosphate

PEP – Phosphoenolpyruvate

PEPC – PEP-Carboxylase

PEPCK – PEP-carboxykinase

PF – Polar Front

PFZ – Polar Front zone

POC – Particulate Organic Carbon

RUBISCO – Ribulose-1, 5-biphosphate carboxylase/oxygenase

SAF – Sub Antarctic Front

SANAE – South African National Antarctic Expedition

SAZ – Sub Antarctic zone

SO – Southern Ocean

SST – Sea surface temperature

STF – Sub Tropical Front

STZ – Sub Tropical zone

WC – Winter Cruise

1. Introduction

1.1. General overview

The ocean plays an important role in regulating and controlling global climate change through the ocean carbon cycle (Sarmiento & Gruber, 2004), which changed dramatically over the past few years (Arrigo, Robinson, Worthen, *et al.*, 1999). The change in the carbon cycle is a result of the rising atmospheric CO_2. The rapidly increasing partial pressure of atmospheric CO_2 leads to increased dissolved CO_2 concentrations in the ocean. As a result of climate change associated with these high levels of CO_2 in the atmosphere, the upper layer stratification, carbon - and nutrient distributions and marine phytoplankton community composition are affected (Arrigo *et al.*, 1999; Bousquet, Peylin & Ciais, 2000). Up until around three decades ago, dissolved inorganic carbon (DIC) was often ignored as an influencing factor of the growth and elementary composition of marine plankton due to the assumed excess availability of DIC in the ocean (Wolf-Gladrow et al., 1999). However, over the past few decades, changes such as productivity, seasonal growth rate and cell size variability in phytoplankton were observed due to changes in carbon resources in the ocean (Finkel, Beardall, Flynn, *et al.*, 2010; Arrigo & van Dijken, 2015; Henson, Cole, Hopkins, *et al.*, 2018).

Phytoplankton are very diverse in the SO and have the ability to take up CO_2 in the ocean and convert it into organic matter. This happens through a process called photosynthesis. Atmospheric CO_2 is made up of the two stable carbon isotopes, 1.1% of the non-radioactive isotope, carbon-13 (^{13}C), and 98.9% of carbon-12 (^{12}C) (O'Leary, Madhavan & Paneth, 1992). During photosynthesis phytoplankton subsume the lighter isotope (^{12}C) and convert it to organic matter, leaving the aqueous pool enriched in the heavier isotope (^{13}C). The $\delta^{13}C$ (reflecting the stable carbon isotopic composition) of marine phytoplankton is determined by the uptake fractionation (ε_p), which is dependent on environmental conditions as well as the physiology of algal cells. This can be of great value when attempting to use the pCO_2 to reconstruct past climatic conditions. The environmental factors and physiology driving the uptake fractionation may include temperature (Wong & Sackett, 1978), light intensities, nutrient supply (Wada, Terazaki, Kabaya, *et al.*, 1986), high CO_2 supply in some Antarctic waters (Rau, Riebesell & Wolf-Gladrow, 1996) and enzyme activities (Fontugne, 1981; Fry & Wainright, 1991).

The $\delta^{13}C$ varies considerably in the ocean (Figure 1.1) and the most notable factor is the relationship between the sea surface temperate (SST) and $\delta^{13}C_{POC}$ (Fielding, Turpin, Guy, *et al.*, 1998) which possibly results from the fact that phytoplankton discriminate less against ^{13}C in higher temperatures. High $[CO_{2(aq)}]$ leads to greater discrimination against the heavier isotope, therefore it is inversely correlated to $\delta^{13}C_{POC}$ (Wong & Sackett, 1978; Rau *et al.*, 1996). With higher discrimination in colder waters, increasing fractionation leads to more ^{12}C taken up, leading

to lower $^{13}C/^{12}C$ ratios in phytoplankton, therefore $\delta^{13}C_{POC}$ becomes more negative (Fielding *et al.*, 1998; Tuerena, Ganeshram, Humphreys, *et al.*, 2019).

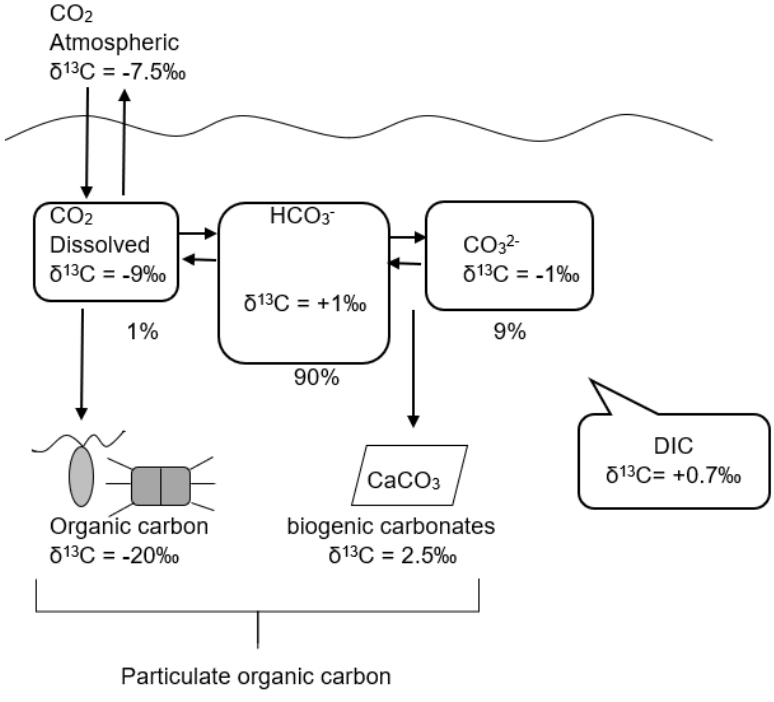

Figure 1.1. The carbon isotopic signature of various reservoirs in the surface ocean. Retrieved from Roy-Barman and Jeandel (2016).

Parameters related to cell physiology such as growth rate, cell size, and cell geometry also have an important influence on $\delta^{13}C_{POC}$ in the surface water (Laws, Popp, Bidigare, *et al.*, 1995; Popp, Trull, Kenig, *et al.*, 1999) and may influence the relationship between $\delta^{13}C_{POC}$ and $[CO_{2(aq)}]$. This is an important aspect to keep in mind when attempting to use $\delta^{13}C_{POC}$ in pCO_2 paleo-reconstruction studies. Such influence can be seen in areas with less variable $[CO_{2(aq)}]$ where factors related to cell physiology have a greater effect on the isotopic fractionation (Popp *et al.*, 1999; Henley, Annett, Ganeshram, *et al.*, 2012). Cells with a slow growth rate or that grow in environments with high concentrations of DIC, have a high ratio of supply to demand for carbon, which then leads to high discrimination against ^{13}C by the carbon fixation enzyme RUBISCO. When the growth rate increases and the carbon supply decreases, the discrimination against ^{13}C decreases and the $\delta^{13}C_{POC}$ values should approach that of the carbon source (Fielding *et al.*, 1998). A model proposed by Rau *et al*. (1997) suggested that growth rates only depend on the diffusive entry of CO_2 across the cell membrane, although a study done by Tuerena *et al*. (2019) concluded that it is more complex. Several phytoplankton groups have a high affinity for DIC which is characteristic of enhanced carbon uptake mechanisms other than passive diffusion (Raven,

Johnston & Turpin, 1993). It is therefore important to consider changes in phytoplankton community when discussing impacts on $\delta^{13}C_{POC}$. Marine organic carbon consists or a $\delta^{13}C$ ranging between -18‰ and -30‰ (Roy-Barman & Jeandel, 2016) and diffusive entry of CO_2 commonly results in more negative $\delta^{13}C_{POC}$ values, whereas carbon concentrating mechanisms (CCM's) or diffusive limitation of carbon supply is associated with more positive $\delta^{13}C_{POC}$ values (Raven, Cockell & De La Rocha, 2008). Some groups can enhance the affinity for CO_2 and actively concentrate DIC, therefore CCM induction can play an important role in determining the $\delta^{13}C_{POC}$ of marine phytoplankton (Raven *et al.*, 2008). For example, in marine diatoms, the induction of CCM's at low concentrations of DIC can result in changes in discrimination against ^{13}C. Furthermore, there are also studies done on some phytoplankton species that use bicarbonate (HCO_3^-) as a source of carbon (Laws *et al.*, 1995; Popp *et al.*, 1999), through active uptake. The conversion of bicarbonate to CO_2, can lead to fractionation of approximately 10.1‰ similar to the use of free CO_2 (Rau *et al.*, 1996).

In this study, we investigate different environmental factors linked with changes in $\delta^{13}C_{POC}$ in the upper layer of the SO. Data from four full transects across the Good Hope Line, the South Georgia leg and the Indian Ocean are reported. The results aim to propose a driver for particulate carbon isotopic signature within the SO, which may help with future studies to interpret $\delta^{13}C_{POC}$ signatures archived in sedimentary records to assess environmental changes in the past, including pCO_2.

1.2. Problem Statement

The history of changes in Earth's CO_2 concentrations over millions of years is bedded in sedimentary archives in the ocean. Research over the last couple of decades clarified the major roles of physical- and inorganic geochemical processes responsible for CO_2 uptake (Hansell & Carlson, 2015), although the response of the biological carbon pump (whether it will amplify or reduce future climate warming as well as ocean deoxygenation) is less understood. To understand past climatic conditions, it is necessary to study the pCO_2 in the underlying sediments. However, it is not possible to measure the pCO_2 directly, it is possible to measure the $\delta^{13}C_{POC}$. It is therefore important to study the relationship the $\delta^{13}C_{POC}$ and pCO_2 in the modern ocean to understand the proportional relationship between $\delta^{13}C_{POC}$ and pCO_2. As mentioned above, several factors can influence the $\delta^{13}C_{POC}$ such as temperature, phytoplankton physiology, but the extent of their influence is not well known in the SO. Furthermore, seasonal changes in ocean frontal dynamics may also influence $\delta^{13}C_{POC}$. Fielding *et al*. (1998) stated the importance of gaining a better understanding of the influential discriminating factors as they can provide important insight when interpreting the variation in $\delta^{13}C_{POC}$ in marine sediment records, which can then lead to insightful information regarding past atmospheric CO_2 conditions.

1.3. Aims and Objectives

The main objective of this study is to determine whether pCO_2 is one of the driving factors of particulate organic carbon isotopic signature and if there is a linear relationship between pCO_2 and $\delta^{13}C_{POC}$. Such linear relationship is an underlying assumption in the paleo-community.

In addition, there is an interest to investigate what the other driving factors are and to what extent they have an influence on $\delta^{13}C_{POC}$.

The above is addressed as follows:

- Previous studies (three cruises along the Good Hope line from Cape Town to Antarctica and one cruise in the Indian Sector of the Southern Ocean, from Cape Town to Antarctica) have collected data on POC, phytoplankton abundance (chl-a), community composition, macronutrients such as nitrate, phosphate, and silicate, as well as data on temperature and salinity in the surface. The relationship of all those parameters with changes in $\delta^{13}C_{POC}$ (data collected from the same voyages) is being examined here to determine their potential influence on the $\delta^{13}C_{POC}$.
- In addition, available pCO_2 data will be used to determine the effect of pCO_2 on the $\delta^{13}C_{POC}$ in the upper layer of the SO.

2. Literature review

2.1. The Southern Ocean

Samples were taken and analysed from four cruises, of which three were across the Good Hope line and one in the Indian Sector of the SO. Surface waters across these fronts were studied. Therefore, here, different physical and chemical processes happening in these waters are described.

The SO is of great significance to the global carbon cycle and a crucial element in regulating anthropogenic CO_2 uptake (Caldeira & Duffy, 2000; Swart, Chang & Fauchereau, 2012). It is also a very important interface between the deep ocean and the atmosphere (Hauck, Völker, Laufkötter, *et al.*, 2015) due to the upwelling that transports carbon- and nutrient-rich waters to the surface where an equilibrium can be reached between the oceanic gas and the atmosphere (Russel, 2006). The SO surrounding Antarctica has one major current, the Antarctic Circumpolar Current (ACC) which mixes waters from the southern parts of the Atlantic -, Pacific – and the Indian Ocean. The ACC is known to be the strongest and longest ocean current (Tynan Cynthia, 1998; Graham, 2013) which rotates clockwise (uninterrupted by landmass) around Antarctica (Figure 2.1). It is made up of different water masses; the Sub Antarctic zone (SAZ), the Polar Frontal zone (PFZ) and the Antarctic zone (AAZ), which are separated by different physical- and chemical properties, such as salinity, temperature, phytoplankton blooms and nutrient concentrations. The boundaries that separate these water masses are called fronts (Pollard, Salter, Sanders, *et al.*, 2009; Graham, 2013) and fronts found along the study area are the Subtropical Front (STF), Sub Antarctic Front (SAF) and the Polar Front (PF). In the Atlantic sector of the SO the position of these fronts shift annually and can be measured by using sea surface height (SSH) and sea surface temperature (SST) observations, based on satellite measurements (Moore, Abbott & Richman, 1999; Graham, Boer, Heywood, *et al.*, 2012).

The temperature in surface water decreases from the north in the Sub Tropical Zone (STZ) to the south in the AAZ with approximately 20ºC (Graham *et al.*, 2012; Graham, 2013). Salinity is also known to decrease from higher to lower latitudes (Tréguer, 2014; Viljoen, Weir, Fietz, *et al.*, 2019), where the AAZ is known to be a region with high amounts of nutrients due to upwelling. The Weddell Gyre and the Ross Gyre are two cyclonic gyres that are characterized by upwelling and exist south of the ACC (Hauck, 2012). Circumpolar Deep Water (CDW) is the dominant water mass in the northern boundary of the gyres. In the subsurface of the Weddell gyre, Central Intermediate Water (CIW) exists and these waters are characterized by high DIC concentration as a result of remineralization of export production, a depletion of oxygen and nutrient enrichment.

The ACC makes up approximately 10% of the world's ocean surface and large areas of it have high surface macronutrient concentrations as well as low chlorophyll concentrations, thus it is called a high-nutrient, low chlorophyll (HNLC) region (Church, Hutchins & Ducklow, 1990; Caldeira & Duffy, 2000; Doney, Lindsay & Moore, 2003) where primary production through phytoplankton is limited. The SO is known to have a significant biogeochemical influence on these HNLC regions (Pollard *et al.*, 2009).

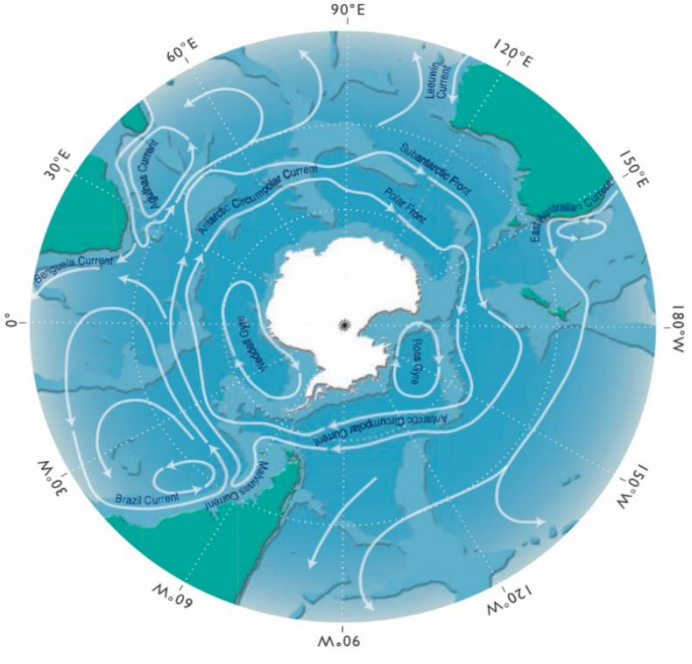

Figure 2.1. The Antarctic Circumpolar Current, the largest current in the world ocean, is presented with the white arrows moving from west to east around the continent, Antarctica (CSIRO, 2002).

The high availability of macronutrients in the SO can be explained by iron limitation, as phytoplankton requires iron to fully utilize macronutrients and due to a large amount of nutrient-rich deep water that gets transported to the surface ocean through upwelling (Pollard *et al.*, 2009). Iron input in HNLC regions is of high importance as it carries the potential to increase productivity and therefore have a positive influence on the atmospheric CO_2 uptake by the oceans (Mahowald, Baker, Bergametti, *et al.*, 2005; Pollard *et al.*, 2009). Due to the low dust inputs of Fe to the SO (Moore & Abbot, 2000; Watson, Bakker, Ridgwell, *et al.*, 2000), most Fe is brought to the surface ocean from the subsurface reservoirs.

Macronutrients also play a very important role as phytoplankton need macronutrients for primary production, which can lead to uptake of anthropogenic CO_2 from the atmosphere. The systematic relationship between nutrient concentrations and CO_2 concentrations in the surface layer of the

ocean shows seasonal changes over a wide range (Takahashi, Olafsson, Goddard, *et al.*, 1993). Within the North Atlantic thermocline, Takahashi *et al*., 1993 stated that the total CO_2 concentration in the surface water has a linear relationship with NO_3 and PO_4. These ratios are greater than that observed in the Icelandic stations, however, the reason for the difference in C/N and C/P ratios are not fully understood. It can either be due to the difference in biological communities in different locations or to the effects of water mass mixing. This proves that several factors are influencing each other, which then affects estimating driving factors for $\delta^{13}C_{POC}$.

Phytoplankton biomass is generally reflected by the phytoplankton pigment, chlorophyll-a: typically, with increasing chlorophyll-a concentration, the biomass increases. This then affects the primary production, although the increased rate varies depending on other factors. Nutrients are also a determining factor of primary production. Primary production can be enhanced through mixing, upwelling and wind which bring nutrients to the surface ocean. Temperature influences species-specific primary production as the enzyme-mediated dark reaction rates of photosynthesis are controlled by temperature. High nutrient, upwelling waters have low temperatures but can still enhance primary production, thus counteracting the effect of temperature on primary production (Sathyendranath, Platt, Brewin, *et al.*, 2019).

2.2. Phytoplankton in the Southern Ocean

Phytoplankton is the main key in the SO food web and plays an essential role in mediating global climate, adding to the importance as to why the biogeochemical processes within the SO should be studied. Phytoplankton is responsible for the transport of biogenic elements, including carbon, from the surface layer of the ocean to the ocean interior and sediments (Bathmann, Scharek, Klaas, *et al.*, 1996; Hauck, 2012; Deppeler & Davidson, 2017)., which will be further outlined below in section 2.4. Several phytoplankton groups are found within the SO; i.e. diatoms, haptophytes, cryptophytes, cyanobacteria, dinoflagellates, prasinophytes and pelagophytes. Diatoms along with *P. antarctica* (a haptophyte) have been reported as the dominant phytoplankton groups and species in several previous studies (Fry & Wainright, 1991; Fry, 1996; Tréguer, 2014; Deppeler & Davidson, 2017).

Diatoms are microscopic phytoplankton which use silica to form their intricate skeletons, known as frustules. They are responsible for 75% of the annual primary production in the surface layer of the SO as well as CO_2 drawdown through photosynthesis. Light – and nutrient availability are controlling factors for primary production, therefore it is important to take note of the season and latitude when studying phytoplankton groups and their ability to take up anthropogenic CO_2 (Smetacek, Klaas, Strass, *et al.*, 2012). Diatoms contribute differently to POC export according to

their life cycle and degree of silicification; thus, diatoms dominate in high latitudes where there is a high availability of silica (Lourey, Trull & Tilbrook, 2004). In warmer waters, the POC export flux of diatoms will be low due to a lower concentration of silicic acid. Diatom blooms also differ in iron-limited and iron-repleted regions (Soppa, Völker & Bracher, 2016), for example, in iron-limited regions diatoms have thick silica shells for grazer protection. When these species are grazed their organic biomass is recycled back into the surface waters, causing an increase of silicic acid in the CDW. Weak silicified diatoms are dominant in iron-repleted regions. These diatoms are called carbon sinkers as they are associated with high growth rates and are responsible for high biomass productions.

Haptophytes are microalgae with red-algal-derived chloroplasts and are very important primary producers (Wong & Sackett, 1978; Endo, Ogata & Suzuki, 2018). *Phaeocystis* genus commonly occurs in high nutrient areas, especially nitrates, and they play a key role in carbon transfer between the ocean and atmosphere (Schoemann, Becquevort, Stefels, *et al.*, 2005), thereby making them ideal organisms to study the role of phytoplankton in climate change regulation. *P. antarctica* can generally be found in higher latitudes of the SO (Figure 2.2) and tend to have faster sinking rates than diatoms (Schoemann *et al.*, 2005; Leeuwe, Visser & Stefels, 2014).

Coccolithophores are calcifying haptophytes in the SO and are mostly found in warmer waters (Viljoen, 2016; Deppeler & Davidson, 2017). They contribute to the carbon cycle as they fix DIC through both photosynthesis and calcification. Calcification is the process in which organic matter is converted into calcite and CO_2 is released via the carbonate counter pump, resulting in higher pCO_2 concentrations near the SAF. Coccolithophores use the DIC to build their shells in two forms of calcium carbonate; (i) aragonite and (ii) calcite, and when they die, they sink out of the surface layer into the ocean floor.

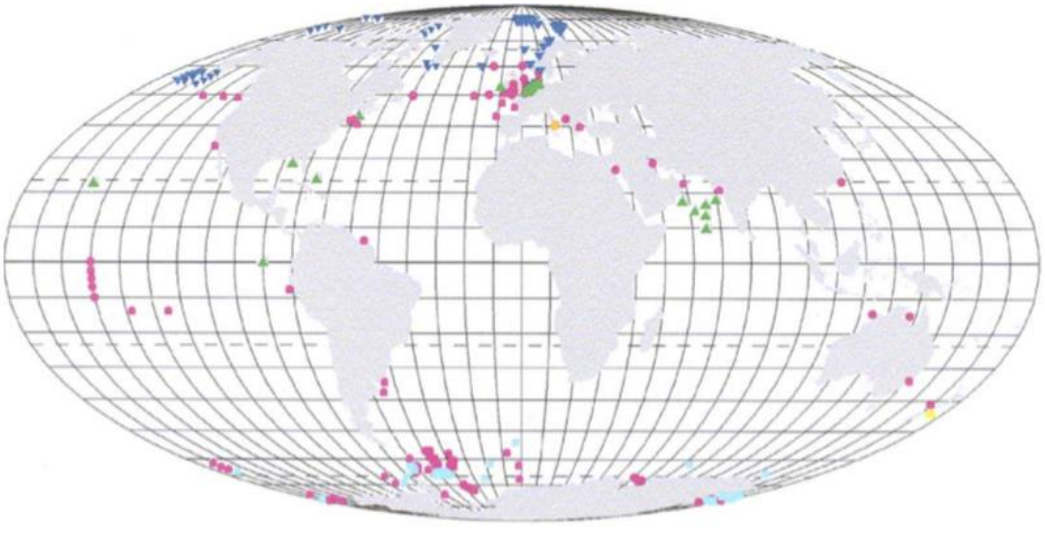

Figure 2.2. Distribution of *Phaeocystis* ssp. around the world. Some of the species have been revised in the past decade. *P. antarctica* is illustrated with light blue circles. Other Phaeocystis species shown here: *P. pouchetti* is illustrated with dark blue triangles, *P. globosa* are indicated by the green triangles, *P. scrobiculata* by yellow triangles, *P. jahnii* and *P. cordata* with an orange circle. Derived from Schoemann *et al*. (2005).

Cryptophytes are another group of algae that contain one or two plastids per cell and two unequal flagella, surrounded by four membranes (Hibberd, Greenwood & Griffiths, 1971; Gillott & Gibbs, 1980). These algae are photosynthetic organisms and thus contribute to the carbon cycle as they fix carbon throughout all kinds of aqueous habitats. Cryptophytes are mostly present in higher latitudes very close to Antarctica in austral summer (Arrigo *et al.*, 1999; Viljoen *et al.*, 2019).

Dinoflagellates are eukaryotic organisms containing two whip-like tails, flagella, which they use to move through the waters. Approximately 90% of dinoflagellates are marine plankton containing chlorophyll-a, chlorophyll-c and carotenoids, which allow them to photosynthesize, the other 10% is symbiotic, benthic and parasitic. Dinoflagellate distributions are dependent on salinity, depth and sea surface temperatures and are susceptible to bloom between the STF and SAF (Eynaud, Giraudeau, Pichon, *et al.*, 1999).

Cyanobacteria are blue-green microscopic organisms that contain chlorophyll-a, thus they are photosynthetic organisms (Palinska & Surosz, 2014). They dominate in warmer waters where nutrients are produced from food webs. Prasinophytes are primarily marine and almost exclusively planktonic (Simon, Cras, Foulon, *et al.*, 2009). They are also classified as the most diversified green algae group among marine phytoplankton and have organic scales on the cell bodies. Pelagophytes are heterokont algae and occur in low latitudes and warmer waters (Schlüter, Henriksen, Nielsen, *et al.*, 2011; Viljoen *et al.*, 2019). All of these different phytoplankton groups have an effect on the global carbon cycle in the oceans as elaborated below.

2.3. Carbon pumps in the Southern Ocean

Carbon moves between four reservoirs (Hauck *et al.*, 2015); the atmosphere, the solid earth, the ocean and the land. CO_2 uptake is regulated within the ocean system through several processes. It is important to understand the different pathways of carbon in the SO, and, here, two of the processes that assist with CO_2 regulation are described. These processes are the biological pump (which consists of the carbonate counter pump and the soft tissue pump) and the solubility pump. The solubility pump is a process of carbon transport that can be influenced by deep vertical mixing. Surface waters are cooled at high latitudes and salinity increases when brine is rejected during the formation of sea-ice (Hauck, 2012; Hauck *et al.*, 2015). The cold-water masses in the SO near Antarctica sink is a result of high density and is rich in carbon as CO_2 is more soluble in colder waters (Henley *et al.*, 2012; Hauck *et al.*, 2015; Landschützer, Gruber, Haumann, *et al.*, 2015). At lower latitudes and slightly higher temperatures, CO_2 is released back into the ocean through upwelling and can be explained by Henry's Law (Figure 2.3) that reflects that the amount of the dissolved gas is proportional to the partial pressure in gas phase. The biological pump is responsible for transporting DIC into organic biomass and exporting it to the deep ocean (Figure 2.3). Carbon storage in the ocean interior (Duckiow, Steinberg & Buesseler, 2001; Passow & Carlson, 2012) can be divided into short-term (several months to decades) and long-term (this can be centuries to millennia).

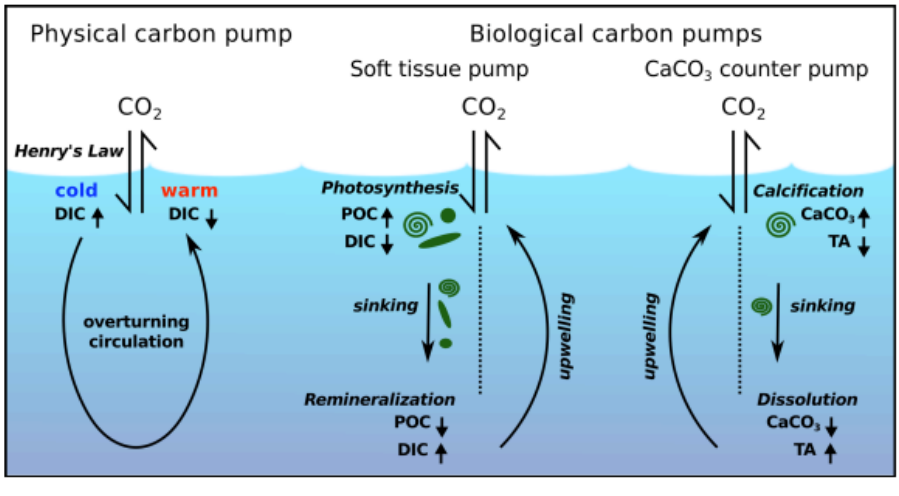

Figure 2.3. Illustration of the biological - and physical carbon pumps in the Southern Ocean responsible for transporting carbon from the surface layer to the deep ocean. Henry's law can be written as $[CO_{2\,(aq)}] = K_0 . pCO_2$ where $[CO_{2\,(aq)}]$ is the concentration of aqueous carbon dioxide, K_0 is the solubility coefficient (dependant on temperature and salinity) and pCO_2 is the partial pressure of carbon dioxide. DIC: dissolved inorganic carbon, POC: particulate organic carbon, TA: total alkalinity. Derived from (Hauck, 2012).

Carbon dioxide emissions can result from natural sources as well as human sources. Natural sources usually include ocean release, respiration and decomposition, whereas human sources come from cement production, deforestation and the burning of fossil fuels like oil, natural gas and coal (Sabine, Feely, Gruber, *et al.*, 2004; Davis & Caldeira, 2010). During the Anthropocene, these emissions increased and a large amount of CO_2 was emitted into the atmosphere (Sabine *et al.*, 2004; Hauck *et al.*, 2015). Griggs and Noguer (2001) proposed that approximately 50% of these CO_2 emissions remained in the atmosphere, whereas the remainder is taken up by the ocean and the land biosphere, or by a combination of both. 40% of these emissions are taken up by the SO, but this may change in the future as there are indications that changes in wind and currents play a crucial role in the weakening of the oceans' ability to take up CO_2 (Scholes et al., 2015). The land- and sea reservoirs transfer CO_2 in a balanced two-way exchange (Andrews, Brimblecombe, Jickells, *et al.*, 2004), thus forming air-to-sea and sea-to-air fluxes. These fluxes are primarily driven by surface water temperature changes, which can alter both the ability to dissolve CO_2 and the biological consumption and production of CO_2 as a result of photosynthesis (Takahashi, Sweeney, Hales, *et al.*, 2012). The subtropical waters of the SO act as a net source of CO_2 to the atmosphere, whereas the higher polar latitudes act as a net sink of CO_2. The biological and physical processes vary both seasonally and spatially.

The total dissolved CO_2 in the ocean consists of three forms: CO_2 in an aqueous environment or as two ionized forms, ($[CO_{2(aq)}]$ or $[H_2CO_3]$) being the former and ($[HCO_3^-]$ and $[CO_3^{2-}]$) the latter. Takahashi *et al*. (2012) stated that 95% of the total dissolved CO_2 is made up by $[HCO_3^-]$, 4% is $[CO_3^{2-}]$ and the remaining 1% is $[CO_{2(aq)}]$, which is the only species directly involved in the air-to-sea and sea-to-air fluxes. The driving force for these fluxes is the partial pressure of surface water CO_2 (pCO_2) and the difference between sea- and air CO_2 partial pressure (ΔpCO_2) is responsible for the direction and the magnitude of the net CO_2 flux between the reservoirs. When the net flux moves in the direction of the ocean, from the air, the pCO_2 of the ocean is greater than that of the air ($\Delta pCO_2 > 0$) and vice versa. Oceanic pCO_2 is controlled by the net community production, i.e. primary production, recycling, respiration and the export of organic carbon to and from the mixed layer (Takahashi *et al.*, 2012; Landschützer *et al.*, 2015). Increasing pCO_2 is due to higher concentrations of atmospheric carbon dioxide. In austral winter the CO_2 sink is related to negative ΔpCO_2 values as a result of high productivity in high chlorophyll zones, approximately 40ºS; thus, cooling of the surface water plays an important role in the formation of the CO_2 net sink. When the temperature rises and the surface is exposed to more sunlight, the sink moves to higher latitudes. Between 50ºS and 60ºS the ΔpCO_2 is very small due to the competing effects of the total dissolved CO_2 and temperature on pCO_2. These sinks are also influenced by $CaCO_3$ neutralization and seawater buffering (Hauck, 2012).

Seawater buffering can be explained by Le Chatelier's principle. When equilibrium is disturbed by a change in partial pressure, temperature, volume or concentration there will be a shift in the equilibrium to counteract the disturbance (Hauck, 2012). Within the ocean carbon cycle, this is applicable, anthropogenic CO_2 taken up by the ocean is buffered because of the chemical reaction that happens with CO_3^{2-}:

$$CO_{2(aq)} + CO_3^{2-} + H_2O \leftrightarrow 2HCO_3^- \quad (2.1)$$

The buffer capacity of the carbon system has a direct effect on the amount of CO_2 that can be buffered, i.e. how much CO_2 can be taken up and how much has already been buffered. Chemical buffering is quantitively the biggest CO_2 sink, as 60-80% of CO_2 emissions are sequestered this way (Hauck, 2012).

2.4. Isotopic fractionation

Isotopes are elements with similar chemical properties, however, they have different masses (Allègre, 2008; Hoefs, 2009). Fractionation is where separation takes place and divides certain quantities (solid, gasses, liquids, suspension, isotopes or enzymes) into smaller quantities during a phase transition. Isotope fractionation is defined as "*The relative partitioning of the heavier and lighter isotopes between two coexisting phases in a natural system"* (Tiwari, Singh & Sinha, 2015). Fractionation emanates from both kinetic – and equilibrium effects (White, 2015). Equilibrium isotope-exchange takes place when isotopes are redistributed in a closed, well-mixed system at chemical equilibrium. When species reach isotopic equilibrium, the reaction rates are identical, although the isotopic composition of the different compounds is not identical. Normally, the heavier isotope accumulates in the species with the higher oxidation state as well as more dense material. In contrast, kinetic isotope fractionation is associated with fast, unidirectional processes, such as evaporation, dissociation reactions, diffusion and biological reactions. Isotope variations in biological systems are a result of kinetic effects, for example where the lighter isotope is enriched in the reaction product, relatively to the substrate. This is a process that happens during photosynthesis. Here fractionation takes place in the rate-determining step, which is the slowest step in the process. This usually happens in a large reservoir, where the material is small in comparison to the size of the reservoir. Kinetic isotopic fractionation is also dependant on the ratio between the masses of isotopes and vibrational energy. In most of the low-temperature environments, kinetic fractionations are larger than the equilibrium fractionation for the same reaction. Bonds between lighter isotopes are broken more effortlessly than the same bond of heavier isotopes, therefore lighter isotopes react faster and become concentrated in species which leads to the enrichment of heavy isotopes in the residual reactants.

These different types of fractionation can happen in different systems, such as biological-, physical- and chemical systems. Biological processes can sometimes involve large isotopic fractionations, i.e. for sulphur, carbon and nitrogen, and are the most important source of isotope fractionation (White, 2015; Condie, 2016). As previously mentioned, during primary production of organic matter by autotrophs, the largest fractionation of carbon occurs (Wolf-Gladrow *et al.*, 1999; White, 2015; Condie, 2016). Autotrophs include bacteria as well as plants. Somewhat smaller fractionation occurs in subsequent reactions as heterotrophs consume primary producers (White, 2015). This autotrophic related fractionation is explained in more detail specifically for carbon fractionation below.

2.4.1. Carbon Isotopic Fractionation

Carbon is found in various compounds, such as carbon dioxide, reduced organic compounds in the biosphere, oxidized inorganic compounds like carbonates, etc. Carbon isotope fractionation is important because it can be used to evaluate the broad spectrum of carbon compounds in high- and low-temperature geological settings. Fractionation analysis can also identify global carbon cycling (Boller, Thomas, Cavanaugh, *et al.*, 2011). Carbon has two stable isotopes; ^{12}C which is in abundance (98.93%) and ^{13}C (1.07%). The fractionation of stable carbon isotopes is affected by numerous environmental factors as well as biological processes (Freeman & Hayes, 1992; Hayes, 1993), and can be measured by the $^{13}C/^{12}C$ ratio through the following equation:

$$\delta\ ^{13}C\ (‰) = \{[(^{13}C/^{12}C)_{\ sample} / (^{13}C/^{12}C)_{\ std}] - 1\} \times 1000 \qquad (2.2)$$

where δ is a relative deviation from the standard, expressed as parts per mil (‰). If δ is positive, the sample is enriched in the heavier isotope than the standard, and if δ is negative there is a decrease in the heavy isotope (Allègre, 2008). This equation can be used to express carbonate (δ_{carb}) and organic (δ_{org}) isotopic ratios (Condie, 2016).

Organic matter and sedimentary carbonates are the two main terrestrial carbon reservoirs (Fritz & Buchardt, 1980; Hoefs, 2009). These two reservoirs have different isotopic characteristics because of two contrasting reaction mechanisms i.e. (i) isotope equilibrium exchange reactions in inorganic carbon systems (atmospheric CO_2 → dissolved bicarbonate → solid carbonate) which leaves carbonates enriched in ^{13}C; and (ii) the kinetic isotope effect during photosynthesis where the lighter isotope ^{12}C, is concentrated in the synthesized organic material. Factors influencing the range and variability of the isotopic fractionation include; the bulk chemical composition of the cell (Hinga, Arthur, Pilson, *et al.*, 1994), temperature due to its ability to affect the equilibrium fractionation between the $[CO_{2(aq)}]$ and $[HCO_3^-]$ (Mook, Bommerson & Staverman, 1974), Rayleigh

distillation of the inorganic carbon source, pH, diffusion trough the unmixed boundary layer and different pathways of carbon fixation (Hinga *et al.*, 1994).

2.4.2. Biological- and physical processes influencing carbon isotope fractionation

2.4.2.1. Photosynthesis

Photosynthetic fractionation of carbon is known to be primarily kinetic and this fractionation can be species-specific, thus depending on growth rate of the marine phytoplankton, geometry, cell size and differences between species (Rau *et al.*, 1996; Burkhardt, Riebesell & Zondervan, 1999; Popp *et al.*, 1999), which is further dependent on environmental factors such as light intensity, nutrient availability, temperature, salinity and the available dissolved carbon dioxide in the water (Burkhardt *et al.*, 1999).

As previously mentioned, surface water in the ocean is enriched in ^{13}C, because the lighter isotope (^{12}C) is subsumed during photosynthesis (Figure 2.4), thereby increasing the $\delta^{13}C$ value in the surface ocean and decreasing the $\delta^{13}C$ in the biogenic matter. In contrast to the surface ocean, the deep ocean is enriched in ^{12}C. The organic matter is transported through the water column (Hauck *et al.*, 2015; White, 2015) and is decomposed or remineralized, thus the biological pump is responsible to transport carbon (^{12}C) from the surface into deep waters. Carbon isotopic signature in the surface ocean is often influenced by changes in the productivity as well as the vertical displacement of POC remineralisation depth (Morée, Schwinger & Heinze, 2018). Nutrients and the preferred ^{12}C are transported from the surface ocean to the deep ocean through POC sinking. Per Morée *et al*. (2018), the mean surface ocean $\delta^{13}C$ increases with higher POC sinking rates, thereby decreasing the fractionation; and decrease due to fractionation being counteracted by remineralization of POC. This correlates with Hinga *et al*. (1994), which stated that with increased productivity, there are more ^{13}C in phytoplankton as they subsume both ^{12}C and ^{13}C, leading to an increase in $\delta^{13}C$ and decrease in fractionation.

The biosynthesis of cellular components, as well as the uptake and intracellular diffusion of CO_2, are the two main steps during biological carbon fixation (Leary, 1980; Hoefs, 2009). This two-step model was first tested by (Park & Epstein, 1960):

$$CO_{2(external)} \leftrightarrow CO_{2(internal)} \rightarrow \text{carbon incorporated into organic compound}$$

Passive carbon diffusion and active transport of bicarbonate into the cells are the primary ways that phytoplankton utilizes carbon. Passive diffusion results in the internal inorganic carbon concentration in growing cells being lower than the external carbon dioxide concentration; whereas the active transport results in the internal carbon dioxide concentration being greater

than that of the ambient environment (Hinga *et al.*, 1994). Sharkey and Berry (1985) proposed that species use passive diffusion in areas with high $CO_{2(aq)}$ concentrations and employ active transport when the external $CO_{2(aq)}$ concentration is low or when bicarbonate is transported into the cell.

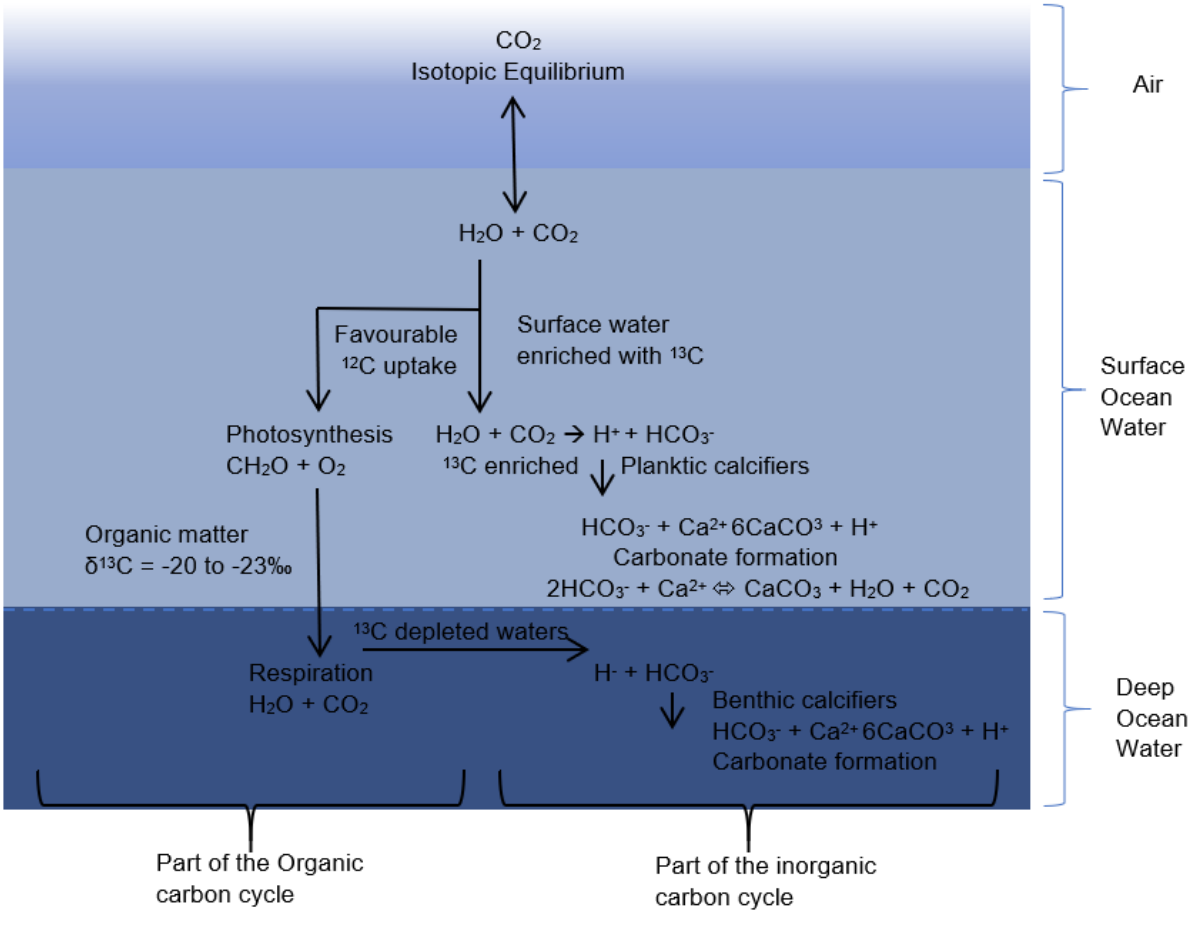

Figure 2.4. The organic carbon cycle (on the left) is driven by photosynthesis and can be in equilibrium. Photosynthesis discriminates against ^{13}C, thus there is a significant isotopic fractionation happening when phytoplankton take up the lighter isotope, leaving the seawater enriched in ^{13}C and $\delta^{13}C$ in the surface water increase. In the deep ocean, there is an export flux which releases ^{12}C back into the water through oxidation of carbon organic matter, decreasing the $\delta^{13}C$ in the seawater. This graph was derived from an online lecture done by (Repeta & Eglinton, 2005).

Biogenic organic matter and carbonates are characterized by different isotopic compositions. Organic matter is isotopically light with a mean $\delta^{13}C$ value around -25‰ and carbonates are isotopically heavy with a mean $\delta^{13}C$ around 0‰ (Figure 2.5).

An isotope mass balance must exist in both sedimentary carbon reservoirs (Hoefs, 2009):

$$\delta^{13}C_{input} = f_{org}\delta^{13}C_{org} + (1 - f_{org})\ \delta^{13}C_{carb}$$

where f_{org} is the fraction of organic carbon entering the sediments and can be calculated if the δ input is determined for a specific time. Note that f_{org} is defined in global mass balance terms, thus independent of biological productivity when looking at the burial rather than the synthesis of organic material. Large f_{org} values may be caused by high productivity and low preservation of organic material or high levels of preservation and low productivity (Hoefs, 2009).

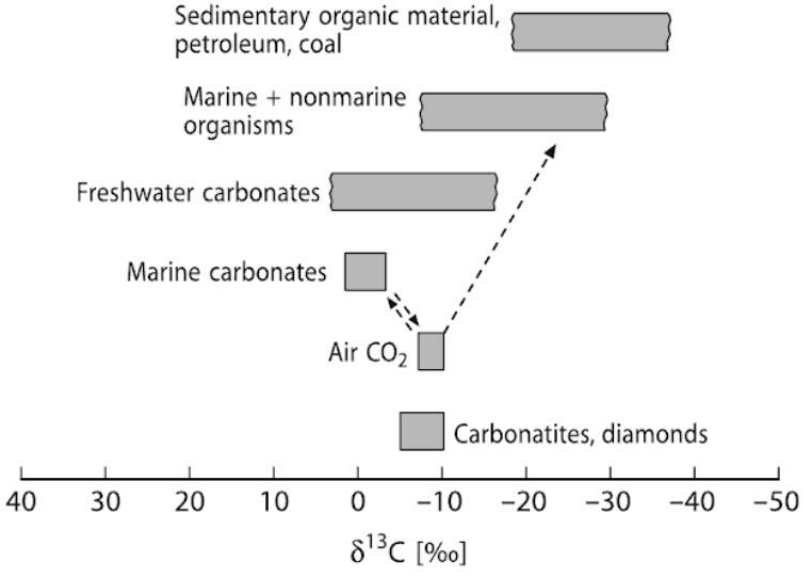

Figure 2.5. Schematic illustration of the $\delta^{13}C$ values of important carbon reservoirs. Retrieved from Hoefs (2009).

2.4.2.2. Enzymatic isotope fractionation during inorganic carbon fixation

Inorganic carbon is predominantly fixed by the enzyme Ribulose-1,5-biphosphate carboxylase/oxygenase (RUBISCO) (Huang, Chen, Kuang, *et al.*, 2016). The second most important enzymes through which inorganic carbon can be converted to organic compounds are the β-carboxylating enzymes, i.e. PEP-carboxykinase (PEPCK) and PEP-Carboxylase (PEPC), which both use phosphoenolpyruvate (PEP) as a substrate, obtained from photosynthesis and can be explained by the Calvin cycle (Burkhardt *et al.*, 1999). There are three basic steps in the Calvin Cycle: fixation, reduction and regeneration. Carbon dioxide along with RUBISCO and ribulose biphosphate (RuBP) is necessary to initiate the Calvin cycle, in this step RUBISCO activates a reaction between RuBP and CO_2 forming a 6-carbon compound which is converted into two 3-carbon compounds. During a reduction in the Calvin Cycle, phytoplankton generates Adenide dinuleotide (ATP) and nicotinamide dinucleotide phosphate (NADPH), through photosynthesis and convert the 3-carbon compound (3-PGA), to another 3-carbon compound

(G3P). These photosynthates must pass through a carbon source, for the cell to use them. At some stage, the G3P molecule leaves the Calvin Cycle to contribute to the carbohydrate molecule (contains 6 carbon atoms) formation. Due to the 6 carbon atoms in carbohydrate, the Calvin Cycle must happen 6 times to make one carbohydrate molecule. The G3P molecules that are not used in the carbohydrate formation, regenerate RuBP, whereafter the system is prepared to start the carbon fixation step again (Figure 2.6).

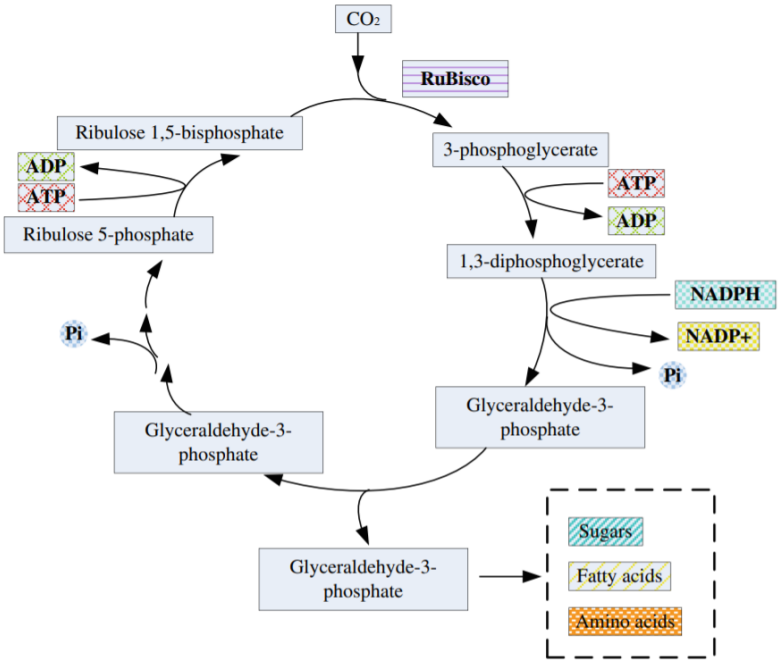

Figure 2.6. The three stages in the Calvin cycle (A) are (i) the carbon fixation where the RUBISCO enzyme incorporates CO_2 into organic molecules, (ii) where the organic molecule is reduced and (iii) where the RuBP molecule is regenerated for the cycle to continue. Derived from (Huang *et al.*, 2016).

Different phytoplankton groups use different pathways to carbon fixation, thus different forms of RUBISCO to catalyse the carboxylation and oxygenation. There are three known forms of RUBISCO; forms I, II and III (Tabita, Satagopan, Hanson, *et al.*, 2008), which only share 25% amino acid similarity. They vary extensively in affinity for CO_2 (K_{CO2}), maximum velocity (V_{max}) and also show some differences in structure. Form I are further subdivided into 4 groups, form IA, IB, IC and ID. Forms IA and IB can be categorized together with 80% shared identities, where forms IC and ID also have some similar traits (Scott, Harmer, Longo, *et al.*, 2007). Under low CO_2 and high O_2 conditions, the catalytic properties of form I is known to be more efficient and although RUBISCO has a low affinity for CO_2 overall, the affinity for form I RUBISCO is higher and it promotes a higher specificity for CO_2 relative to O_2 (Tabita *et al.*, 2008). Each phytoplankton species consists of a dominant form along with at least 3 other forms to successfully employ carboxylation. Form IB is mostly found in cyanobacterium and green algae, although Scott *et al*.

(2007) suggested that some cyanobacterium consists of form IA, as dominant RUBISCO form, too. In coccolithophores, form ID is used to activate the carboxylation process (Puerta, Bachvaroff & Delwiche, 2005), while diatoms and dinoflagellates use type IB RUBISCO (Boschker, Kromkamp & Middelburg, 2005) and type II RUBISCO (Hoins, Eberlein, Van de Waal, *et al.*, 2016), respectively. Form ID is ubiquitous in dominant primary producers; such as diatoms; therefore it is important to study the isotope discrimination step by form ID RUBISCO to elucidate $\delta^{13}C$ values in culture-based as well as environmental studies for global effects and paleo-oceanography (Boller *et al.*, 2011). In contrast with from II, form I discriminates conspicuously against ^{13}C, thus it may result in more negative $\delta^{13}C$ values due to a higher fractionation, especially by form IA RUBISCO (Scott *et al.*, 2007). The considerable variety in $\delta^{13}C$ values (-16‰ to -36‰), in phytoplankton, may be a result of the enzymatic reactions of the different types of RUBISCO found in algae (Freeman & Hayes, 1992). Carboxylation and decarboxylation reactions involve 40‰ fractionation (O'Leary *et al.*, 1992), therefore it can affect the isotopic composition of the cells. The discrimination degree against ^{13}C can be measured as a ratio of the reaction rate constants for every isotope, i.e. k^{12}:k^{13}, which can be described as $\varepsilon_f = 1000\ [(k^{12}/k^{13}) - 1]$. This is the discrimination due to specific carboxylation and it is directly proportional to the discrimination against ^{13}C that happens between the product and the substrate pool (CO_2).

RUBISCO contributes to the upper limit of fractionation only, as other processes determine the degree of this contribution, such as leakage and bicarbonate which plays a role in CCM's of phytoplankton. Leakage can be referred to as the amount of CO_2 diffusing out of the cell, parallel to the inorganic carbon source uptake. High leakage may cause the intracellular inorganic carbon pool to regenerate, thus preventing the ^{13}C uptake, which allows RUBISCO to approach the upper fractionation values (Hoins *et al.*, 2016). By understanding the CCM's, it may help to understand the CO_2 dependent results found linked to changes in the fractionation and the species-specific differences (Hoins *et al.*, 2016).

2.4.2.3. Carbon Dioxide Concentrating Mechanisms

The CO_2 concentration in surface water, the growth rate of the phytoplankton species, cell membrane permeability, the relative contribution of bicarbonate to the total inorganic uptake, as well as inorganic carbon leakage (Hinga *et al.*, 1994; Rau *et al.*, 1996) all influence the CCM's of phytoplankton. CCM's are adapted to environments with low carbon dioxide concentrations (Moroney & Ynalvez, 2007) to enhance carbon fixation as RUBISCO has a low affinity for CO_2. There are 3 types of carbon concentrating mechanisms: (i) C_4 mechanism and crassulaceous acid metabolism (CAM), (ii) active transport of inorganic carbon and (iii) carbon dioxide concentration by acidification.

Active transport of inorganic carbon has primarily been studied in cyanobacteria (Moroney & Ynalvez, 2007). Carboxysome is a sophisticated CCM found in cyanobacteria which is responsible for the active uptake and transport of CO_2 and HCO_3^- (Price & Badger, 1989). In this specialized microcompartment, α-carboxysome is where accumulated HCO_3^- are converted to carbon dioxide and β-carboxysome is responsible for the dehydration of HCO_3^- (Figure 2.6). At this location of RUBISCO, CO_2 increases because of diffusion restrictions on efflux through the carboxysome protein shell structure. The last type of CCM found in eukaryotic algae is dependent on the pH gradient in light. Within cyanobacteria, the predominant inorganic carbon in the chloroplast is HCO_3^- (Moroney & Ynalvez, 2007) and CO_2 is the most abundant form of inorganic carbon in the cell. Bicarbonate requires a proton for each HCO_3^- molecule that is converted to $CO_{2(aq)}$, which is catalysed by the carbonic anhydrase (CA) enzyme.

2.5. Indications on potential drivers of $\delta^{13}C$ in POC from previous studies

In this section, the aim is to focus the attention on the results obtained from previous studies and how different factors already proved to influence $\delta^{13}C_{POC,}$ although the extent of the effects is not well understood.

Impact of primary productivity and growth rate: Primary productivity is linked to biomass, which is often assessed by measuring chlorophyll-a concentration. Henley *et al*. (2012) observed a significant relationship between $\delta^{13}C_{POC}$ and the total biomass in the surface waters near Ryder Bay. The $\delta^{13}C_{POC}$ values can also be affected by phytoplankton growth rates. Wada *et al*. (1986) proposed a decrease in $\delta^{13}C_{POC}$ values with slow growth rates and vice versa, this was also confirmed by Henley *et al*. (2012), which proposed a positive relationship between $\delta^{13}C_{POC}$ and growth rate as higher growth rates increase internal carbon demand and restrict ε_p. Hinga *et al*. (1994) stated that the sizable difference in fractionation between different phytoplankton species might be a major limitation to the precision by which one should be able to specify the $\delta^{13}C_{POC}$ of carbon fixed by phytoplankton. Blooms across different latitudes and water masses will constantly provide a changing isotopic signature of the organic matter entering the cell. Scott *et al*. (2007) hypothesized that more negative $\delta^{13}C$ values are the result of a higher degree of fractionation by type IA RUBISCO.

Impact of phytoplankton groups: Diatoms are a dominant phytoplankton group in the SO (Henley *et al.*, 2012), occurring in high productivity in some areas of the SO. High productivity in the SO is linked to ^{13}C enrichment within phytoplankton carbon, thus a decrease in fractionation is observed (Fischer, 1991). Diatoms use form IB as well as form II RUBISCO to fix inorganic carbon through passive diffusion at very low rates (Laws, Bidigare & Popp, 1997). These results agree

with a model assuming that active transport moves CO_2 into the cell to the site of carboxylation to such an extent that the minimum energy is required for CO_2 concentration at the site of RUBISCO. In the case of light limitation, RUBISCO is inactive (Burkhardt *et al.*, 1999), having the result that no net fixation of inorganic carbon will happen. This leads to the use of carbohydrate to fuel the metabolic reactions and provide the carbon skeleton for major compounds such as proteins and lipids. Therefore, the effect of decarboxylation on $\delta^{13}C_{POC}$ is definite during light limitation, i.e. the place where carbon fluxes are dominated by respiratory activity. When respired CO_2 is not effectively re-fixed in other cellular substrates, the $\delta^{13}C_{POC}$ will be affected by isotopic fractionation associated with decarboxylation, which range from 9‰ - 32‰. It is important to know that the synthesis of organic matter by marine phytoplankton is predominantly based on the uptake and fixation of CO_2 through the C_3/C_4 pathway rather than by the active transport of bicarbonate.

The cysts found in dinoflagellates are maintained in marine sediments and their CO_2 dependency of isotopic composition may be reflected in their cysts. Hoins *et al*. (2015) investigated the elevated effects of pCO_2 and low light conditions in combination with the fractionation factor in dinoflagellates and proven that POC production stayed unchanged with CO_2 availability under low light conditions but showed increasing results under the availability of light. Some species of dinoflagellates showed flexibility in low light conditions, which allowed the cells to synthesize more, showing an increase in chlorophyll-a concentrations. The above mentioned suggests the presence of a CCM in dinoflagellates is important to maintain the growth under low concentrations of inorganic carbon. Other dinoflagellates species tend to take up HCO_3^- through active transport thereby increasing the intracellular inorganic carbon pool, this is a result of high CA activities within the species. A few studies (Sharkey & Berry, 1985; Fontugne, Descolas-Gros & de Billy, 1991; Laws *et al.*, 1995) reported that carbon dioxide concentrating mechanisms are employed by different phytoplankton species to buffer the impact of $[CO_{2(aq)}]$ variability and therefore play an important role in the $\delta^{13}C_{POC}$ values of the species. It can thus be said that a greater variability of $\delta^{13}C_{POC}$ values can be attributed to species-specific effects. Rau *et al*. (1996) suggested that cells with greater diameters, contribute to large negative shifts in $\delta^{13}C_{POC}$, these values range between -24‰ and -25.5‰. These negative shifts are hypothesized to be a result of fractionation by form IA RUBISCO, although it could not be proven to be correct.

Sharkey and Berry (1985) stated the possibility that some species, to avoid the energetic cost of active transport, use passive diffusion when the external $[CO_{2(aq)}]$ is abundant, in contrast with this when the $[CO_{2(aq)}]$ is low, active transport/uptake of HCO_3^- happens. This active uptake can drive the $\delta^{13}C_{POC}$ values to above -10‰, because it is isotopically enriched relative to CO_2 by approximately 12‰ at 0ºC. In low $[CO_2]$ conditions, phytoplankton take up HCO_3^-. Although Fischer (1991) showed no direct relationship between temperature and $\delta^{13}C_{POC}$, Rau *et al*. (1992)

proposed low $\delta^{13}C_{POC}$ values as a result of high [$CO_{2(aq)}$], which is a result of low temperatures. Bicarbonate utilization brought about by PEPC would have a positive effect on $\delta^{13}C_{POC}$, due to smaller ε_p than the initial HCO_3^- enrichment relative to CO_2 and is supported by the results stated in Laws & Bidigare (1997). Freeman and Hayes (1992) suggested that temperature strongly influences the isotopic differences between dissolved inorganic carbon and CO_2, as well as the isotopic differences between carbonate minerals and CO_2. A high concentration of external carbon dioxide usually increases the ε_p of the inorganic carbon assimilation and as a result the $\delta^{13}C_{POC}$ decreases independent of the initial $\delta^{13}C_{CO2.}$ In the results obtained by Hoins *et al*. (2015), the fractionation increase due to the uptake of more ^{13}C depleted carbon in comparison to the ^{12}C enriched HCO_3^- and decreases with increasing POC production as inorganic carbon is fixed by a higher rate than the total carbon uptake, thereby reducing the ability of RUBISCO to evince the full presence of the lighter $^{12}CO_2$. This significant drop observed in isotope fractionation may also be the result of increased cellular carbon contents.

Potential impact of temperature: Carbon fixation through phytoplankton takes place in an open system, therefore the isotope effect (ε_p) can be directly measured through the isotopic difference between dissolved CO_2 and the primary photosynthate (Freeman & Hayes, 1992). Studies done by Pop *et al*. (1989), Cooper, Fimer & Wishnick *et a*l. (1969) and Freeman & Hayes (1992) stated that the substrate for the immense carbon fixation happening is dissolved carbon dioxide, thus ε_p can be cast in terms of the carbon isotopic composition of dissolved CO_2, in other words, there is less isotope fractionation with a decrease in CO_2 concentrations. Freeman and Hayes (1992) also showed positive results between temperature and $\delta^{13}C_{POC}$ (values ranged between 15‰ and 30‰), although Fischer 1991 showed no clear relationship between temperature and $\delta^{13}C_{POC.}$ Increasing fractionation with increasing temperature may be a result of higher molecular diffusion rates that happens at higher temperatures (Hinga *et al.*, 1994), thus supporting the results found in (Sarnthein, Winn, Duplessy, *et al.*, 1988) that there might be a positive relationship between the $\delta^{13}C_{POC}$ and ocean productivity. Results obtained from Freeman and Hayes (1992) revealed strong evidence about the considerable effect that temperature has on the isotopic difference between dissolved CO_2 and DIC, as well as dissolved CO_2 and carbonate minerals found in the ocean. A simple mechanism like temperature cannot be completely responsible for the effect of fractionation but temperature likely influences a wide variety of cellular functions, which influences the fractionation factor (Hinga *et al.*, 1994; Boller *et al.*, 2011). Thermal stratification can happen due to the warming of the surface ocean, thereby decreasing the light limitation in the SO, while it can cause nutrient limitation in the subtropics. Therefore, different responses from phytoplankton groups will be observed due to climate change as these responses will affect the fractionation process. Freeman and Hayes (1992) suggested that temperature strongly influences

the isotopic differences between dissolved inorganic carbon and CO_2, as well as the isotopic differences between carbonate minerals and CO_2. High concentration of external carbon dioxide usually increases the ε_p of the inorganic carbon assimilation and as a result the $\delta^{13}C_{POC}$ decreases independent of the initial $\delta^{13}C_{CO2.}$

Potential impact of CO_2: Tuerena *et al.* (2019) compared the relationships between $\delta^{13}C_{POC}$, $\delta^{13}C_{CO2}$ and $CO_{2(aq)}$ to modelled estimates for passive diffusion to better understand conditions where the ambient $[CO_{2(aq)}]$ dominate the determination of $\delta^{13}C_{POC}$ in the surface water. The results showed no significant correlation between these parameters, both at $p > 0.05$, indicating that $[CO_{2(aq)}]$ may be a determining factor of $\delta^{13}C_{POC}$, however, other factors are playing an important role in the fractionation process.

3. Methodology

Existing data for the South African National Antarctic Expedition (SANAE) 54, Winter Cruise (WC) 2015 and WC 2017 were used to analyse all the parameters. This data was collected by team members of the Department of Earth Sciences, Stellenbosch University. For SANAE 56, available data on all parameters from team members of the Department of Earth Sciences, Stellenbosch University, were used, except for nutrients. I analysed the nutrients for SANAE 56 in the Geochemistry lab at the Department of Earth Sciences, Stellenbosch University. However, even though existing data were mainly used for this study (except nutrients of SANAE56), methodologies are briefly reflected here for those readers unfamiliar with the team's previous studies. Statistical analyses were applied newly in this study as described in section 3.1 for all 4 cruises.

3.1. SANAE 54

SANAE 54 took place from 5 December 2014 to 17 February 2015. The research vessel SA Agulhas II was used for this voyage. The SA Agulhas II went from Cape Town down to Antarctica (Figure 3.1), crossing 3 major water masses along the Good Hope line, the Sub Tropical Front (STF) at 40.1ºS, the Sub Antarctic Front (SAF) at 44.1ºS and the Polar Front (PF) at 50.4ºS, then sailed west to South Georgia and back to South Africa again.

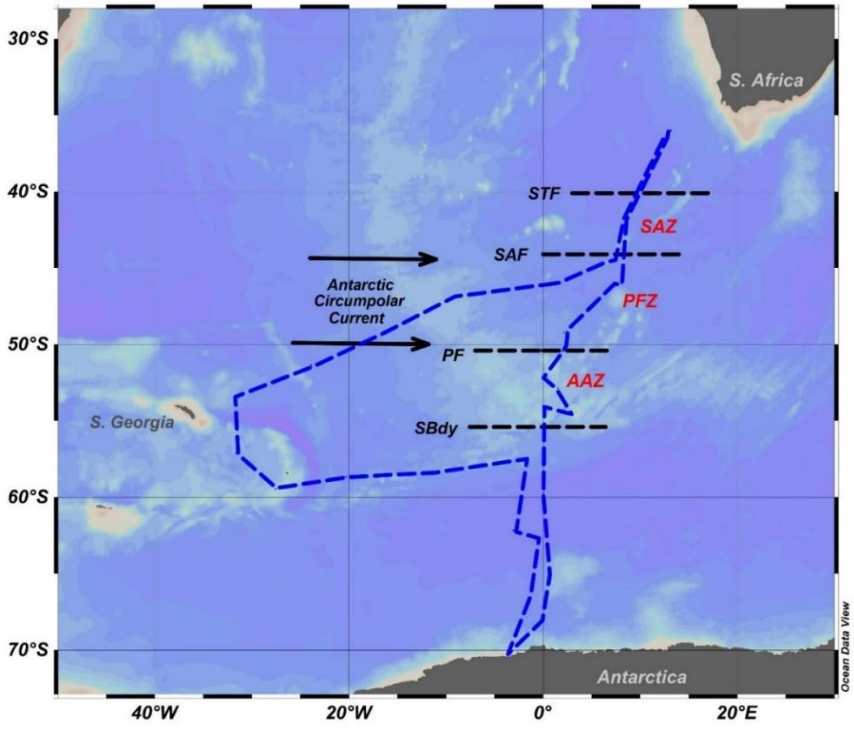

Figure 3.1. Schematic illustration of the SANAE 54 cruise track during the summer months of 2014/2015. The ship crossed major fronts and zones as indicated. STF: Subtropical Front; SAF: Sub-Antarctic Front; PF: Polar Front. This graph was made using Ocean Data View (Schlitzer, 2016) based on the previous version in (Viljoen, 2016).

3.1.1. Sampling and analytical methods for ancillary parameters

The team collected seawater from the continuous underway supply at a depth of 5 m from the ship's bow. Nutrient samples were taken every two hours and the chlorophyll samples were taken every four hours during leg one. A 0.2 µm pore size syringe filter was used; first, 5 - 10 mL sample water was filtered through the filter to clean the filter, thereafter the falcon tube was filled with filtrate and immediately frozen at -20ºC (Viljoen *et al.*, 2019). Nutrient samples were analysed at the University of Cape Town, within two months after sampling by postdoctoral fellow R. Philibert, SU Earth Sciences (pers. communication). Nitrate, nitrite (García-Robledo, Corzo & Papaspyrou, 2014) and silicic acid analysis were done using a Lachat Quick-Chem Flow injection auto analyser and phosphate was manually analysed at 880 nm with a Spectronic Helios Epsilon spectrophotometer according to protocols described by (Grasshof, Kremling & Ehrhard, 1983)

Twenty-four underway water samples were used to determine the surface phytoplankton groups across the major water masses. Using a Whatmann GF/F glass fibre filter (0.7 µm pore size) under dim light conditions, the samples were filtered and immediately stored at -80ºC. Hereafter, an analysis using High-Performance Liquid Chromatography (HPLC) at Laboratoire d'Océanographie de Villefranche/Mer (LOV – CNRS), a CHEMTAX matrix factorization program was done by Ph.D. student J. Viljoen, SU Earth Sciences. This method was used to calculate the phytoplankton community composition, thus the phytoplankton groups' contribution to the total chl-a (Viljoen *et al.*, 2019).

For POC, water from the bow intake of the ship was sub-sampled into 1-L LDPE bottles. These bottles were pre-rinsed 3 times prior to sampling. Samples were filtered through 25 mm GF/F filters where after the filters were stored at -25ºC. 20 mm filter discs were punched out from 47 mm filter paper and freeze-dried for roughly 6 hours before POC analysis (Pienaar, 2017). Petri dishes with POC samples and drying silica gel beads were placed in a desiccator and acid fumed, hereby removing the inorganic carbon from the samples. Samples were then transferred to tin foil sample cups and placed into microplates. The blank filter paper was placed into every 7th slot of the microplate. Samples were then sent to the University of Pretoria for analysis and results were first reported in Honours thesis (Pienaar, 2017).

Sea surface temperature and sea surface salinity data were continuously measured by a thermosalinograph in 10-minute intervals during this voyage.

The surface water pCO_2 was measured using an underway system described by (Pierrot, Neill, Sullivan, *et al.*, 2009). The system directs seawater flow through a chamber, which is known as the equilibrator. Within the equilibrator the CO_2 present in the water equilibrates with the adjacent gas in the chamber, also referred to as the headspace gas. The CO_2 in the headspace gas is

determined by pumping it through a non-dispersive infrared analyser to measure the mole fraction of the CO_2 (xCO_2) and returned to the equilibrator to form a closed system. Air is also pumped through the analyser to measure the mole fraction of CO_2.This analyser is calibrated using four CO_2 standard gases at recurring intervals (Pierrot *et al.*, 2009).

3.1.2. Sampling analysis for carbon isotopic composition

Laboratory analysis was done on $\delta^{13}C$ (carbon isotopic composition) and reported as follow:

$$\delta^{13}C\ (‰) = [\ (^{13}C\ /^{12}C_{sample}\ /\ ^{13}C\ /^{12}C_{\text{standard}}) - 1] \times 1000$$

The analysis of carbon isotopic signature was done at the University of Pretoria, Stable Isotope Laboratory, Mammal Research institute and data first reported in Honours thesis Pienaar (2017). A Flash EA 1112 Series was coupled to a Delta V Plus stable light isotope ratio mass spectrometer via a ConFlo IV system and two laboratory running standards (Merck Gel: $\delta^{13}C$ = 20.26‰, $\delta^{15}N$ = 7.89‰, C% = 41.28, N% = 15.29) and (DL-Valine: $\delta^{13}C$ = -10.57‰, $\delta^{15}N$ = -6.15‰, C% = 55.50, N% = 11.86) were used as well as a blank sample (Pienaar, 2017). The running standards were calibrated against international standards, which include the National Institute of Standards and Technology (NIST): NIST 1557b (Bovine liver); NIST 2978 (Muscle tissue) and NIST 1547 (peach leaves) (Pienaar, 2017).

3.1.3. Statistical analysis

A statistical correlation was done using Statistica, XLStat and SPSS, where $\delta 13C_{POC}$ is the dependant variable and the independent variables include POC, macronutrients (PO_4, $Si(OH)_4$, NO_2 and NO_3), chlorophyll-a concentration, nine different phytoplankton groups, pCO_2, salinity and temperature.

There are three possible correlation tests to use, but to determine which one to use, it is important to know whether the data is normally distributed or not. Pearson's correlation test only requires that datasets are presented in intervals (Field, 2009), although when it is needed to establish the significance of the data, it is required to know whether the dataset is normally distributed or not. For the statistics to be valid, the data should be normally distributed. Spearman's correlation coefficient is used for non-parametric datasets, thus there is no requirement for the data to be normally distributed. The last correlation test that can be used is Kendall's Tau, which is also a non-parametric correlation and should be used in Spearman's place in the case of very small datasets. Normality testing can be done by using skewness and kurtosis. Skewness measures the asymmetry of the probability distribution of random variables about their means, thus indicating the amount and direction of skew. The distribution is highly skewed for values less than

-1 and greater than 1, a moderately skewed dataset has skewness between -1 and -0.5 or 0.5 and 1, and skewness values between -0.5 and 0.5 are roughly symmetric and can be accepted as normally distributed data. Kurtosis indicates the height and sharpness of the central peak. Acceptable values for kurtosis are between -0.5 and 3. Anything outside this parameter cannot be accepted as normally distributed data.

Skewness and kurtosis need to be looked at together, both values should fall in the ranges above for a dataset to be normally distributed. For all four cruises, skewness and kurtosis tests were done, whereafter it was decided whether to use Pearson, Spearman of Kendall's tau correlation tests.

After the statistic tests on the data sets, the relationship between two variables was used to draw a scatter plot to indicate linearity using the correlation coefficient (R-values). By comparing the p-value to the significance level (α or alpha) which is 0.05, the significance of the correlation coefficient was determined. A p-value ≤ α, indicates that the correlation is statistically significant and when the p-value > α, it indicates that the correlation is not statistically significant.

3.2. Winter Cruise 2015

Team members of the Department of Earth Sciences, Stellenbosch University collected most (except pCO_2) here described samples. From 22 July 2015 – 15 August 2015, when the SA Agulhas II travelled along the Good Hope line as well as the SAMBA line, the latter indicated in red (inserted to show cruise track) in figure 3.2 (Monteiro, Ansorge, Fietz, *et al.*, 2015). The autonomous underway pCO_2 measurements were taken by members of the SOCCO team, CSIR, as per (Pierrot *et al.*, 2009). For this study, we focus on the Good Hope line between Cape Town and Antarctica along the Greenwich Meridian. The objective of choosing the Good Hope line for sampling is to continue the repeat of high density biogeochemical and physical data collection along the cruise track (Monteiro *et al.*, 2015). There was a total of 12 stations along the Good Hope line during this cruise.

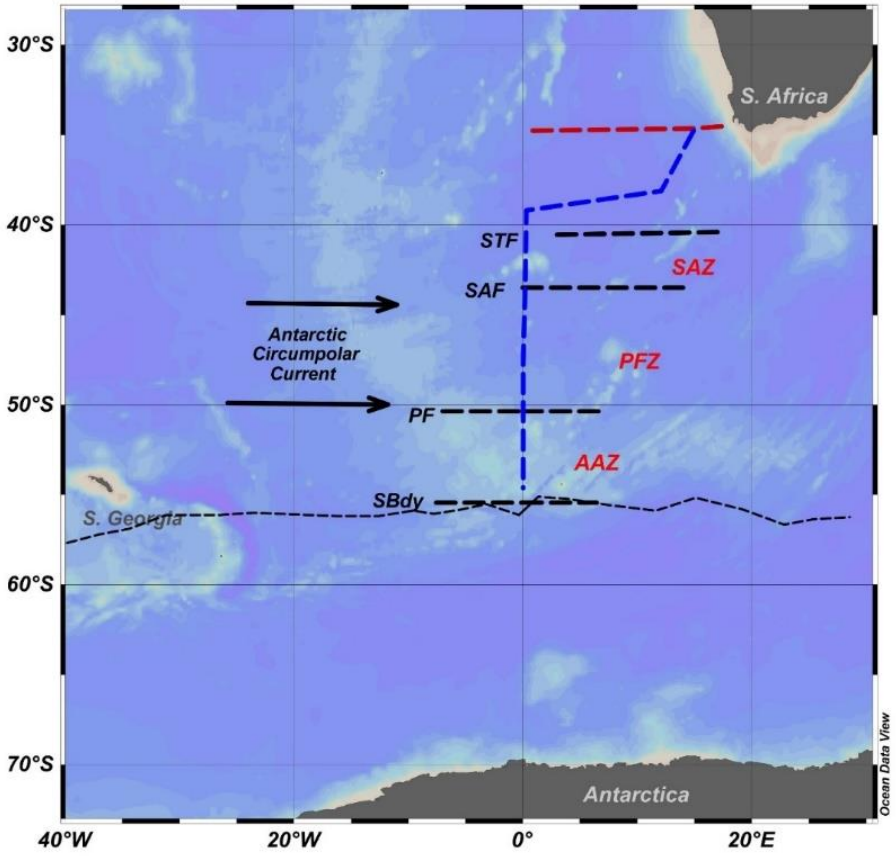

Figure 3.2. Cruise map (Schlitzer, 2016) of the Winter 2015 voyage along the Good Hope line (indicated in blue) and the SAMBA line (indicated in red). The sea ice edge was reached at 56˚S.

3.2.1. Sampling and analysis for ancillary parameters

Surface pCO_2 was collected from the ship's underway supply (Monteiro *et al.*, 2015) and was measured using an infrared gas analyser. This instrument was sequenced to change between atmospheric air, seawater and reference standards every four hours. LABVIEW was used to log the data collected from the instrument and to control the operation of the instrumentation. To ensure appropriate water– and gas flow as well as equilibrator levels, the instrument was monitored approximately every two hours. Sampling and analyses for all other parameters were done the same way as mentioned in section 3.1.

3.3. SANAE 56

Team members of the Department of Earth Sciences, Stellenbosch University collected most (except pCO_2) here described samples during the 56th SANAE cruise that took place from 2 December 2016 to 13 February 2017 where 3 major fronts were crossed along the Good Hope line; the Sub Tropical Front (STF) at 40.94ºS, the Sub Antarctic Front (SAF) at 43.6ºS and the Polar Front (PF) at 49.2ºS (Figure 3.3). The ACC and the Southern Boundary (SBdy) was

identified at approximately 55.44ºS for this cruise (Viljoen *et al.*, 2019). Samples for pCO_2 were taken by members of the SOCCO team, CSIR, as per (Pierrot *et al.*, 2009).

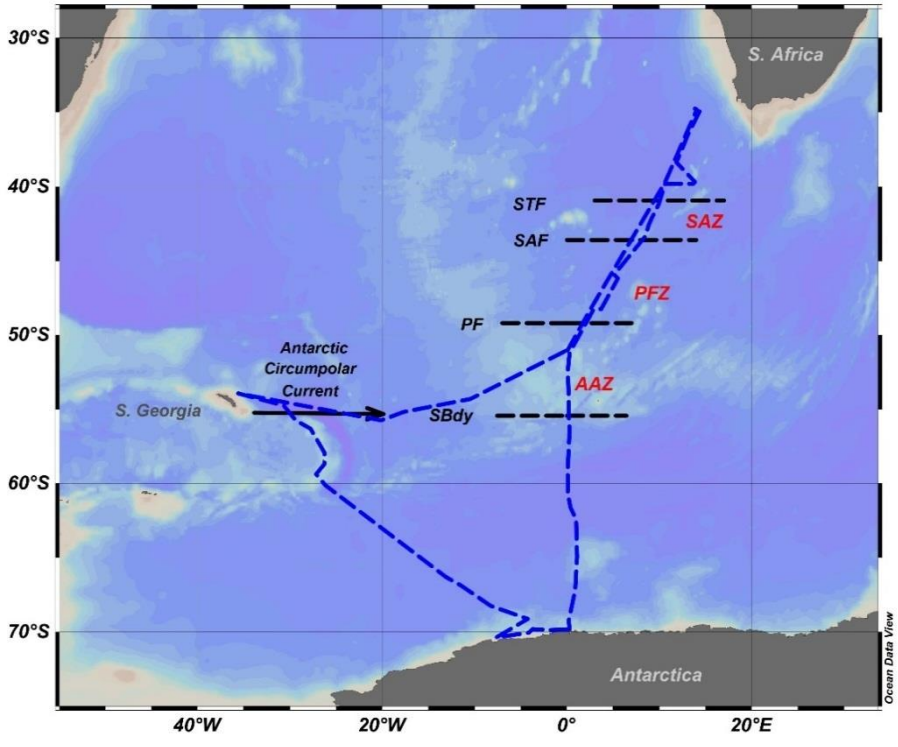

Figure 3.3. Schematic illustration of the SANAE 56 cruise that took place for the 2016/2017 summer (Schlitzer, 2016). The Agulhas II travelled along the Good Hope Line from South Africa to Antarctica and on the way back sailed via South Georgia. All major fronts were crossed on the way south.

3.3.1. Sampling and analysis for ancillary parameters

Temperature and salinity data were collected from continuous underway sampling at 10-minute intervals and were recorded on the scientific data system of the ship. For all other parameters, samples from the ship's underway supply were taken at 6 m depth and at a high resolution, where after analysis, calculations and statistics were done as explained in section 3.1. However, since I conducted the nutrient analysis for SANAE 56 specifically for the here presented MSc thesis, the methodology is provided in more detail hereafter.

3.3.2. Nutrient Analysis

As mentioned above, surface water was collected from the underway supply and samples used for the macronutrients were frozen at -20ºC immediately after sampling, until analysis after the cruise. Nutrient analysis for SANAE 56 was done manually on a Genesys 10-S UV Spectrophotometer at the Earth Science department, Stellenbosch University. Both silicic acid and phosphate were determined using modified colorimetric methods of (Grasshof *et al.*, 1983) while nitrate and nitrite were determined using methods of (García-Robledo *et al.*, 2014).

3.3.2.1. Silicic acid

Glassware was avoided while preparing the reagents and standards for silicic acid. The standards and actual samples were treated the same way every day to calculate the sample concentrations from the standard absorbance readings. Four reagents were used during the analysis for silicic acid: Solution 1 was made by dissolving 2 g ammonium molybdate tetrahydrate ($(NH_4)_6 Mo_7O_{24}{\cdot}4H_2O$) in 10 mL deionized water. Solution 2, also called the working solution, was prepared from a 95 - 99% 18.2 M H_2SO_4 bulk solution, using the equation $C_1V_1 = C_2V_2$ (18.2 M) (V_1) = (3.6 M) (10 mL), where V_1 = 1.98 mL H_2SO_4 and was made up to 10mL with deionized water (DIW). Solution 1 was added to solution 2. It is very important to add solution 1 to solution 2 and not the other way around. This solution was prepared fresh every week.

The oxalic acid solution was made up by dissolving 10 g of oxalic acid in 100 mL DIW. This reagent was stored in a dark place and it was not refrigerated due to recrystallization. The ascorbic acid solution was made by adding 1.75 g ascorbic acid to 100 mL DIW. This reagent was stored in a fridge wrapped in tinfoil and prepared fresh once a week. As long as the reagent remains colourless, it is effective. The silicic acid standard was prepped by dissolving 0.9403 g silicofluoride in 1-L DIW to make a Silicocluride (Na_2SiF_6) bulk solution (5 Mm) where after a 100 µM working standard was made up by adding 1000 mL DIW to 20 mL of the 5 mM standard.

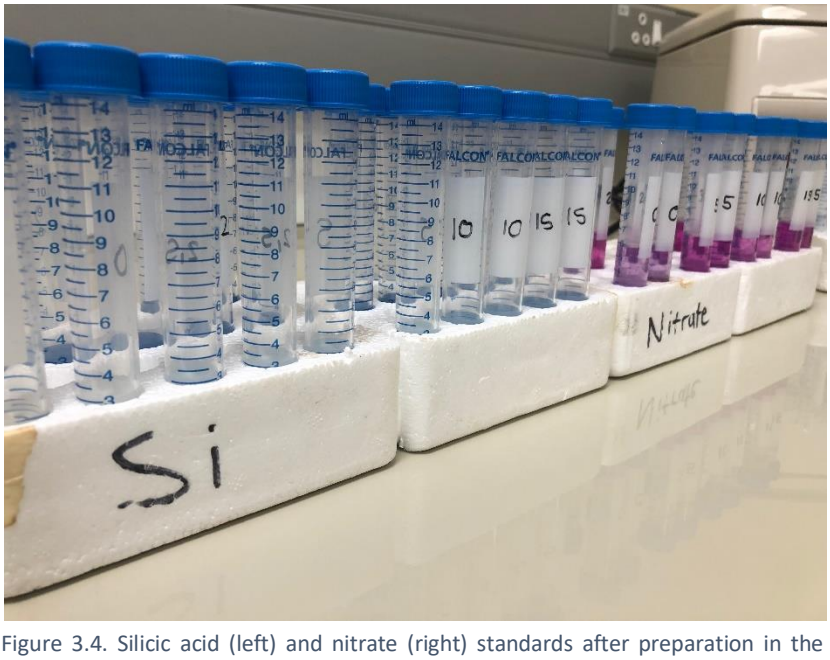

Figure 3.4. Silicic acid (left) and nitrate (right) standards after preparation in the Geochemistry Labarotory at Stellenbosch University, just before the absorbance was read. Silicic acid showed a blue-purple colour and became darker with higher concentrations and the nitrate standards turned pink after the Griess reagent was added.

Samples (3 mL) were prepared by adding 90 µL of solution 2 to all samples and standards, after which they were vortexed. After waiting 10 minutes for the solution to react, 90 µL of solution 3 and 4 were added to all samples, vortexed and allowed to react for 20 minutes. After 20 minutes a purple-blue colour was observed with darker colours at higher concentrations (Figure 3.4). The spectrophotometer was calibrated using a plastic cuvette filled with DIW and the absorbance was read at 810 nm, where after a calibration curve was made by plotting the absorbance against standard concentrations. This line graph gave a simple y = mx + c equation, where y is the absorbance, m is the slope already calculated for each graph, x is the concentration and c is the y-intercept where the line crosses the y-axis. The analysis took place over 5 days and the calibration curve for each day and freshly prepared standards can be seen in figure 3.5.

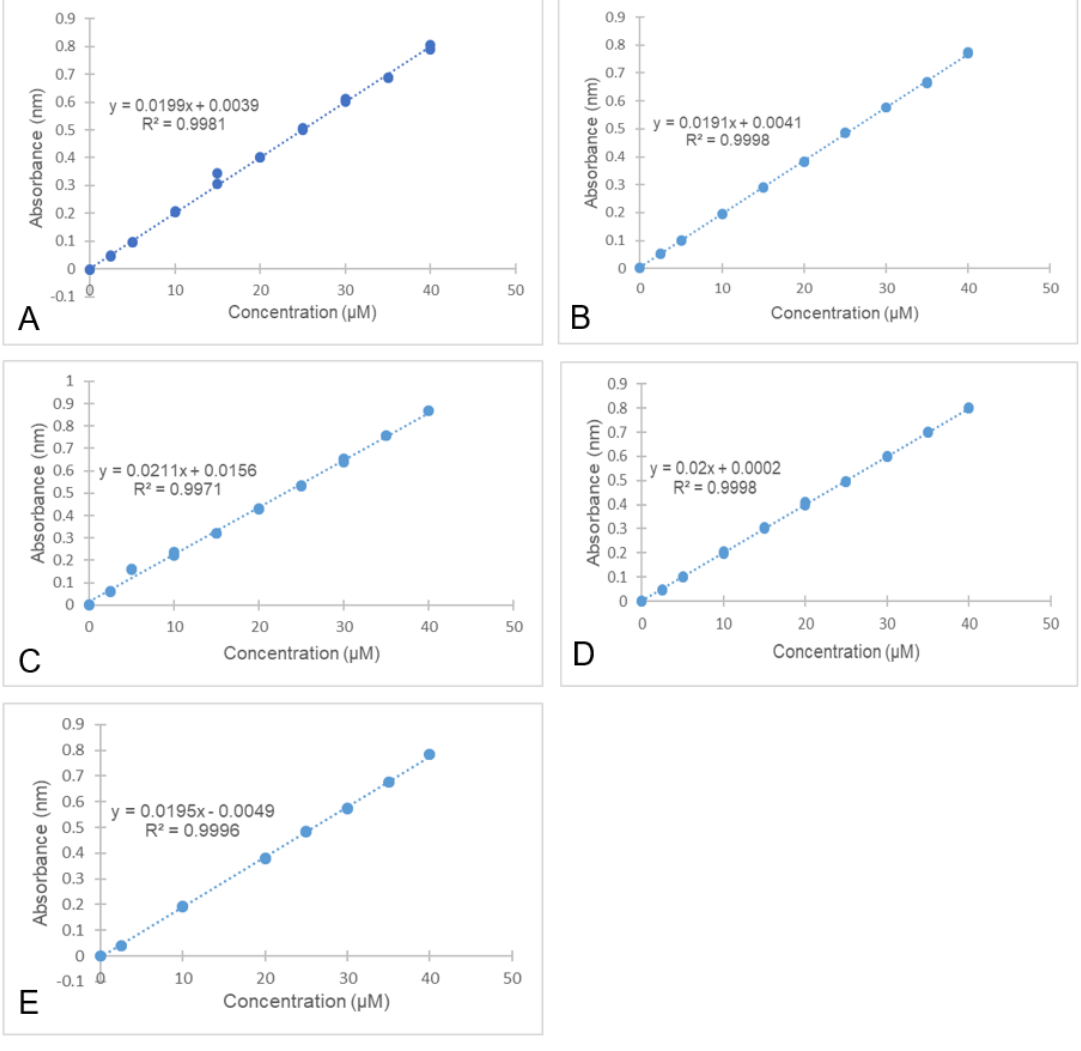

Figure 3.5. Calibration standards for silicic acid for 87 nutrient samples taken during the SANAE 56 cruise analysed over 5 days. Each day standards were prepped fresh to make the calibration curves. The first day of analysing, 3 samples were analysed with the standards (A); on the second day 16 samples were analysed (B), the third day 20 samples were analysed (C), 23 samples were analysed on the fourth day (D) and the last 25 samples were analysed on the fifth day (E).

3.3.2.2. Phosphate

Reagents for phosphate analysis were prepared as follows; ammonium molybdate tetrahydrate ($(NH_4)_6$ $Mo_7O_{24}{\cdot}4H_2O$) solution was made up by dissolving 7.5 g ammonium molybdate tetrahydrate in 250 mL DIW and was stored in a plastic bottle out of direct sunlight. The sulphuric acid solution was made by adding 70 mL sulphuric acid to 450 mL DIW and stored in a cool place. Ascorbic acid (13.5 g) was dissolved in 250 mL DIW and stored in a fridge wrapped in tinfoil. This solution was made fresh once a week. Potassium antimonyl-tartrate ($C_8H_{10}O_{15}Sb_2$) was made up by dissolving 0.34 g of potassium antimonyl-tartrate in 250 mL DIW and stored in a glass bottle. This reagent stays stable for a few months. The mixed reagent for phosphate was made up by mixing the above-mentioned reagents in the following order: (i) 10 mL of ammonium molybdate, (ii) 25 mL sulphuric acid, (iii) 10 mL ascorbic acid and (iv) 5 mL of potassium antimonyl-tartrate.

A bulk solution (10 µM) of anhydrous potassium dihydrogen phosphate (KH_2PO_4) was made up by dissolving 0.816 g anhydrous potassium dihydrogen phosphate in 1000 mL DIW which was stored in a dark bottle with 1 mL of chloroform. From this concentrated standard, 0.2 mL was made up to 200 mL with DIW to make a 6 µm working standard. 5 mL standards were prepared directly from the bulk solution.

For all 5 mL samples and standards, 0.5 mL of the mixed reagent was added, vortexed and allowed to react for 30 minutes. The spectrophotometer was calibrated once again using a cuvette filled with DIW and the absorbance was read at 880 nm. Calibration curves were made after each day of analysis (Figure 3.6) to calculate the phosphate concentration from the linear regression equation $y = mx + c$.

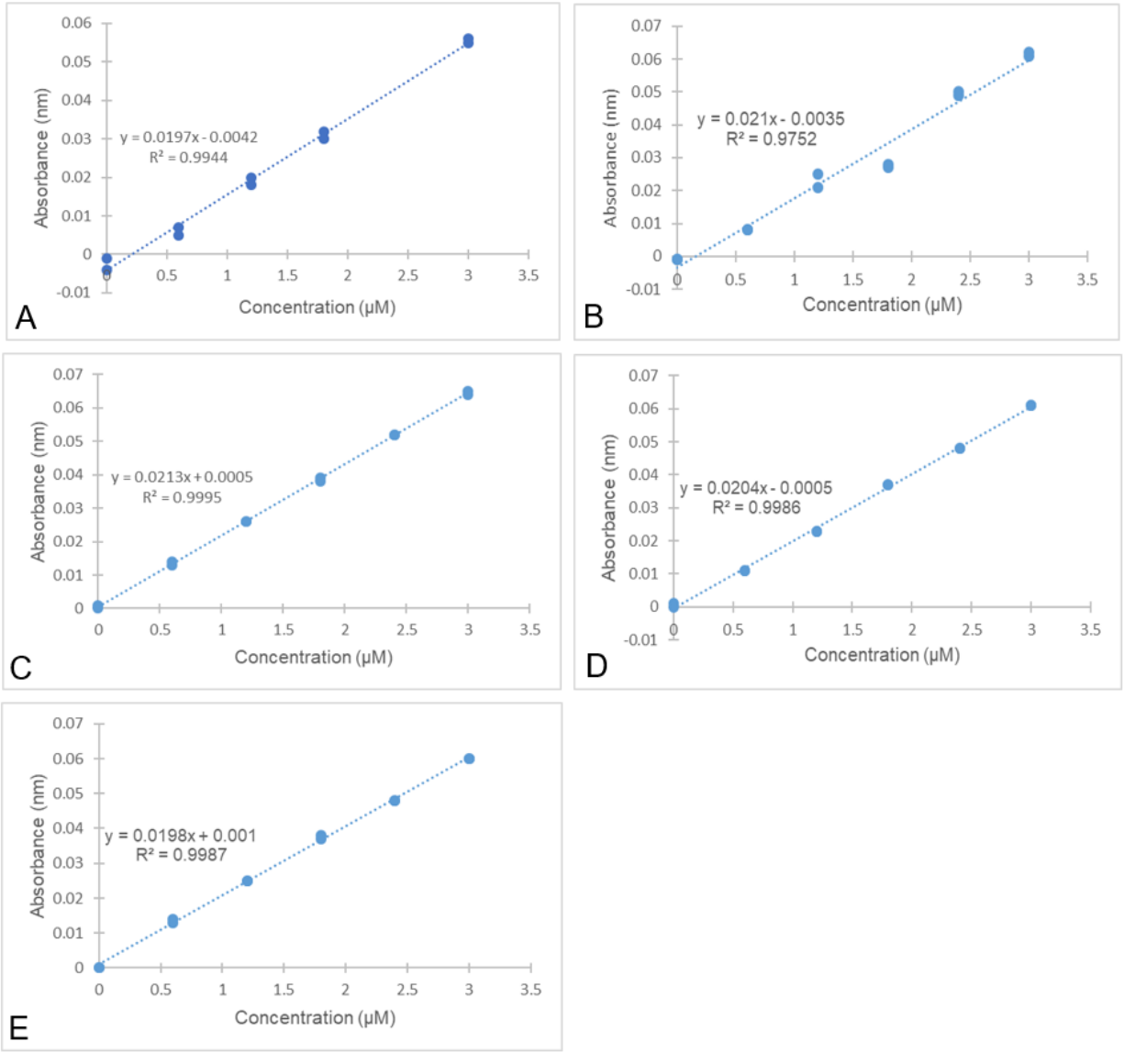

Figure 3.6. Calibration standards for phosphate for 87 nutrient samples taken during the SANAE 56 cruise analysed over 5 days. Each day standards were prepped fresh to make the calibration curves. The first day of analysing, 3 samples were analysed with the standards (A); on the second day 16 samples were analysed (B), the third day, 20 samples were analysed (C), 23 samples were then analysed on the fourth day (D) and the last 25 samples were analysed on the fifth day (E).

3.3.2.3. Nitrate and Nitrite

All reagents used for this analysis were stored in dark glass bottles and maintained at 4ºC. Sulphanilamide (1 g) was dissolved in 11.76 mL HCl and diluted in 60 mL milli-Q water. This is an exothermic reaction; thus, it was allowed to cool down and then made up to 100 mL. 90.1 g N-(1-naphthyl)-ethylenediamine dihydrochloride (NEDI) was dissolved in 100 mL milli-Q water. NEDI is stable for approximately one month after mixing and can be used until a brown discoloration occurs. Just before analysis, 10 mL sulphanilamide and 10 mL NEDI were mixed, this is called the Griess-reagent. Vanadium (III) chloride was prepared by dissolving 0.5 g of VCl_3

in 14.71 mL 10.2M HCl solution. Dissolution normally takes about 1 hour, but in this case, it sometimes took up to 3 hours. Complete dissolution can be observed when there is a shift from a turbid to a transparent solution. The solution was filtered through a 0.7 µm nominal pore size glass filter (Whatman GF/F filters) to eliminate any impurities. This solution is stable for several months.

Both nitrite and nitrate determinations can be affected by salinity, thus calibration curves were performed using standards at salinity values like those of the samples. It is important to note that NO_2 molar absorptivity will decrease once analysing for NO_3 due to several factors ranging from dilution to VCl_3 reagent interferences, etc.

Stock solutions were prepared using DIW and not synthetic seawater.

Calibration standards for seawater samples were prepared using synthetic seawater in the place of DIW. All reagents are of analytical quality. Synthetic seawater was prepared by dissolving 310 g NaCl, 100 g of magnesium sulphate ($MgSO_4 \cdot 7H_2O$), and 0.50 g of sodium bicarbonate ($NaHCO_3 \cdot H_2O$) in 10-L of distilled water.

A 5 mM stock nitrate solution was prepared by dissolving 0.5055 g KNO_3 (which was oven-dried at 100ºC for 1 hour) in 1-L pure water. It is important to remember that nitrate analysis is most effective for samples <30 µM, therefore dilution is recommended for samples greater than this. The solution is stable indefinitely in the absence of evaporation. Working solutions were always prepared fresh before use. A working solution (500 µM) was prepared by diluting 25 mL of stock solution in 250 mL artificial seawater. 250 µL Griess reagent was then added to 5 mL of standard and gently mixed. Falcon tubes were incubated at ambient temperature (~25ºC) for 20min (Figure 3.7).

Figure 3.7. Nitrate and nitrite standards and solutions were placed in the water bath after Griess reagent was added.

500 µL VCl_3 was then added to every 5 mL sample. The falcon tubes were then closed to prevent evaporation, gently mixed and incubated in a temperature-controlled bath at 60°C for 25 minutes. A water bath was used to cool down the falcon tubes to room temperature. Absorbance was then measured at 540 nm where after calibration curves were plotted for nitrate (Figure 3.8) and nitrite (Figure 3.9).

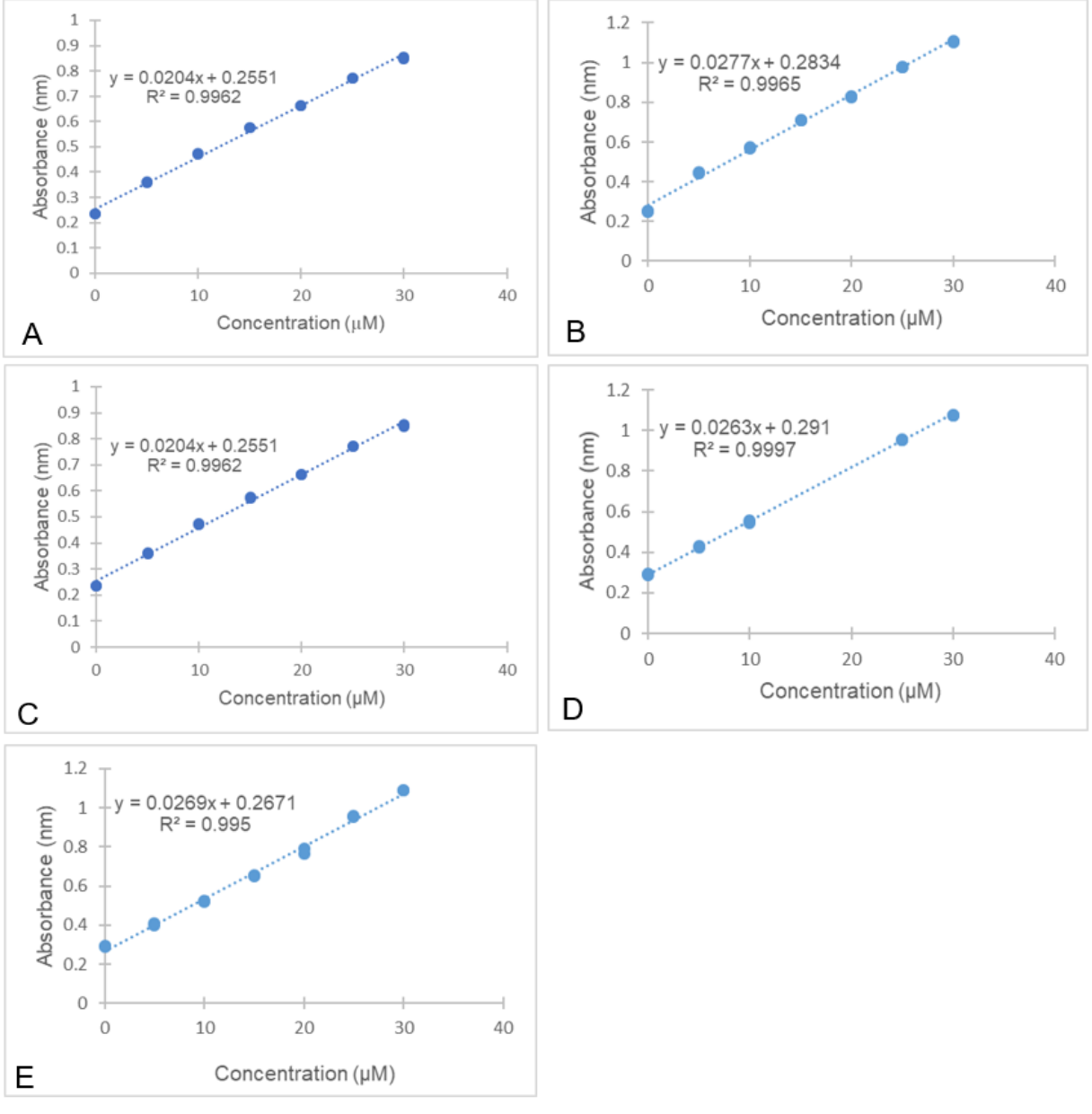

Figure 3.8. Calibration standards for nitrate for 87 nutrient samples taken during the SANAE 56 cruise analysed over 5 days. Each day standards were prepped fresh to make the calibration curves. The first day of analysing, 3 samples were analysed with the standards (A); on the second day 16 samples were analysed (B), the third day 20 samples were analysed (C), 23 samples were analysed on the fourth day (D) and the last 25 samples were analysed on the fifth day (E).

A 5 mM stock nitrite solution was prepared by dissolving 0.345 g $NaNO_2$ in 1-L pure water and stored in a dark bottle with 1 mL of chloroform as a preservative. This solution is stable for 1-2 months. A working solution was prepared by diluting 0.2 mL of the 5 mM stock solution in 250 mL synthetic seawater. After that, 250 µL of the Griess reagent was added to 5 mL standard and gently mixed. The falcon tubes were then closed to prevent evaporation and incubated in a temperature-controlled bath at 60ºC for 25 minutes. Absorbance was read at 540 nm.

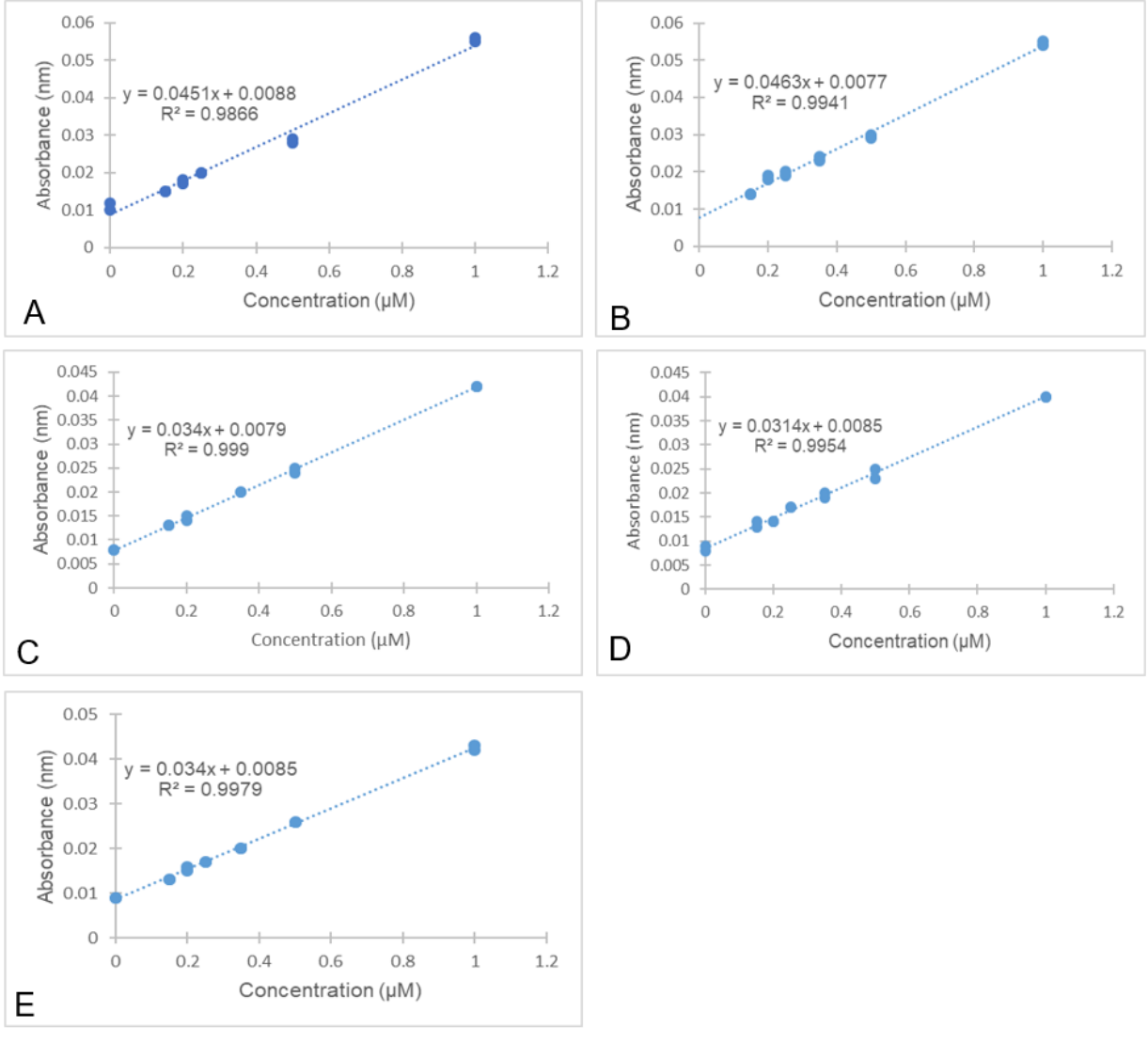

Figure 3.9. Calibration standards for nitrite for 87 nutrient samples taken during the SANAE 56 cruise analysed over 5 days. Each day standards were prepped fresh to make the calibration curves. The first day of analysing, 3 samples were analysed with the standards (A); on the second day 16 samples were analysed (B), the third day 20 samples were analysed (C), 23 samples were analysed on the fourth day (D) and the last 25 samples were analysed on the fifth day (E).

3.3.3. Carbon isotopic composition

Sampling protocols, analysis and calculations were done the same way as described in chapter 3.1.2 for SANAE54.

3.4. Winter Cruise 2017

Team members of the Department of Earth Sciences, Stellenbosch University collected most of here described samples during Winter Cruise 2017 that took place from 28 June 2017 to 13 July 2017 and consisted of three legs (Figure 3.10). Samples for pCO_2 were taken by members of the SA Weather Service team, using a system described by (Pierrot *et al.*, 2009) This cruise focused on capturing the winter recharge conditions in the Atlantic-Indian Ocean sector of the SO and crossed the major water masses at the following positions; STF at 42.4ºS, the SAF at 46.2ºS, the PF at 49.3ºS and the SBdy at 58.5ºS (Weir, 2018).

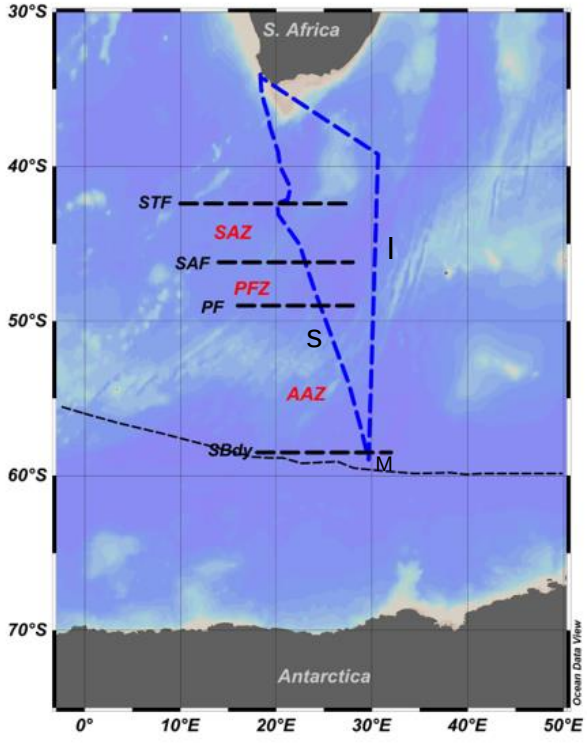

Figure 3.10. Actual cruise track of WC 2017 indicating 15% sea ice concentration (Vichi, 2017) with the thin dashed black line bordering 60˚S at approximately 30˚E. This graph was made using Ocean Data View (Schlitzer, 2016).

3.4.1. Sampling and analysis for ancillary parameters

Through the entire cruise, continuous temperature data were measured at 1 hourly intervals using a Vaisala Humicap HMP155 probe and was logged using a Campbell Scientific CR1000 logger (Vichi, 2017). Underway salinity samples were taken at 4-hour intervals and were analysed using a Salinometer to calibrate the TSG system. A total of 99 pCO_2 samples were taken during the

cruise, on leg S, 62 samples were collected from the underway system, in 4-hours intervals. During leg M, 5 samples were collected using two handheld Niskin bottles at 5 different ice stations and 32 samples were taken during leg I, in duplicate Niskin bottles and the underway system. pCO_2 samples were collected in 500 mL glass bottles and a short Tygon tube was used for the underway as well as the Niskin bottles using the method described in section 3.1.

Nutrient underway samples, 32 to be exact were taken during the voyage and were measured in the Marine Biogeochemistry Laboratory at UCT (Weir, 2018). Pigment samples (38) and POC samples (32) were sampled with additional pigment samples taken at a higher resolution at the frontal zones. POC, $\delta^{13}C_{POC}$ and pigment sampling and analysis were done as explained in section 3.1 and Viljoen *et al.* (2019).

4. Results

4.1. SANAE 54

4.1.1. $\delta^{13}C_{POC}$

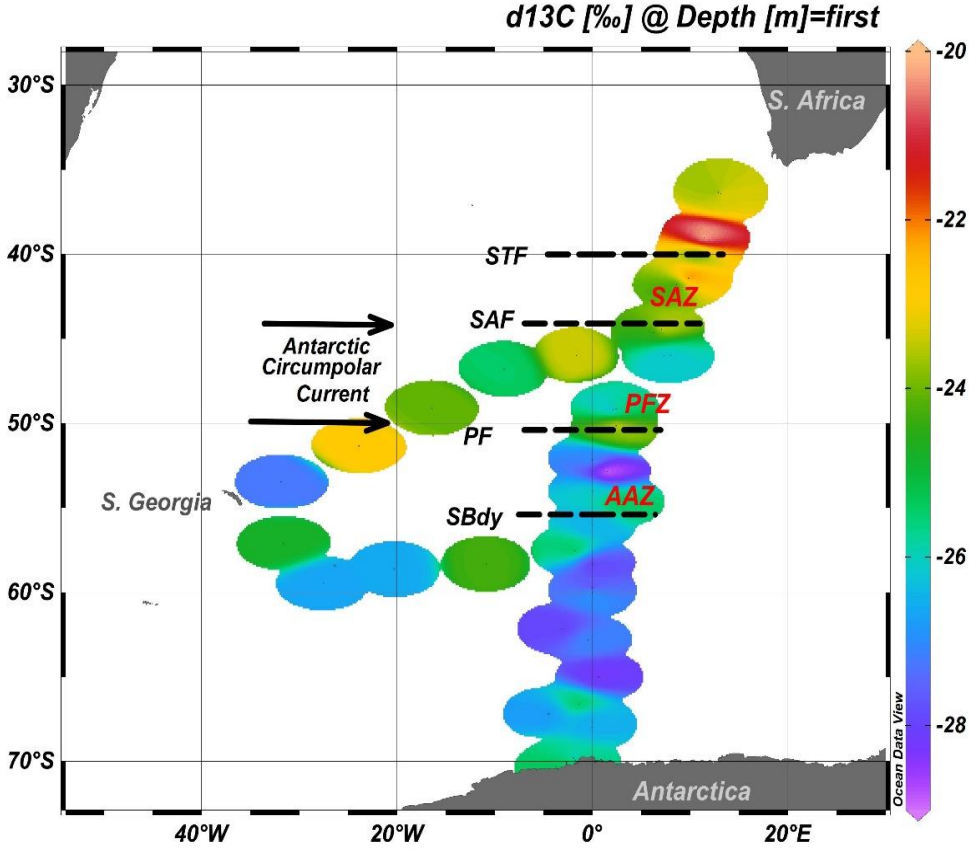

Figure 4.1. Carbon isotopic signature ($\delta^{13}C_{POC}$) along the Good Hope line from South Africa to Antarctica during the SANAE 54 voyage that took place in December2014-February2016. The highest value can be observed at -39°S just before crossing the STF.

Along the transect from Cape Town to Antarctica, the $\delta^{13}C_{POC}$ vary between -24‰ and -28‰, with a general trend of decreasing $\delta^{13}C_{POC}$ values (Figure 4.1). A peak of ca. -20‰ is observed just north of the STF at 39ºS. The South Georgia leg shows a slight decrease (-24.3‰ to -26.7‰) in $\delta^{13}C_{POC}$ from 10ºW to approximately 35ºW and an increase to -22.9‰ at 20ºW crossing the PF.

4.1.2. Macronutrients

The correlation coefficient used for all nutrients with $\delta^{13}C_{POC}$ for the SANAE 54 results is the Pearson correlation, due to their skewness and kurtosis values, see appendix A, table A1.

Silicic acid: Silica plays a very important role in controlling biological production in the ocean (Roy-Barman & Jeandel, 2016) and the lack thereof limits diatom development (see section 4.1.3). Silicic acid is negatively related to $\delta^{13}C_{POC}$ with a correlation coefficient of -0.550, which is also significant at p = 0.003 (Table 4.1). This negative relationship between $Si(OH)_4$ and $\delta^{13}C_{POC}$ can

be seen in figure 4.2-A; with an increase in $Si(OH)_4$, the $\delta^{13}C_{POC}$ becomes more negative. This may be a result of phytoplankton groups taking up ^{12}C as there is a depletion in ^{13}C and fractionation increases. Previous studies (Coale, Johnson, Chavez, *et al.*, 2004; Egan, Rickaby, Leng, *et al.*, 2012) support the results found in this study as it is known that silicic acid increases from north to south in the SO, which can be seen in figure 4.2-B. This does not necessarily mean that silicic acid has a direct effect on the fractionation. The significant correlation between silicic acid and $\delta^{13}C_{POC}$ can be explained by the increase of siliceous phytoplankton along the transect (Figure 4.5-F). On the South Georgia leg, there is a peak in silicic acid concentration at 30ºW and 60ºS from ca. 40 µM to ca. 80 µM, where after the concentration gradually decreases until reaching 0 µM when the PF is crossed back southwards.

Phosphate: In the surface ocean, phosphate is present in much lower concentrations than that of silicic acid and nitrate (Figure 4.2-H). PO_4 concentrations increase from Cape Town to Antarctica, with a maximum concentration at 66.6ºS close to the Antarctic shelf. The PO_4 spike at this point coincides with the high productivity that is observed in high latitude waters, although just before the spike a fall in concentration from 1.5 µM to 0.5 µM is observed. On the South Georgia leg, crossing the Southern Boundary the concentration does not show a steady trend; it varies between 1 and 2 µM. Along the Good Hope Line and the South Georgia leg, a negative relationship is observed between $\delta^{13}C_{POC}$ and PO_4 concentrations. With increasing PO_4 concentration, the $\delta^{13}C_{POC}$ decrease, resulting from an increase in fractionation. This relationship is however not significant with $p = 0.084$.

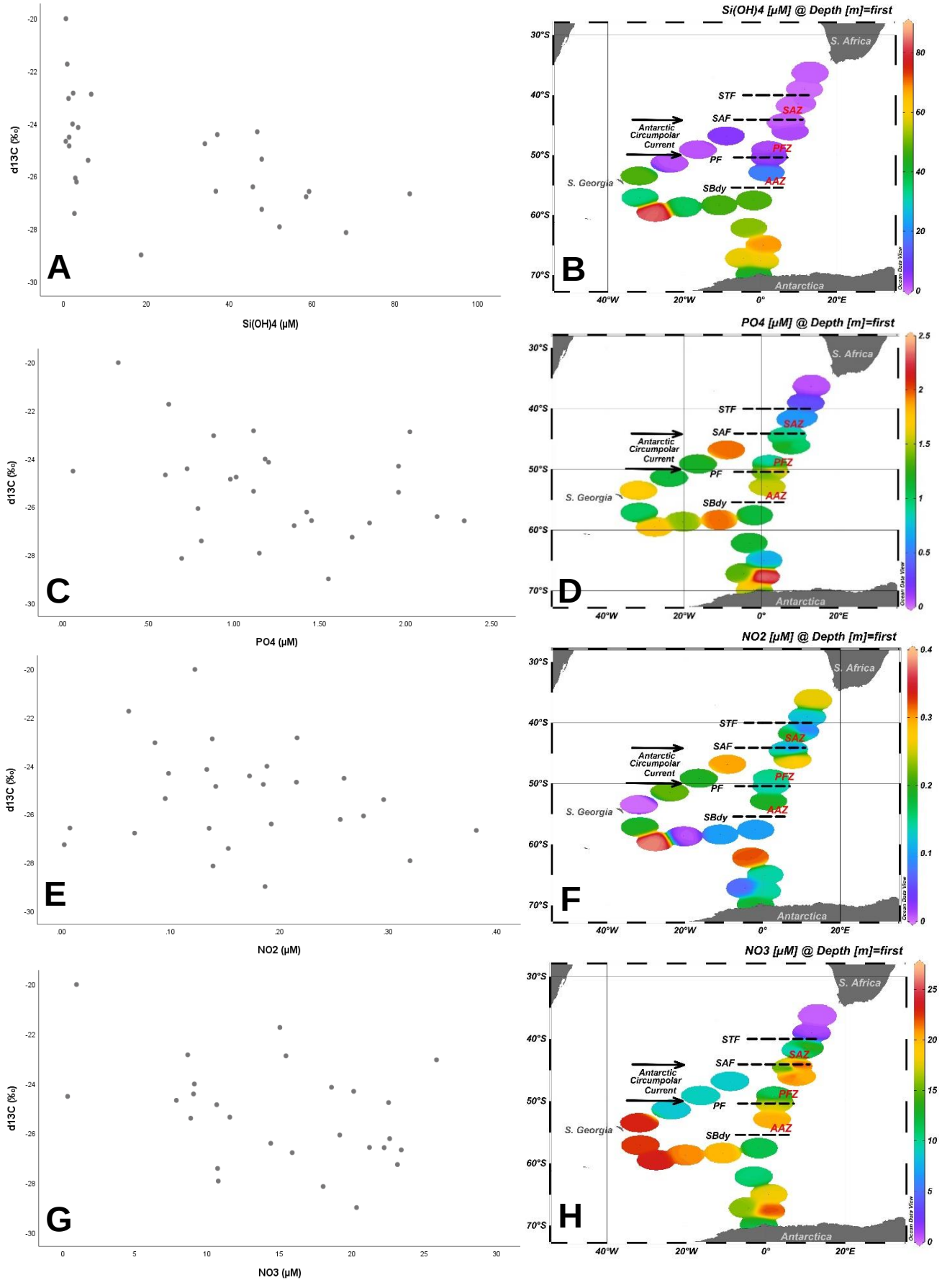

Figure 4.2. Macronutrients results for $Si(OH)_4$ (A&B), PO_4 (C&D), NO_2 (E&F) and NO_3 (G&H) during SANAE 54 as plotted using SPSS (A, C, E & G) and ODV (B, D, F & H). The x-y graphs for each nutrient (A, C, E, G) indicate whether there is a positive or negative relationship between the nutrient and $\delta^{13}C_{POC}$. The horizontal dashed lines on the ODV maps indicate the frontal positions.

Nitrite and Nitrate: Nitrate is the second most abundant nutrient in surface waters of the SO, where nitrite concentrations are very low relative to nitrate. Negative relationships between $\delta^{13}C_{POC}$ and concentrations of nitrite (NO_2) and nitrate (NO_3) are observed (Figures 4.2-E&G). However, the negative relationship observed between NO_2 and $\delta^{13}C_{POC,}$ shows a low correlation coefficient of r = -0.176 and no significance at p = 0.379. In contrast with this result, NO_3 has a negative relationship with $\delta^{13}C_{POC}$ at r = -0.391 and is significant at p = 0.044 (Table 4.1). NO_2 concentrations show a slight peak at approximately 60ºS on the Good Hope line and the South Georgia leg (Figure 4.2-F). NO_3 increase from 0 µM – 15 µM when the STF is crossed at 40.1ºS. From the SAF to Antarctica, the concentration varies between 15 µM and 20 µM with a slight increase to ca. 23 µM at 69ºS. On the South Georgia leg, south of the SBdy, the concentration shows an increase to 25 µM, whereafter it drops to 10 µM north of the PF at 50.4ºS. This high concentration near South Georgia can be explained by HNLC regions where nutrients are underutilized. Potential macronutrient impact will be discussed below (Section 5.1.1 and section 5.2.1), especially concerning the simultaneous impact on $\delta^{13}C$ fractionation.

Table 4.1. A correlation test was done using SPSS showing results for $\delta^{13}C_{POC,}$ POC and macronutrients. The Pearson correlation firstly indicates if the relationship between the parameters is positive or negative and also indicates the significance at level 0.05 and 0.01 respectively. N represents the number of samples analysed.

		$d13C_{POC}$ (‰)	POC (µg/L)	NO_2 (µM)	NO_3 (µM)	$Si(OH)_4$ (µM)	PO_4 (µM)
$d13C_{POC}$ (‰)	Pearson Correlation	1	.106	-.176	-.391*	-.550**	-.339
	Sig. (2-tailed)		.478	.379	.044	.003	.084
	N	47	47	27	27	27	27

*. Correlation is significant at the 0.05 level (2-tailed).

4.1.3. POC, Chlorophyll-a and phytoplankton groups

**. Correlation is significant at the 0.01 level (2-tailed).

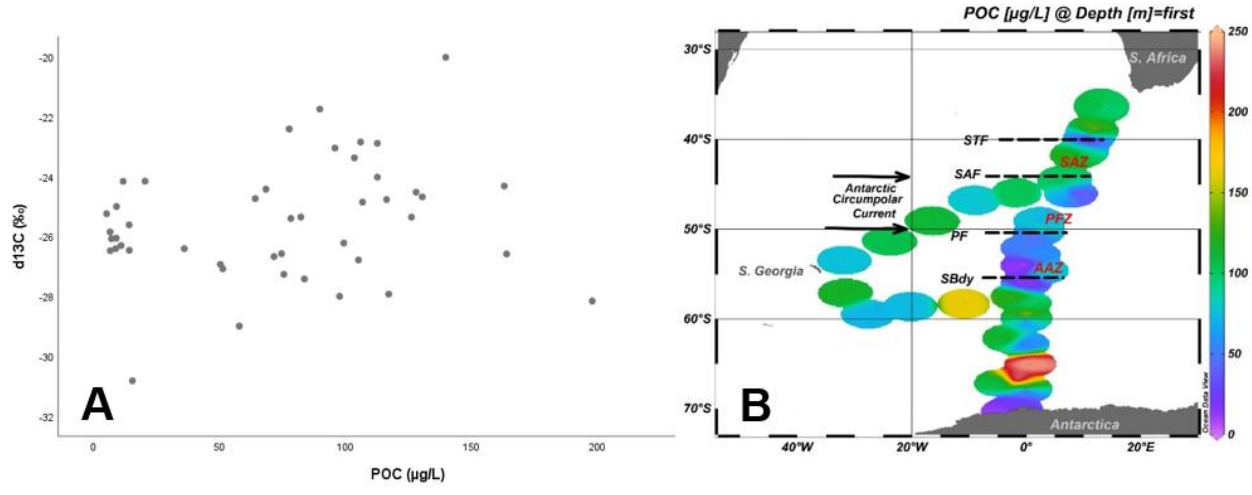

Figure 4.3. POC show a negative relationship with $\delta^{13}C_{POC}$ (A); POC in the surface water along the Good Hope line and the South Georgia transect for SANAE 54 (B).

POC: Particulate organic carbon concentrations slightly decrease (Figure 4.3-B) when crossing the STF from the warmer tropical waters to the PFZ and when crossing the PF, it shows a low concentration of approximately 50 µg/L in the AAZ. South of the Southern Boundary, the concentration starts to increase again, where it reaches a high of about 250 µg/L at 65ºS, decreasing to >50 µg/L at 70ºS. This increase near the Antarctic shelf indicates high productivity and growth and correlates with increasing phytoplankton blooms. This may also be a result of high CO_2 concentration in the surface water or due to the release of macronutrients through upwelling or as the sea ice melts. Upwelling usually results in higher productivity as nutrients are released back into surface water and then can be utilized through phytoplankton again, thus it was expected that the fractionations should decrease and the $\delta^{13}C_{POC}$ increase. This is however not the case (Figure 4.3-A) for results obtained from SANAE 54. There is little to no correlation between POC and $\delta^{13}C_{POC}$ with r = 0.106 and no significant correlation at p = 0.478 (Table 4.1).

Chlorophyll a: Chl-a concentrations in the SO tend to increase with a higher nutrient supply as seen in section 4.1.2. Chlorophyll-a concentrations increase from 0.1 µg/L at the STF to approximately 0.5 µg/L in Antarctic waters. In the PFZ there is a slightly higher concentration of 0.2 µg/L (Figure 4.4-B) and correlates with a higher concentration of PO_4 (Figure 4.2-D) and NO_3 (Figure 4.2-H) in the PFZ of 1 µM and 20 µM respectively. Crossing the SBdy, the concentration of chlorophyll-a continues to increase to the south as well as to the west towards South Georgia, but a clear decrease can be observed at approximately 25ºW and increasing again when the

SBdy is crossed back to the north. $\delta^{13}C_{POC}$ becomes more negative along the transect from Cape Town to Antarctica, thus phytoplankton subsumed more ^{12}C, leaving the surface ocean enriched in ^{13}C. This is an indication of phytoplankton blooms further South as the chlorophyll-a concentration increases and the $\delta^{13}C_{POC}$ decreases. Chlorophyll-a shows to be negatively correlated to $\delta^{13}C_{POC}$ at r = - 0.409 and significant at p = 0.025 (Table 4.2). Correlations between $\delta^{13}C_{POC}$ and Chlorophyll-a and all the phytoplankton groups, except diatoms, were calculated using spearman's rho, due to non-parametric datasets.

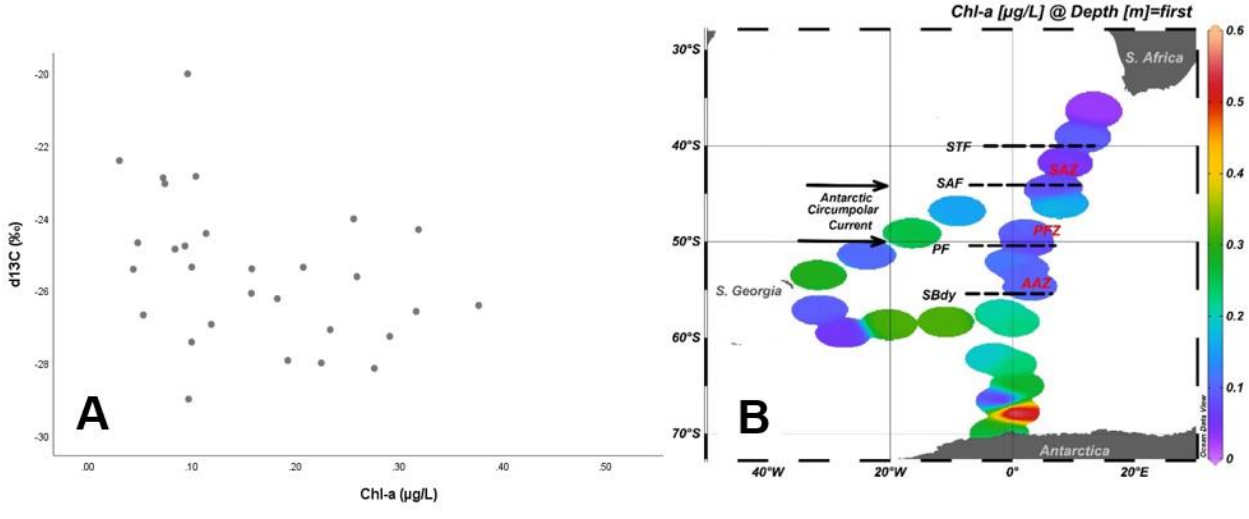

Figure 4.4. Scatter plot (phytoplankton groups's contribution to total chl-a in µg/L represented on the x-axis) of chlorophyll-a concentrations versus $\delta^{13}C_{POC}$ for SANAE 54, showing a negative relationship between these parameters and the total chl-a concentrations in the surface water (A) chlorophyll-a concentrations along the transect (B).

Phytoplankton community composition: The contribution of phytoplankton groups to total chl-a was estimated as chemotaxonomic composition for 9 different phytoplankton groups (Viljoen *et al.*, 2019). The three groups that showed the best correlation to $\delta^{13}C_{POC}$ during this cruise, were cyanobacteria, coccolithophores (Table 4.2) and diatoms (Table 4.3), although the three dominant groups contributing to total chl-a concentration in the surface water, are *P. antarctica* (10%), coccolithophores (11%) and diatoms (72%) (Figure 4.6). *P. antarctica* and diatoms are two ubiquitous groups and play a very important role in the ocean carbon cycle (Schoemann *et al.*, 2005; Cermeno, Dutkiewicz, Harris, *et al.*, 2008; Viljoen *et al.*, 2019). Diatoms are the group that is the most abundant in the surface water of the transect with 72% contribution to total chl-a and there is also an increase in the diatom-derived chl-a from north to south from 0 µg/L at 36ºS to 0.3 µg/L at 67ºS (Figure 4.5-F). An increase in *P. antarctica* to total chl-a (Figure 4.5-B) and coccolithophores to total chl-a (Figure 4.5-D) can also be seen at ca. 67ºS, with 0.05 µg/L and 0.2 µg/L respectively.

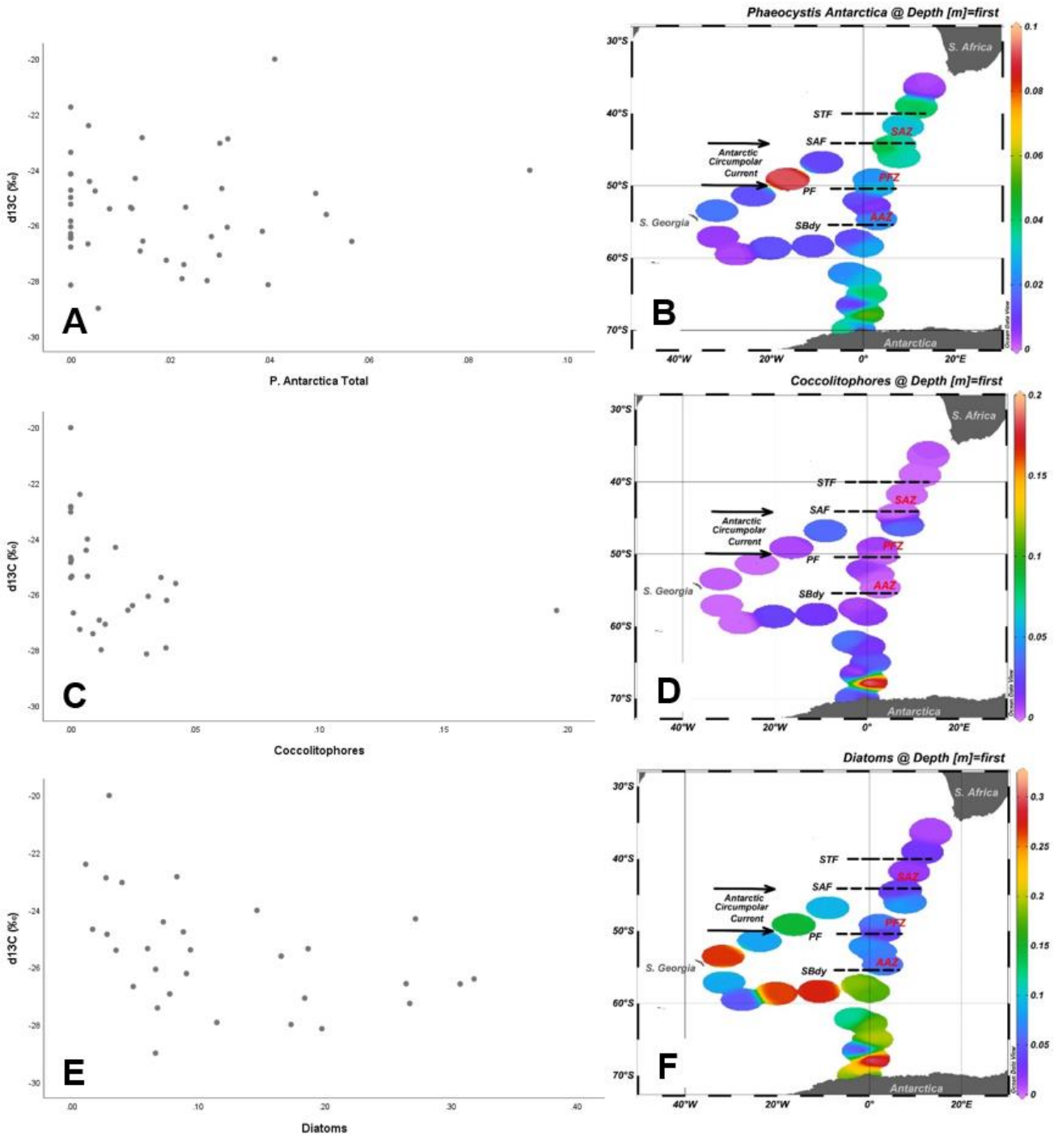

Figure 4.5. Scatterplots (phytoplankton groups's contribution to total chl-a in µg/L represented on the x-axis) of selected parameters versus $\delta^{13}C_{POC}$ (A, C, E) and distribution in surface waters (B, D, F). The three dominant phytoplankton groups in the surface ocean during the SANAE 54 cruise: P. antarctica (B), coccolithophores (D) & diatoms (F) and their contribution to total chl-a concentration (µg/L), with coccolithophores and diatoms showing significant relationships towards $\delta^{13}C_{POC}$ (C&E respectively) as P. antarctica shows

On the South Georgia leg, there is a depletion in almost all phytoplankton groups' contribution to total chl-a, except for a diatom bloom at about 5 - 20ºW and 30ºW (Figure 4.5-F) and a slight increase in *P. antarctica* from 0 µg/L to 0.1 µg/L in the PFZ and a bloom of dinoflagellates in the SBdy at about 20ºW and in the PFZ. Coccolithophores show small contributions to total chl-a along the Good Hope line and the South Georgia leg. In the PFZ there is a slight bloom of coccolithophores, with another increase from 0 µg/L to about 0.2 µg/L contribution to total chl-a south of the PF. Coccolithophores do not show a prominent increase from lower to higher latitudes as to those of *P. antarctica* and diatoms. Both diatoms and *P. antarctica* depend on available nutrients in the SO, in contrast, coccolithophores require $CaCO_3$ for their coccolith shells (Monteiro, Bach, Brownlee, *et al.*, 2016). Chlorophytes are almost completely depleted in the surface water along the transect, except for a small contribution in the tropical waters north of the STF (Figure A.2-B; Appendix A). Cryptophytes have a small peak in the AAZ of about 0.0175 µg/L cryptophyte-chl-a (Figure A.2-C; Appendix A). On the Good Hope line, dinoflagellates show a small increase in the AAZ, south of the PF with a contribution to the total chl-a of 0.01 µg/L (Figure A.2-F; Appendix A) and on the South Georgia leg south of the SBdy at ca. 30ºW, a contribution of 0.015 µg/L to total chl-a can be observed. Pelagophytes seems to be depleted throughout the transect with a small bloom in the PFZ (Figure A.2-D; Appendix A). Prasinophytes are completely depleted on the South Georgia leg with small contributions to total chl-a to be seen just north of the STF, in the PFZ and south of the SBdy at about 62ºS (Figure A.2-E; Appendix A). The three groups that show to be significantly correlated to $\delta^{13}C_{POC}$ are cyanobacteria, coccolithophores (Table 4.2) and diatoms (Table 4.3). Cyanobacteria are positively correlated to $\delta^{13}C_{POC}$ at $r = 0.382$ and are significant at $p = 0.037$. Coccolithophores and diatoms are both negatively correlated to $\delta^{13}C_{POC}$ at $r = -0.520$ for the former and $r = -0.401$ for the latter and are significant ($p = 0.003$ and $p = 0.028$, respectively).

Table 4.2. Correlation test using Spearman's rho to indicate the confidence levels for chlorophyll-a and all phytoplankton groups' contribution to total chl-a (µg/L), except for diatoms. All the data is tested using a two-tailed correlation. N represents the number of data points used.

			d13C$_{POC}$ (‰)	Chl-a (µg/L)	Cyanobacteria	Prasino phytes	Dinoflagellates	Crypto phytes	*P. antarctica* Total	Coccolithophores	Pelagophytes	Chloro phytes
Spearman's rho	d13C$_{POC}$ (‰)	Correlation Coefficient	1.000	-.409*	.382*	.108	-.194	.135	-.031	-.520**	.178	.085
		Sig. (2-tailed)	.	.025	.037	.569	.305	.477	.841	.003	.346	.654
		N	47	30	30	30	30	30	45	30	30	30

*. Correlation is significant at the 0.05 level (2-tailed).

**. Correlation is significant at the 0.01 level (2-tailed).

Table 4.3. Results of a Pearson Correlation test was used to determine whether the contribution of diatoms to total chl-a (µg/L) are significantly correlated to $\delta^{13}C_{POC}$.

		d13C$_{POC}$ (‰)	Diatoms
d13C$_{POC}$ (‰)	Pearson Correlation	1	-.401*
	Sig. (2-tailed)		.028
	N	47	30

*. Correlation is significant at the 0.05 level (2-tailed).

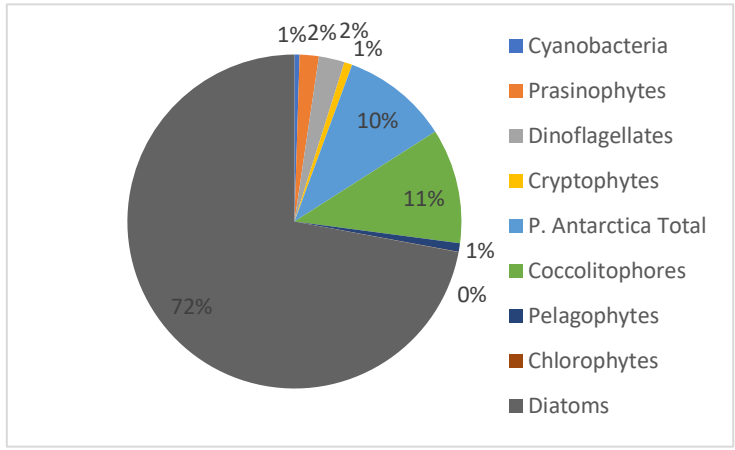

Figure 4.6. Visual representation of the contribution to total chl-a (%) of the phytoplankton groups within the surface water of the SO along the Good Hope Line and South Georgia leg in the summer of 2014/2015.

4.1.4. Temperature and Salinity

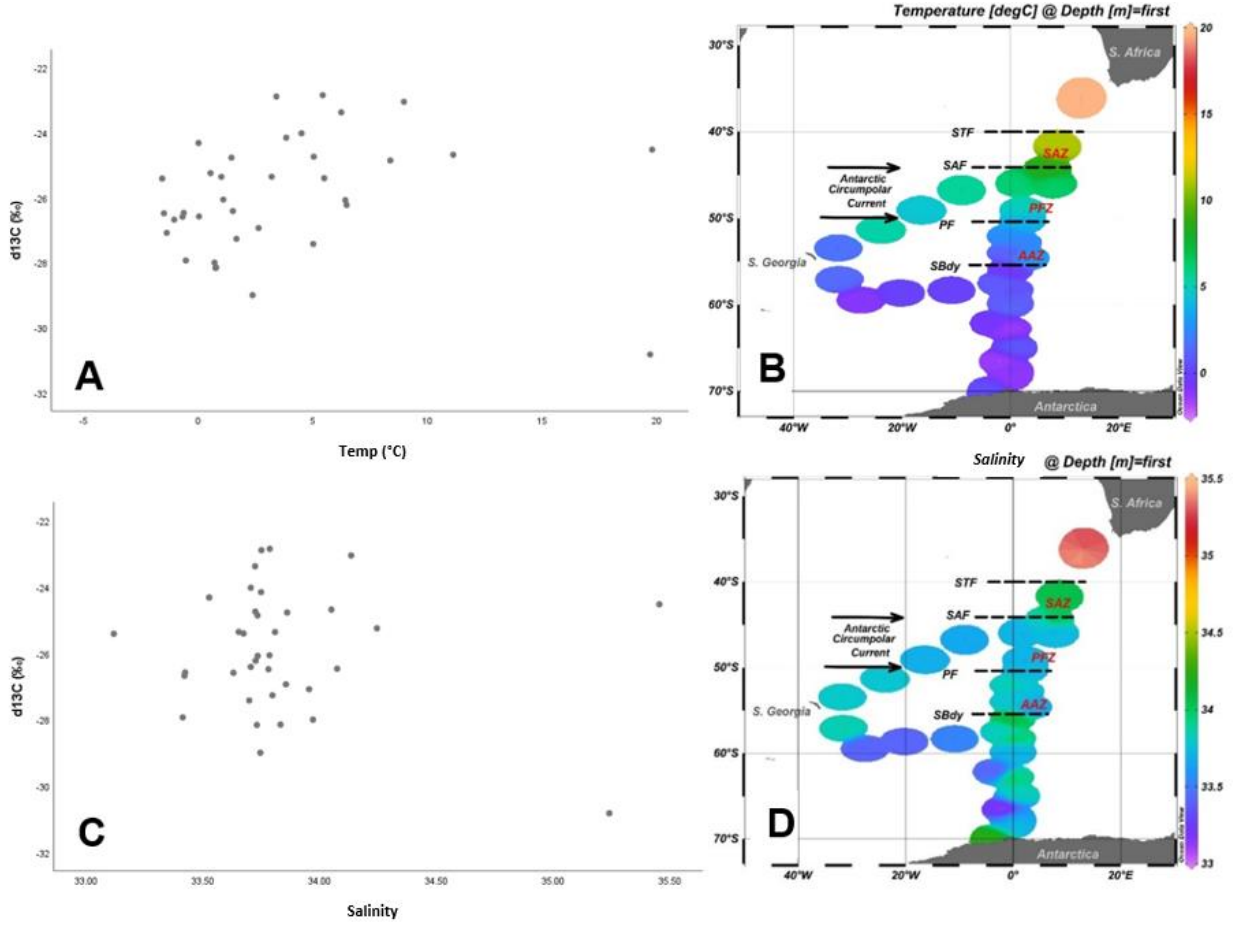

Figure 4.7. Scatterplots of temperature (A) and salinity (C) against $\delta^{13}C_{POC}$ during SANAE 54 made using SPSS and ODV graphs showing results of temperature (B) and salinity (D) in the surface water.

Temperature: In the SO surface temperature decreases when approaching Antarctica (Figure 4.7-B). The highest temperature of 20ºC is observed in the subtropical waters and decreases to 0ºC when approaching the Antarctic. Crossing the SBdy there is a decrease to the South, as well when moving eastwards towards South Georgia. There is only an increase when crossing the PF northwards at approximately 20ºW. With decreasing temperature from Cape Town to Antarctica, the $\delta^{13}C_{POC}$ value becomes more negative (Figure 4.7-A) and the correlation is significant at p = 0.017 (Table 4.4). Previous studies (Wong and Sackett 1978; Fritz and Buchardt 1980) have reported that temperature has a direct effect on fractionation as fractionation is temperature dependant for different phytoplankton species. The high solubility of CO_2 may also affect the temperature-dependent fractionation by phytoplankton; however, temperature alone is not the controlling factor of the fractionation (Fielding *et al.*, 1998).

Salinity: Salinity is thought to have little to no effect on carbon isotopic fractionation by phytoplankton during photosynthesis (Wong & Sackett, 1978). For SANAE 54, the salinity results

across the transect can be seen in figure 4.7-D, where it shows that the salinity of the surface water range between 33.4 and 34.5, with only 3 points falling outside of that range (35.99ºS, 36.35ºS and 66.61ºS). Excluding these points from the dataset, salinity still shows no significant correlation to $\delta^{13}C_{POC}$.

Table 4.4. Spearman's rho correlation test was done for temperature and salinity during the voyage. All the data is tested using a two-tailed correlation. N represents the number of data points used.

			d13C$_{POC}$ (‰)	Temp (ºC)	Salinity
Spearman's rho	d13C$_{POC}$ (‰)	Correlation Coefficient	1.000	.397*	.037
		Sig. (2-tailed)	.	.017	.831
		N	47	36	36

*. Correlation is significant at the 0.05 level (2-tailed).

4.1.5. pCO_2

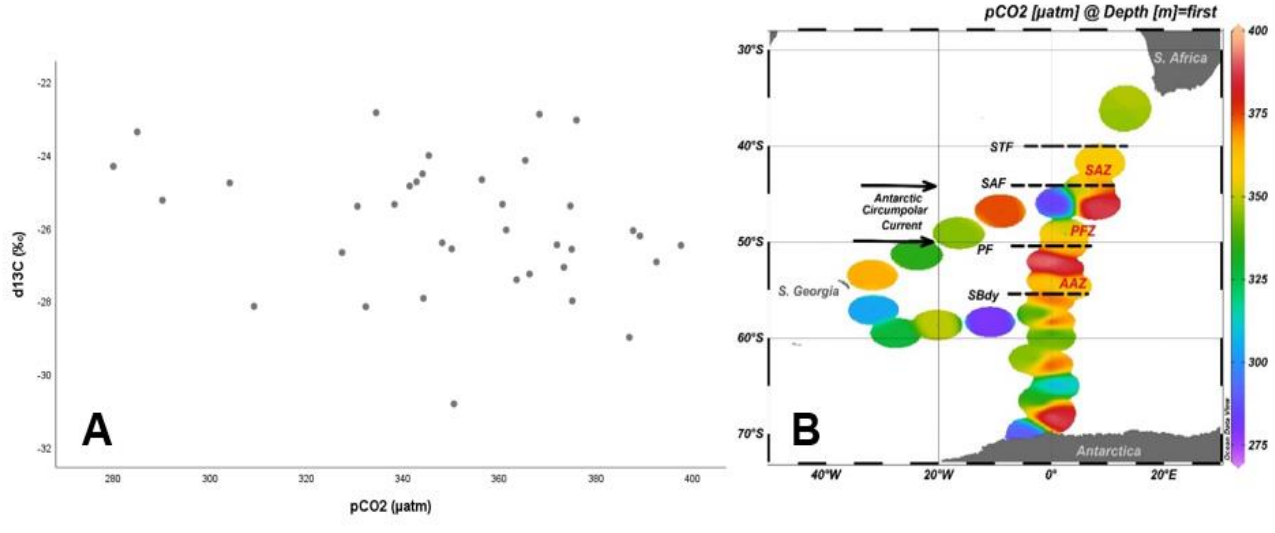

Figure 4.8. A scatter plot of pCO_2 concentrations in the surface water plotted against $\delta^{13}C_{POC}$ (A) to indicate a negative relationship between these parameters and pCO2 concentrations in the surface water along the Good Hope line from South Africa to Antarctica (B), during the SANAE 54 voyage.

Along the transect the pCO_2 concentrations increase when the STF is crossed towards the south and again when the SAF is crossed, although a decrease to ca. 275 µatm can be observed in the PFZ at 0º. Crossing the PF, there is another increase to 392 µatm in the AAZ, whereafter it seems to be more stable between 300 and 350 µatm with another increase at 67ºS right at the Antarctic shelf to 398 µatm. On the South Georgia leg, the concentration varies between 275 and 375 µatm, with no major decrease or increase, except in the PFZ at about 10ºE, there is an increase to 389 µatm northwards. It was expected that pCO_2 would have a significant relationship with $\delta^{13}C_{POC}$,

however, this is not the case (Figure 4.8-A and Table 4.5). There is a weak negative relationship between pCO_2 and $\delta^{13}C_{POC}$ at r = -0.256 but no significance at p = 0.132 (Table 4.5).

Table 4.5. Pearson correlation test for pCO_2 against $\delta^{13}C_{POC}$. All the data is tested using a two-tailed correlation. N represents the number of data points used.

		$d13C_{POC}$ (‰)	pCO_2 (µatm)
$d13C_{POC}$ (‰)	Pearson Correlation	1	-.256
	Sig. (2-tailed)		.132
	N	47	36

4.2. Winter Cruise 2015

4.2.1. $\delta^{13}C_{POC}$

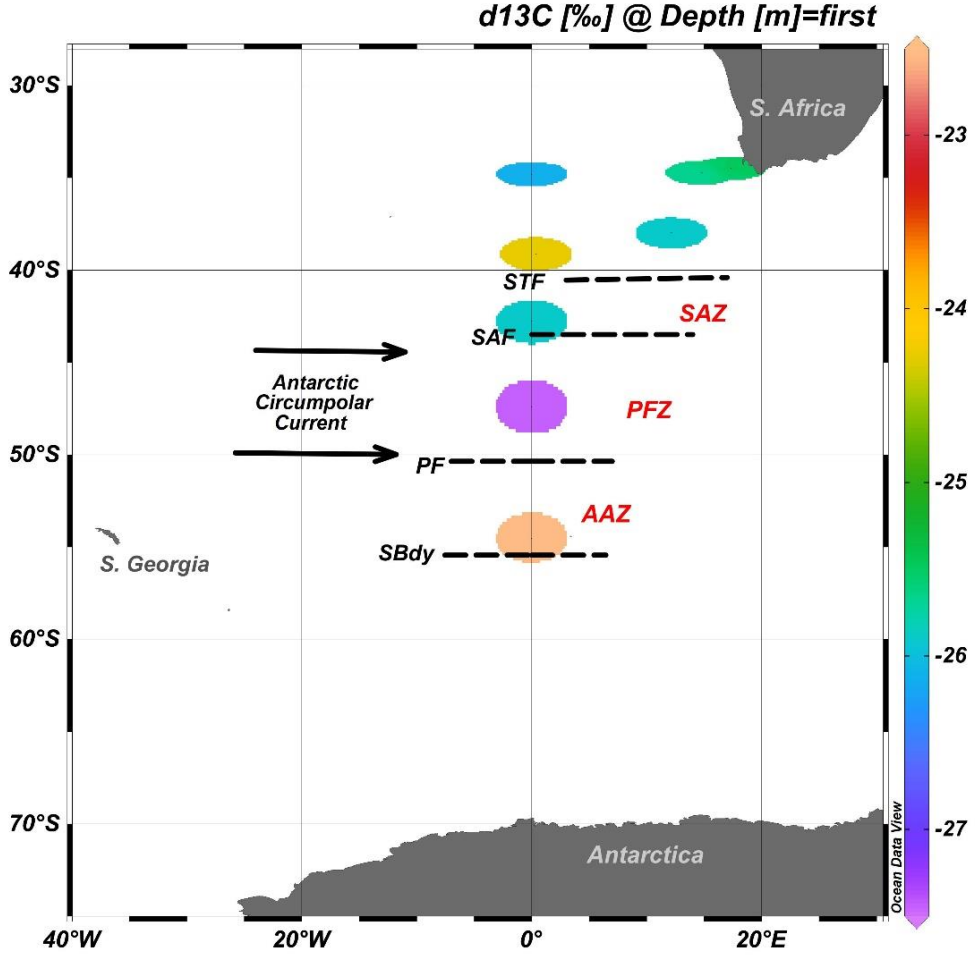

Figure 4.9. Carbon isotopic signature in the surface water of the SO during the winter months of July and August 2015. Horizontal dashed lines are indicative of the major fronts crossed during the voyage.

The average $\delta^{13}C_{POC}$ value observed in the water masses of the SO during this cruise was -25.40‰. Due to ice formation during this period of the year, the ship was only capable to reach approximately 55ºS (Section 3.2), thus there are no data points after 54.5ºS (Figure 4.9). Following the Good Hope line, north of the STF in the Subtropical waters, the $\delta^{13}C_{POC}$ is ca. -26‰ and decreases in the PFZ to -27‰. When the PF is crossed into colder waters, the $\delta^{13}C_{POC}$ increases to -22.5‰. These results contradict the suggestion of Rau *et al*. (1997) that $\delta^{13}C$ of phytoplankton is more negative in colder waters, due to the lower diffusional limitation of CO_2 in colder water. The descriptive statistics table for skewness and kurtosis values can be seen in appendix B, table B.1.

4.2.2. Macronutrients

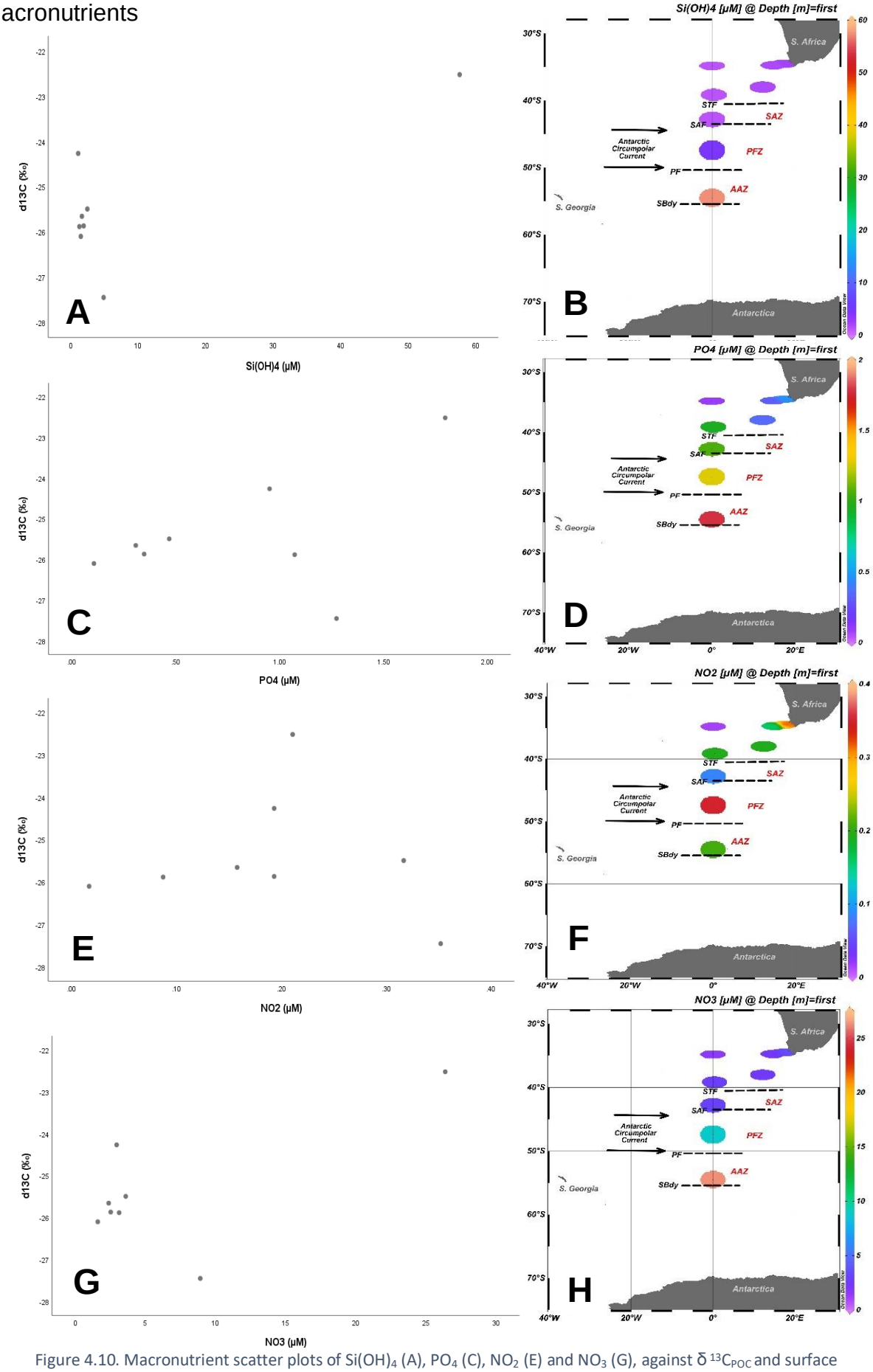

Figure 4.10. Macronutrient scatter plots of $Si(OH)_4$ (A), PO_4 (C), NO_2 (E) and NO_3 (G), against $\delta^{13}C_{POC}$ and surface water distribution along the transect (B, D, F & H) for the WC 2015.

As a HNLC region, the SO typically contains high concentrations of dissolved phosphate, silicate and nitrate (Clarke & Leakey, 1996; Lourey *et al.*, 2004), which correlates with high productivity of phytoplankton blooms and low chlorophyll concentrations. However, the extent of the relationships between these parameters may differ from season to season. The available macronutrient data during WC 2015 in the surface water, is much less when comparing the results to SANAE 54 (Figure 4.10 (B, D, F&H). NO_3 concentrations increase from lower latitude waters near Cape Town to the higher latitudes of the PFZ and when crossing the PF, a maximum concentration of 26.4 µM is observed. Moving back to the north, the NO_3 concentration starts to decrease, ending with a concentration of 1.6 µM in the subtropical waters (Figure 4.10-H). The correlation between NO_3 and $\delta^{13}C_{POC,}$ indicates that with increasing NO_3 concentration, the $\delta^{13}C_{POC}$ decreases to -27.5‰ (Figure 4.10-G) at 47.4ºS, indicating increased fractionation. However, there is no significant correlation between these two factors at p = 0.439 (Table 4.6). $Si(OH)_4$ concentrations in the surface water shows a similar correlation to those of NO_3 as the concentration peaks at 54.5ºS to 57.6 µM just before the SBdy (Figure 4.10-B). There is no relationship between $Si(OH)_4$ and $\delta^{13}C_{POC}$ with r = 0.095 and p = 0.823 (Table 4.6). PO_4 and NO_2 concentrations are very low in the surface waters with a maximum of 1.79 µM at the edge of the SBdy and 0.35 µM in the PFZ, respectively (Figure 4.10-D&F). Neither PO_4 nor NO_2 is significantly correlated with $\delta^{13}C_{POC}$ at r = 0.473 and p = 0.236 for PO_4 and r = -0.092 and p = 0.828 for NO_2 (Table 4.6).

Table 4.6. Correlation tests between surface macronutrients and $\delta^{13}C_{POC}$ throughout the transect. Spearman's rho was done for $Si(OH)_4$ and NO_3 (left) and a Pearson correlation was done for NO_2 and PO_4 (right). All the data is tested using a two-tailed correlation. N represents the number of data points used.

			d13C$_{POC}$ (‰)	Si(OH)$_4$ (µM)	NO$_3$ (µM)
Spear-	d13C$_{POC}$	Correlation Coefficient	1.000	.095	.286
man's	(‰)	Sig. (2-tailed)	.	.823	.493
rho		N	8	8	8

		d13C$_{POC}$ (‰)	NO$_2$ (µM)	PO$_4$ (µM)
d13C$_{POC}$	Pearson	1	-.092	.473
(‰)	Correlation			
	Sig. (2-tailed)		.828	.236
	N	8	8	8

4.2.3. POC, Chlorophyll-a and phytoplankton groups

POC: is often related to productivity in the euphotic layer of the SO. In the warmer subtropical water during WC 2015, the POC increases from ca. 60 µg/L to above 100 µg/L just north of the STF. Moving in a northerly direction back towards Cape Town, the overall trend is that the POC decrease, except where an increase is observed when crossing the PF (Figure 4.11-B). POC is not significantly correlated to $\delta^{13}C_{POC}$, with r = -0.024 and p = 0.995 (Table B.2; Appendix B) (Figure 4.11-A).

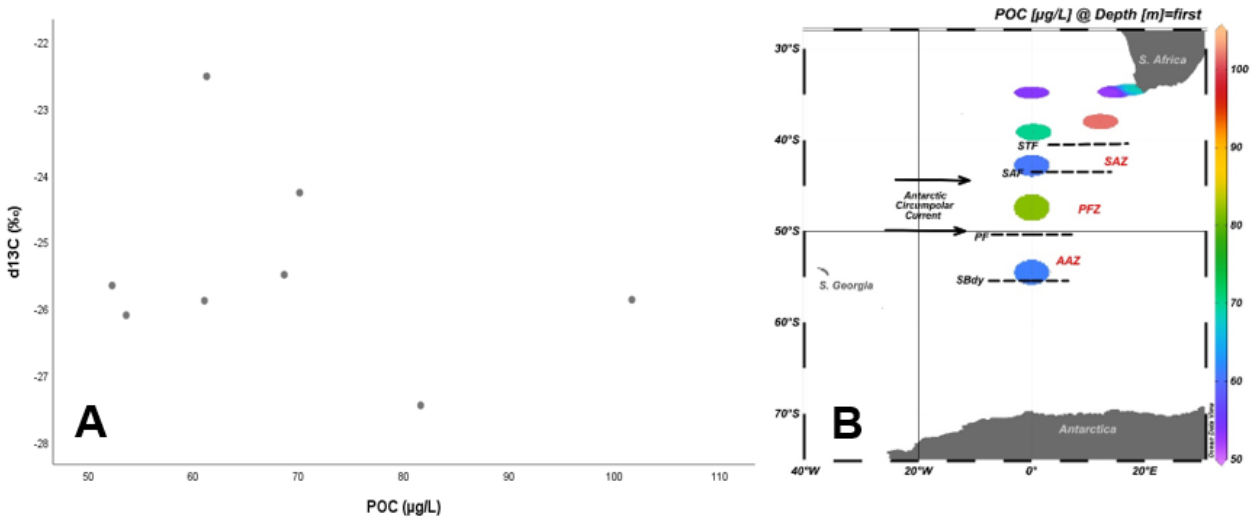

Figure 4.11. $\delta^{13}C_{POC}$ vs POC scatterplot show a negative relationship along during WC 2015 (A) and the surface POC concentrations along the transect (B).

Chlorophyll-a: Chl-a is used to indicate biomass in the sea surface; thus, the highest phytoplankton blooms can be detected using chl-a as an indicator. Chl-a concentrations are approximately 0.12 µg/L in the warmer tropical waters north of the STF during this cruise. The highest concentration is observed in the SAZ (Figure 4.12-B), whereafter it decreases towards the ice shelf, indicating that phytoplankton blooms may also decrease from north to south. A peak is observed at the SAF with a concentration of 0.15 µg/L. The highest $\delta^{13}C_{POC}$ value (-22.52‰) correlates with the lowest chl-a concentration of 0.077 µg/L at the border of the SBdy (Figure 4.12-A), hence it can be argued that fractionation decreases in the AAZ. Accordingly, fractionation should then increase in the PFZ where the chl-a concentration increases to 0.087 µg/L and in the subtropical waters where the chl-a concentration is 0.12 µg/L. There is no significant correlation between chl-a concentrations and $\delta^{13}C_{POC}$ at r = -0.024 and p = 0.995 (Table B.3; Appendix B) as there is quite a large scatter of these data (Figure 4.11-A).

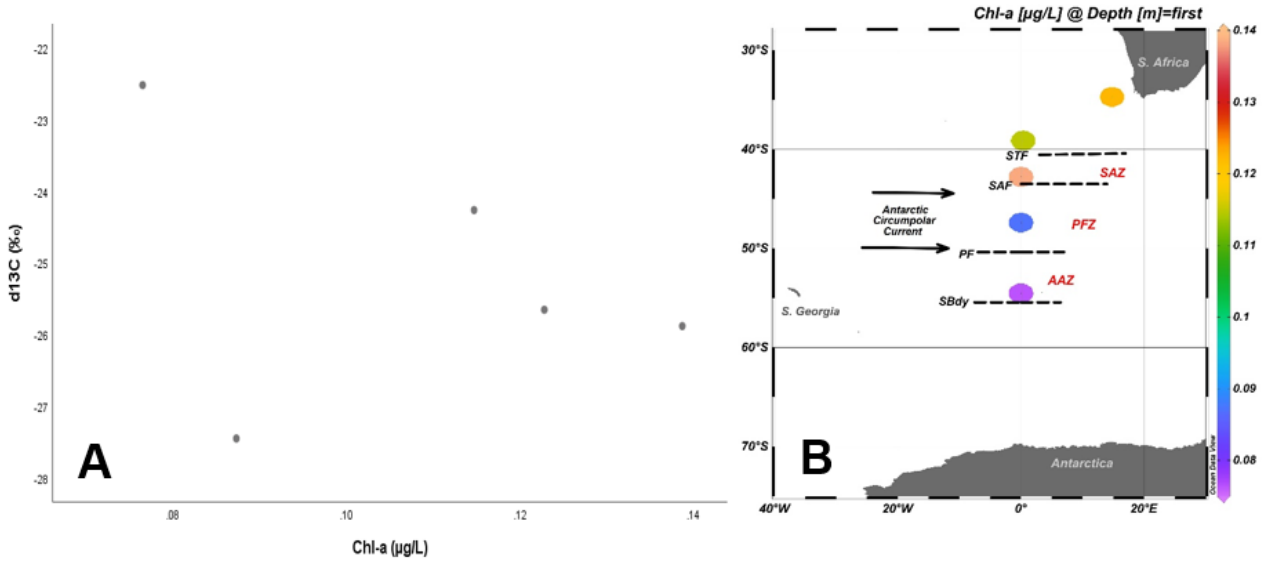

Figure 4.12. Chlorophyll-a concentration plotted against $\delta^{13}C_{POC}$ (A) and surface chlorophyll-a in the SO during WC 2015 (B) crossing major waterfronts.

Phytoplankton community composition: During winter 2015, the surface water phytoplankton blooms differ from that of the summer, with prasinophytes contributing 50% to the total phytoplankton bloom (Figure 4.13) and *P. antarctica* making up 37% of the contribution to total chl-a.

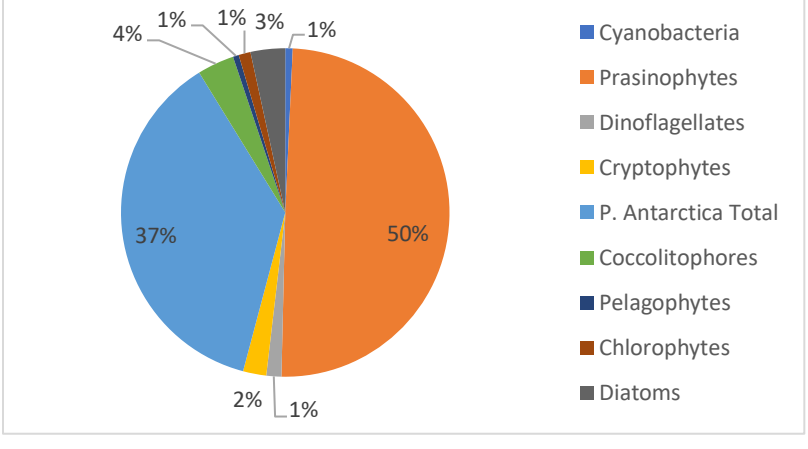

Figure 4.13. Visual representation of the phytoplankton groups (%) contributing to total chl-a within the surface water of the SO along the Good Hope Line during WC 2015.

The highest contribution to chl-a through prasinophytes can be seen in the SAZ just south of the SAF at 42.8ºS and the second largest is close to South Africa in the warmer waters at 34.70ºS. The lowest contribution is at the furthest point south in the AAZ. A negative relationship can be seen between prasinophytes and $\delta^{13}C_{POC}$ as prasinophytes increases with increasing

fractionation (Figure 4.14-A). Although a trend is observed, there is no significant correlation between chl-a and prasinophyes at r = -0.700 and p = 0.505 (Table B.3; Appendix B).

When looking at *P. antarctica* and coccolithophores' contribution to total chl-a (Figure 4.14-D&F), there is no trend observed from north to south. Coccolithophores contribution to total chl-a, was the highest in lower latitudes and *P. antarctica* shows a slight increase south of the STF and the SAZ. There is also no significant correlation between these 2 groups and $\delta^{13}C_{POC}$ with r = -0.100 and p = 0.873 for coccolithophores (Table B.3; Appendix B) and r = 0.396 and p = 0.510 for *P. antarctica* (Table B.2; Appendix B). The remaining six phytoplankton groups examined show a very small contribution to the total chl-a and overall phytoplankton community and no correlation with $\delta^{13}C_{POC}$ (Appendix B), as the p-values are as follow: cyanobacteria (0.624), cryptophytes (0.747), dinoflagellates (0.873), pelagophytes (0.553), diatoms (0.873) and chlorophytes (0.718).

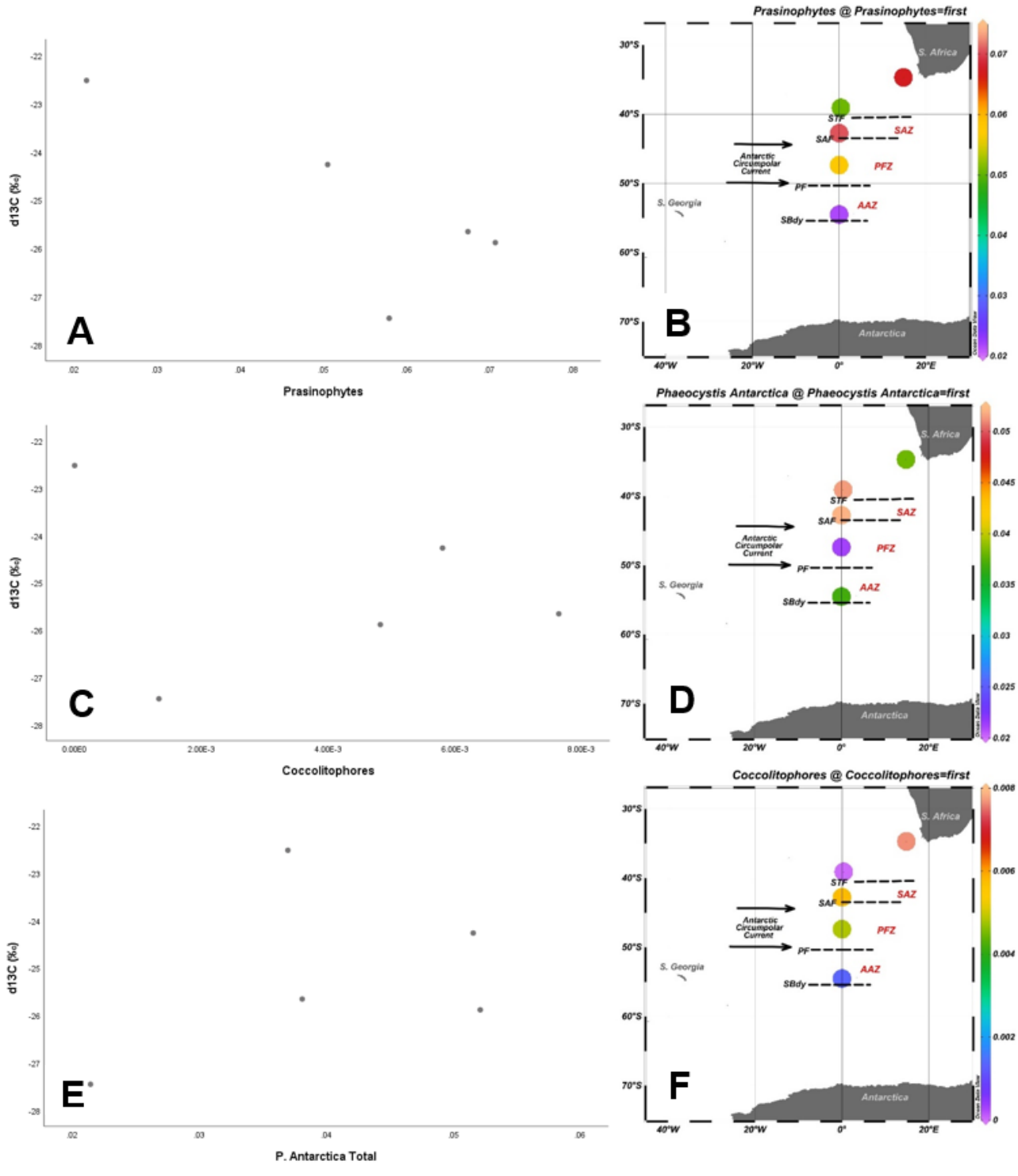

Figure 4.14. Dominant phytoplankton groups in the surface water of the SO during the WC 2015 along the Good Hope line. Relationships with $\delta^{13}C_{POC}$ can be seen in the scatterplots (phytoplankton groups's contribution to total chl-a in µg/L represented on the x-axis) for prasinophytes (A), coccolithophores (C) and P. antarctica (E). Their contribution to total chl-a in the surface water along the cruise track is recorded in B, D and F for each community respectively.

4.2.4. Temperature and salinity

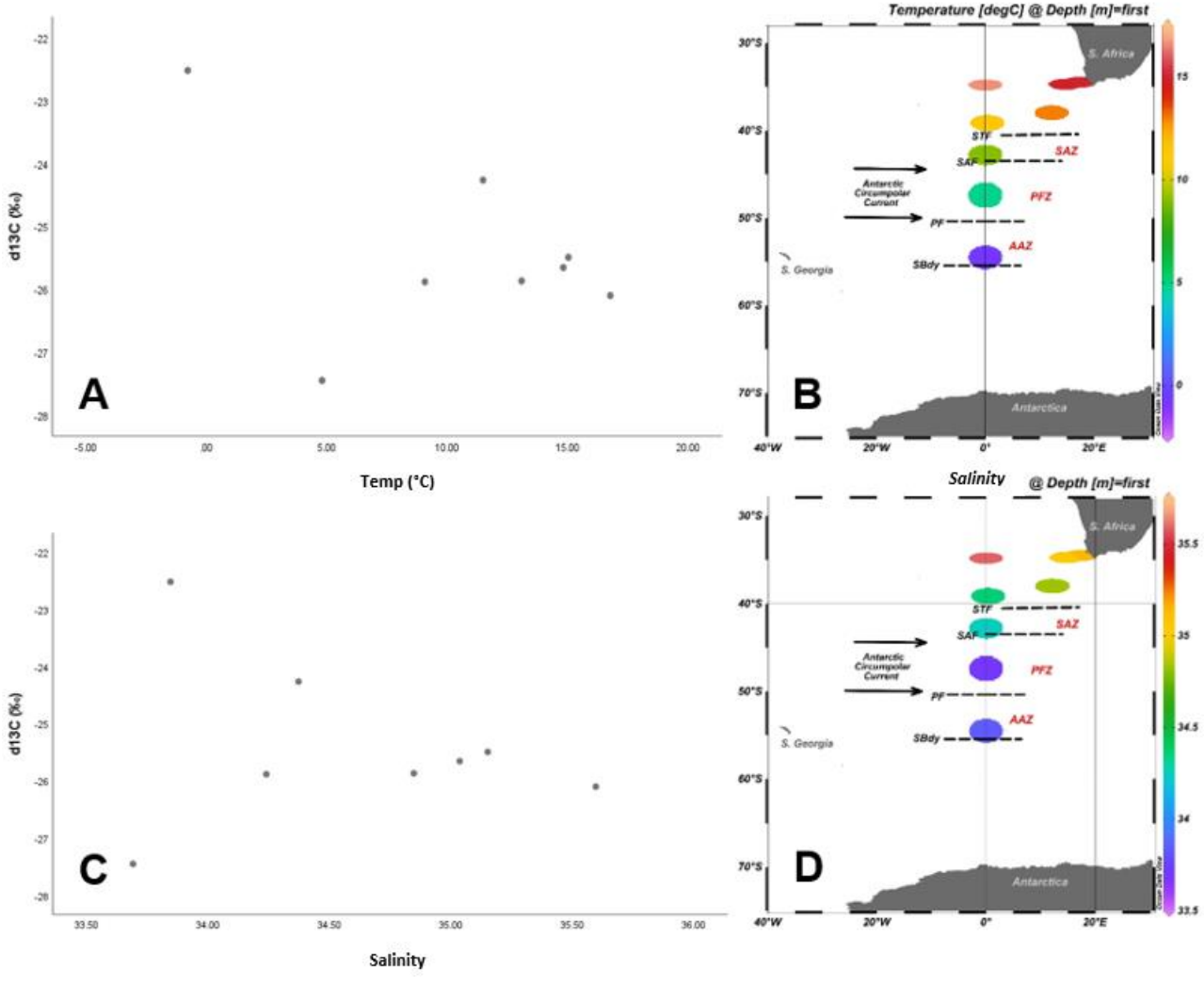

Figure 4.15. Scatterplots for temperature (A) and salinity (C) against $\delta^{13}C_{POC}$ during the WC 2015 voyage and surface temperature (B) and salinity (D) results obtained.

Sea surface temperature of the SO decrease from north to south as already mentioned and can also be seen in figure 4.15-B, where the temperature falls with 10ºC from Cape Town going into the PFZ, increasing again when moving back to the north. Salinity slightly decreases from 35.15 to 33.6 when moving towards the south and increase again when moving back north to Cape Town, reaching a maximum of 35.59 at 34.8ºS (Figure 4.15-D). Both temperature and salinity show no overall latitudinal trend. Salinity and temperature do not have a significant correlation to the carbon isotope fractionation, at r = 0.000, p = 1.000 and r = -0.167 and p = 0.693 (Table 4.7) respectively.

4.2.5. pCO_2

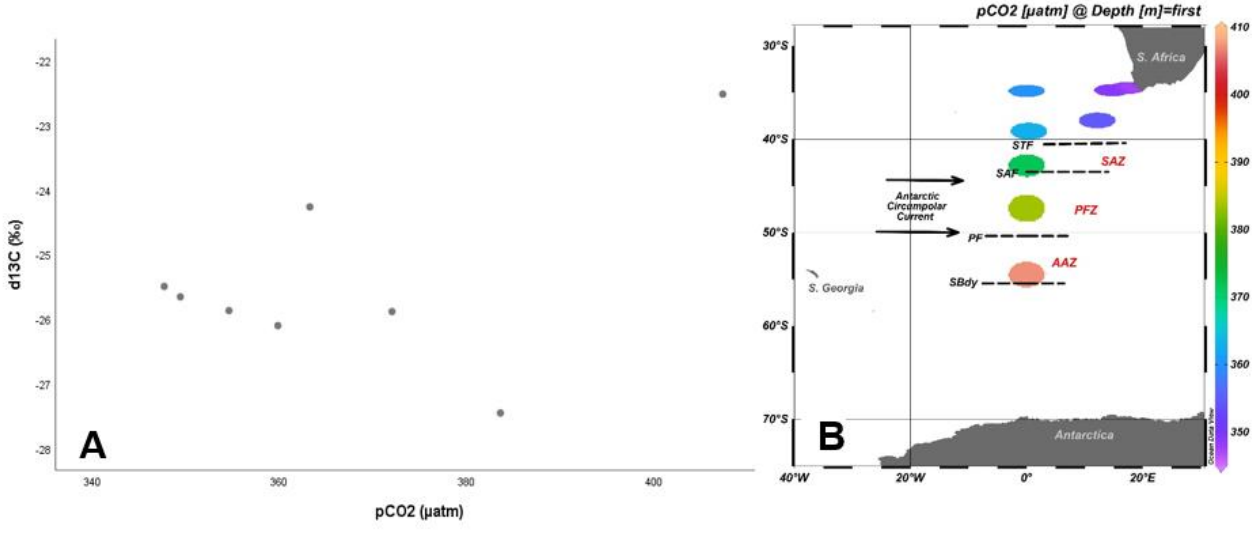

Figure 4.16. WC 2015 pCO_2 concentrations plotted against $\delta^{13}C_{POC}$ (A), and surface concentrations along the Good Hope line (B) for WC 2015.

The pCO_2 concentrations increase as $\delta^{13}C_{POC}$ becomes more negative (Figure 4.16-A); with increasing pCO_2 concentrations in the surface water of the SO, the $\delta^{13}C_{POC}$ decreases (Figure 4.16-B), thus the phytoplankton groups become more depleted in ^{13}C and the fractionation increases with increasing pCO_2 concentrations. This coincides with an increase in diatoms (Figure B.4-E; Appendix B), $Si(OH)_4$ (Figure 4.10-A), PO_4 (Figure 4.10-C) as well as NO_3 (Figure 4.10-G) at the same point. pCO_2 shows a negative relationship at r = -0.048 and p = 0.991, therefore this correlation is not significant. When the data point with the highest pCO_2 and highest $\delta^{13}C_{POC}$ (Figure 4.10-A) is omitted from this graph, there is still no significant correlation between these parameters. pCO_2 gradually increases along the transect from 350 µatm in subtropical waters near Cape Town to 410 µatm just before crossing the SBdy, the latter is the highest concentration observed during this cruise.

Table 4.7. Spearman's rho correlation test done between $\delta^{13}C_{POC}$ and temperature, salinity and pCO_2 where (**) indicates a significance level at 99% and (*) indicates a significance level at 95%. All the data is tested using a two-tailed correlation. N represents the number of data points used.

			$d13C_{POC}$ (‰)	pCO_2 (µatm)	Temp (ºC)	Salinity
Spearman's rho	$d13C_{POC}$ (‰)	Correlation Coefficient	1.000	-.048	-.167	.000
		Sig. (2-tailed)	.	.911	.693	1.000
		N	8	8	8	8

4.3. SANAE 56

4.3.1. $\delta^{13}C_{POC}$

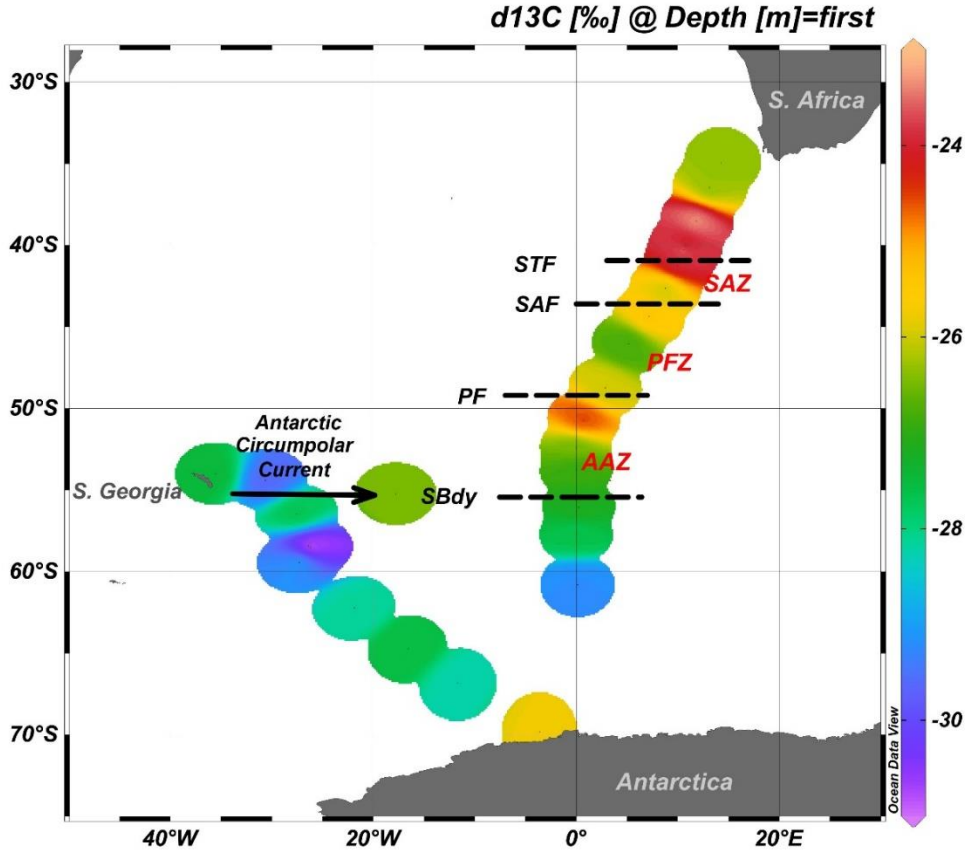

Figure 4.17. Carbon isotopic signature in the surface layer of the SO in the summer months of December 2016, January and February 2017 during the SANAE 56 voyage. Major fronts were crossed along the Good Hope line (horizontal dashed lines) and data were also collected on the South Georgia leg.

The $\delta^{13}C_{POC}$ decreases from north to south along the Good Hope line. $\delta^{13}C_{POC}$ increases at 46.ºS in the PFZ and at 50.7ºS at the PF. $\delta^{13}C_{POC}$ peaks north of the STF (Figure 4.17) in the subtropical waters and south of the STF in the SAZ. At the Antarctic shelf the $\delta^{13}C_{POC}$ increases to -25.8‰, (Figure 4.17). The lowest $\delta^{13}C_{POC}$, i.e. highest fractionation, can be observed on the South Georgia leg at 30.6ºW and 54.4ºS where the $\delta^{13}C_{POC}$ reaches a minimum of -29.6‰. The descriptive statistics table for skewness and kurtosis values for this cruise can be seen in table C.1, appendix C.

4.3.2. M.acronutrients

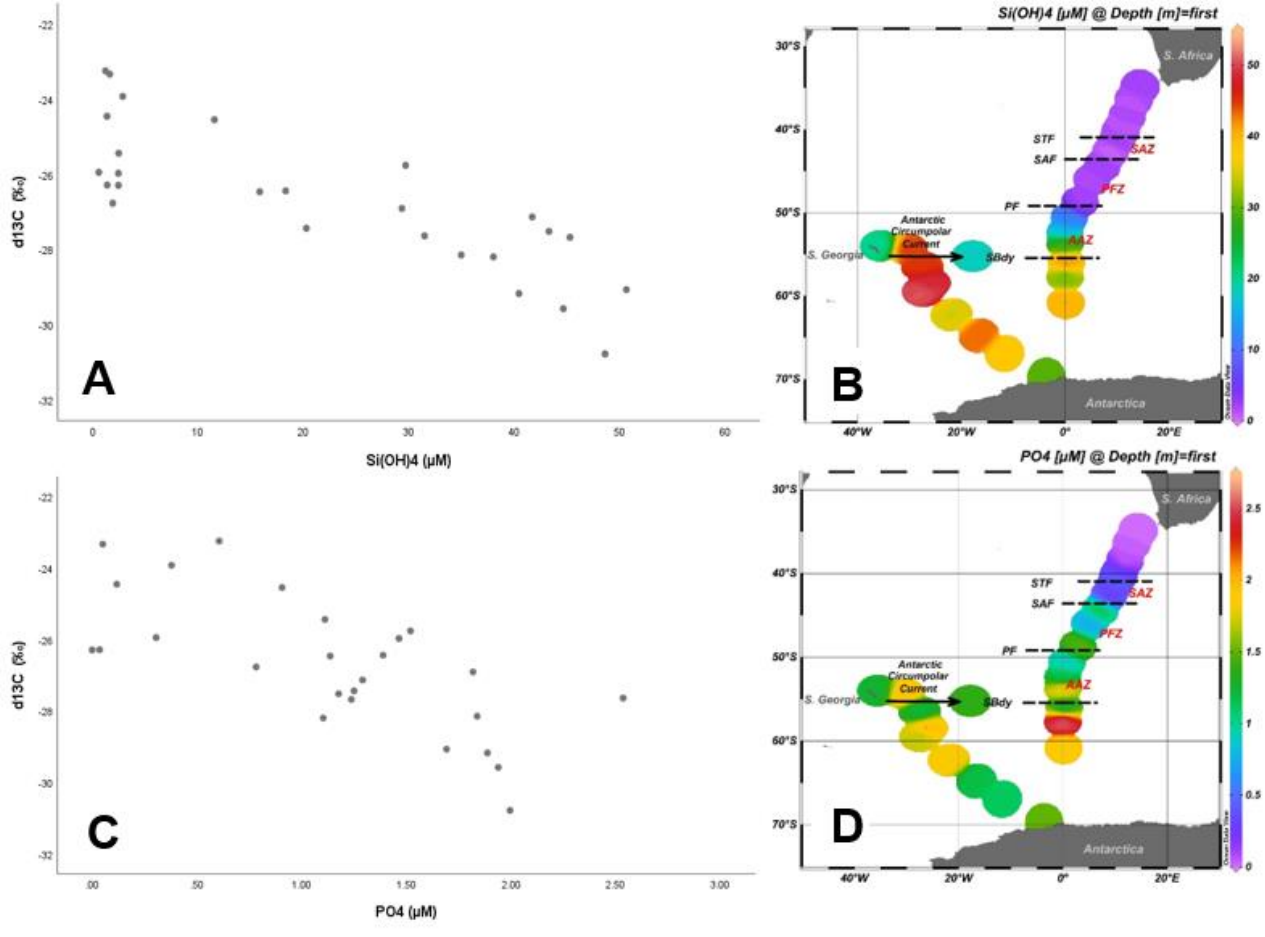

Figure 4.18. $Si(OH)_4$ (A) and PO_4 (C) scatterplots against $\delta^{13}C_{POC}$ to determine correlation during SANAE 56. $Si(OH)_4$ concentrations in the surface water (B) and PO_4 concentrations (D) along the Good Hope line.

All four macronutrients show a significant negative correlation to $\delta^{13}C_{POC}$ during SANAE 56 (Table 4.8). With increased nutrient concentration in the surface water along the cruise track, the $\delta^{13}C_{POC}$ becomes more negative, therefore increasing the fractionation.

Silicic acid: $Si(OH)_4$ is almost depleted north of the PF, however towards the south the concentrations increase (Figure 4.18-B). From Antarctica to South Georgia the concentration increases and a peak of 50.6 µM is observed at 27.3ºW and 59.4ºS. $Si(OH)_4$ has a negative relationship with $\delta^{13}C_{POC}$ at r = -0.839 and is significant at p = 0.000.

Phosphate: PO_4 shows a similar trend as to $Si(OH)_4$ along the Good Hope line where the concentration is almost depleted in the subtropical waters south of the STF. There is an increase in concentration when the SAF is crossed and again when the PF is crossed (Figure 4.18-D). PO_4 is the most abundant at 58.5ºS, with 1.99 µM, when the SBdy is crossed towards Antarctica. On

the South Georgia leg, the concentration seems to increase until South Georgia is reached. PO_4 has a significant negative relationship with $\delta^{13}C_{POC}$ at r = -0.703 and at p = 0.000.

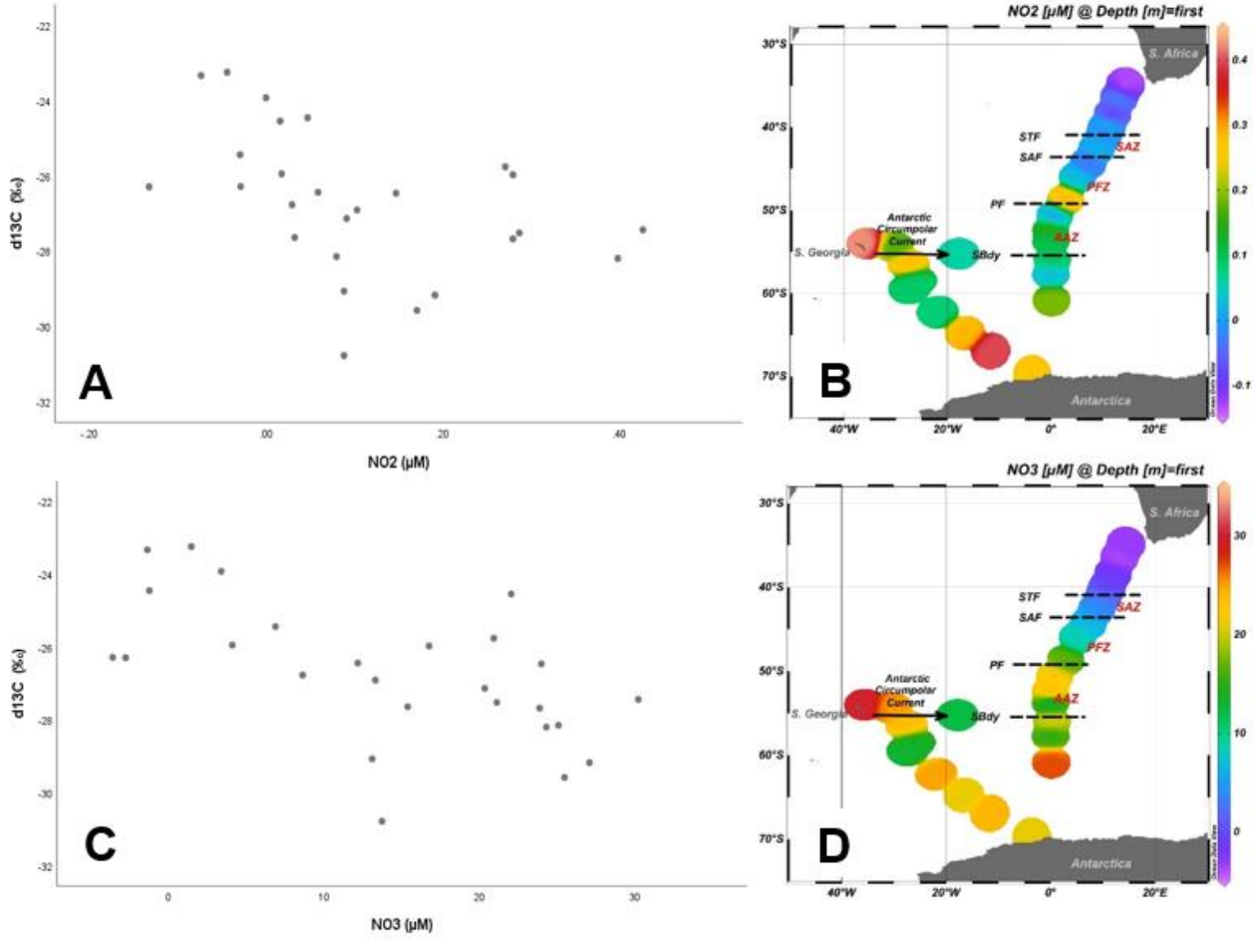

Figure 4.19. Scatterplots of nitrite (A) and nitrate (C) concentrations against $\delta^{13}C_{POC}$ during SANAE 54, made using SPSS correlation tests nitrite (B) and nitrate (D) concentrations in the surface ocean made using ODV.

Nitrite and nitrate: NO_2 concentrations are very low in the surface waters, although they increase from north to south on the Good Hope line and reaches the highest concentrations on the South Georgia leg at 11.7ºW and 66.83ºS and right at the South Georgia border at 35.5ºW and 54.01ºS, 0.39 µM and 0.42 µM respectively (Figure 4.19-B). NO_3 follows a similar trend to those of $Si(OH)_4$ and NO_2, as it is depleted in the warmer regions of the transect and increases when the PF is crossed towards Antarctica. Figure 4.19-D shows that the concentration stays stable on the South Georgia leg with a slight decrease south of the ACC and an increase to 30.2 µM close to South Georgia. Both NO_2 and NO_3 have negative relationships towards $\delta^{13}C_{POC}$ and is significantly correlated at r = -0.445 and p = 0.023 and r = -0.640 and p = 0.000, respectively.

Table 4.8. Correlation tests for macronutrients with $\delta^{13}C_{POC}$ during SANAE 56. Spearman's rho was calculated for $Si(OH)_4$ and NO_3 (left) and a Pearson correlation was done for NO_2 and PO_4 (right). All the data is tested using a two-tailed correlation. N represents the number of data points used.

			d13C$_{POC}$ (‰)	NO_3 (µM)	$Si(OH)_4$ (µM)
Spear-	d13C$_{POC}$	Correlation Coefficient	1.000	-.640**	-.839**
man's	(‰)	Sig. (2-tailed)	.	.000	.000
rho		N	26	26	26

		d13C$_{POC}$ (‰)	NO_2 (µM)	PO_4 (µM)
d13C$_{POC}$	Pearson Correlation	1	-.445*	-.703**
(‰)	Sig. (2-tailed)		.023	.000
	N	26	26	26

*. Correlation is significant at the 0.05 level (2-tailed).

**. Correlation is significant at the 0.01 level (2-tailed).

4.3.3. POC, Chlorophyll-a and phytoplankton groups

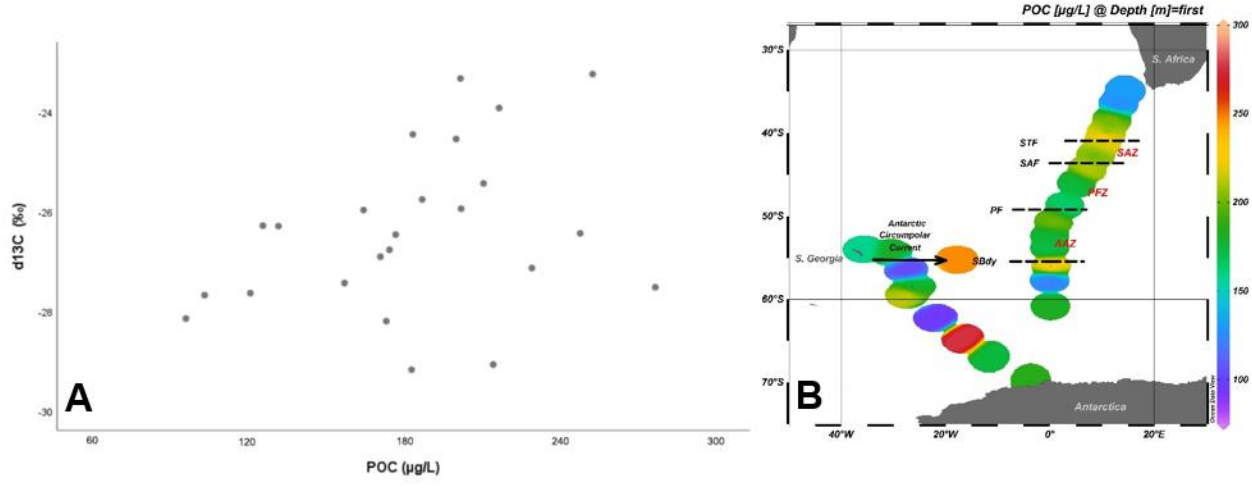

Figure 4.20. Scatterplot of POC versus $\delta^{13}C_{POC}$ (A) shows a positive relationship. POC in the surface water along the Good Hope line and the South Georgia transect for SANAE 56 (B).

POC: POC concentrations along the Good Hope line alternate between ca. 120 µg/L and 220 µg/L with the lowest concentrations at the highest latitudes and just south of the SBdy (Figure 4.20-B). From Antarctica moving towards South Georgia there is an increase from ca. 180 µg/L to ca. 270 µg/L, whereafter there is a decrease to 100 µg/L. This variation in POC might be due to the different phytoplankton blooms on this transect. POC seems to increase with increasing $\delta^{13}C_{POC}$ values (Figure 4.16-E), although there is no significant correlation to $\delta^{13}C_{POC}$ as r = 0.328 at p = 0.118 (Table C.2; Appendix C).

Chlorophyll a: Chl-a concentrations are low in the surface water during summer 2017, especially north of the SBdy (Figure 4.21-B). There is a peak just south of the SBdy at 56.05ºS from 0.18

µg/L to 1.02 µg/L. Moving towards South Georgia from Antarctica the chl-a concentration varies and reaches another peak at 26.15ºW and 58.5ºS with 1.09 µg/L and at 17.79ºW and 55.24ºS with 1.12 µg/L. There is no significant correlation between chl-a and $\delta^{13}C_{POC}$ at r = 0.053 and p = 0.797 (Table 4.9). Figure 4.21-A shows that the $\delta^{13}C_{POC}$ obtain a rather average value with increasing chl-a concentrations, except between 0.20 and 0.50 µg/L where the $\delta^{13}C_{POC}$ varies between -24 and -29‰.

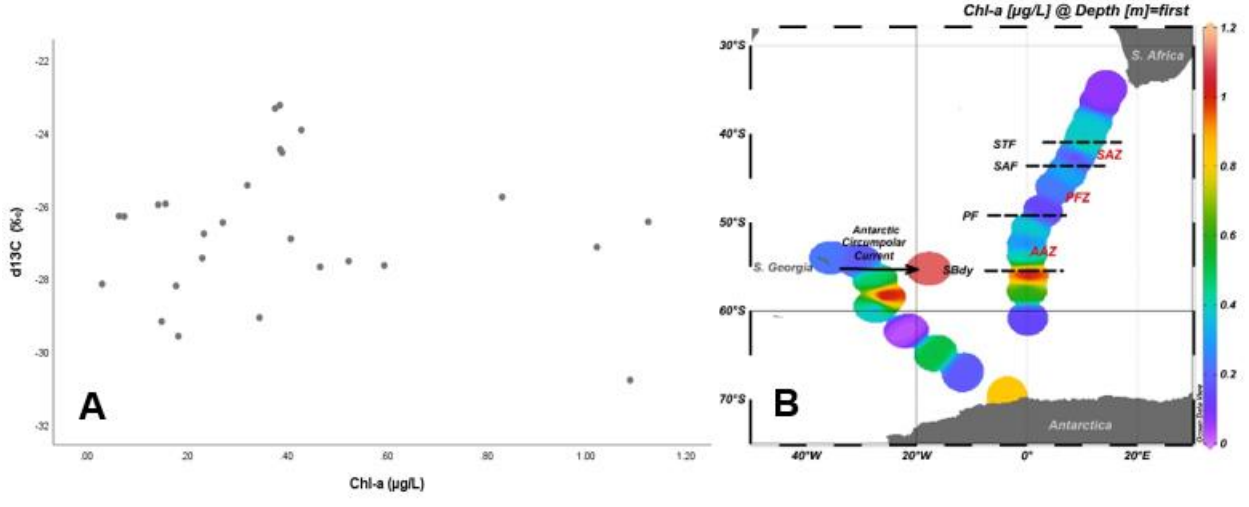

Figure 4.21. Scatterplot of chlorophyll-a concentrations plotted against $\delta^{13}C_{POC}$ (A) chl-a concentration in the surface water along the Good Hope line in the austral summer 2016/2017 during SANAE 56 (B).

Phytoplankton community composition: The dominant phytoplankton groups during the 2016-2017 summer with the highest contributions towards total chl-a, includes diatoms (43%), *P. antarctica (18%)*, cryptophytes (12%) and coccolithophores (8%) (Figure 4.22). Out of 9 phytoplankton groups investigated during this cruise, 7 groups are significantly correlated to $\delta^{13}C_{POC}$ (Table 4.9). Cyanobacteria are almost completely depleted along the transect, except in the tropical waters where the contribution to the total phytoplankton community ranges between 0.01 - 0.06 µg/L (Figure 4.23-B). Looking at figure 4.23-A, there seems to be no correlation between cyanobacteria and $\delta^{13}C_{POC}$, although when using Spearman's rho correlation, there is a significant correlation at r = 0.510 and p = 0.008 (Table 4.9). Dinoflagellates are almost depleted throughout the transect, with small peaks in the tropical waters south of the STF and crossing the PF at 49.2ºS where the contribution to total chl-a reaches a high of 0.2 µg/L (Figure 4.23-D). There is a positive correlation between dinoflagellates contribution to total chl-a and $\delta^{13}C_{POC}$ at r = 0.562 and it is significant at p = 0.003 (Table 4.9). $\delta 13C_{POC}$ becomes less negative (increase), i.e. fractionation decrease, with increasing dinoflagellates contribution as there is more available ^{13}C, thereby increasing productivity. There is also a positive relationship between the *P. antarctica*

contribution to total chl-a and $\delta^{13}C_{POC}$ at r = 0.426, indicating fractionation decreases with increasing *P. antarctica* contribution to the total chl- a (Figure 4.23-E) and it is significant at p = 0.030 (Table 4.9). *P. antarctica* contribution to total chl-a does not vary largely along the Good Hope line with a peak to 0.29 µg/L south of the SBdy at 56.05ºS (Figure 4.23-F). Diatoms contribute to the total community in the AAZ and when the SBdy is crossed, with the highest contribution of 0.89 µg/L to total chl-a on the South Georgia line at 55.24ºS (Figure 4.24-B). There is a negative relationship between diatoms contribution to total chl-a and $\delta^{13}C_{POC}$ at r = -0.431 and is significant at p = 0.028 (Table 4.9).

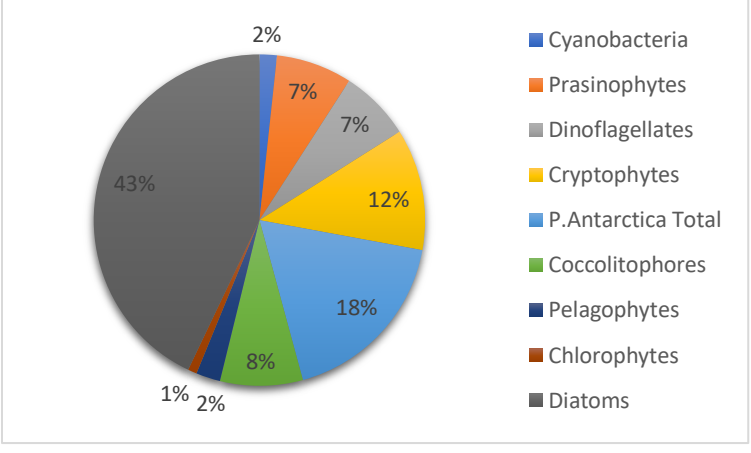

Figure 4.22. Visual representation of the average phytoplankton groups within all the surface water of the SO along the Good Hope Line and South Georgia leg in the summer of 2016/2017 for SANAE 56.

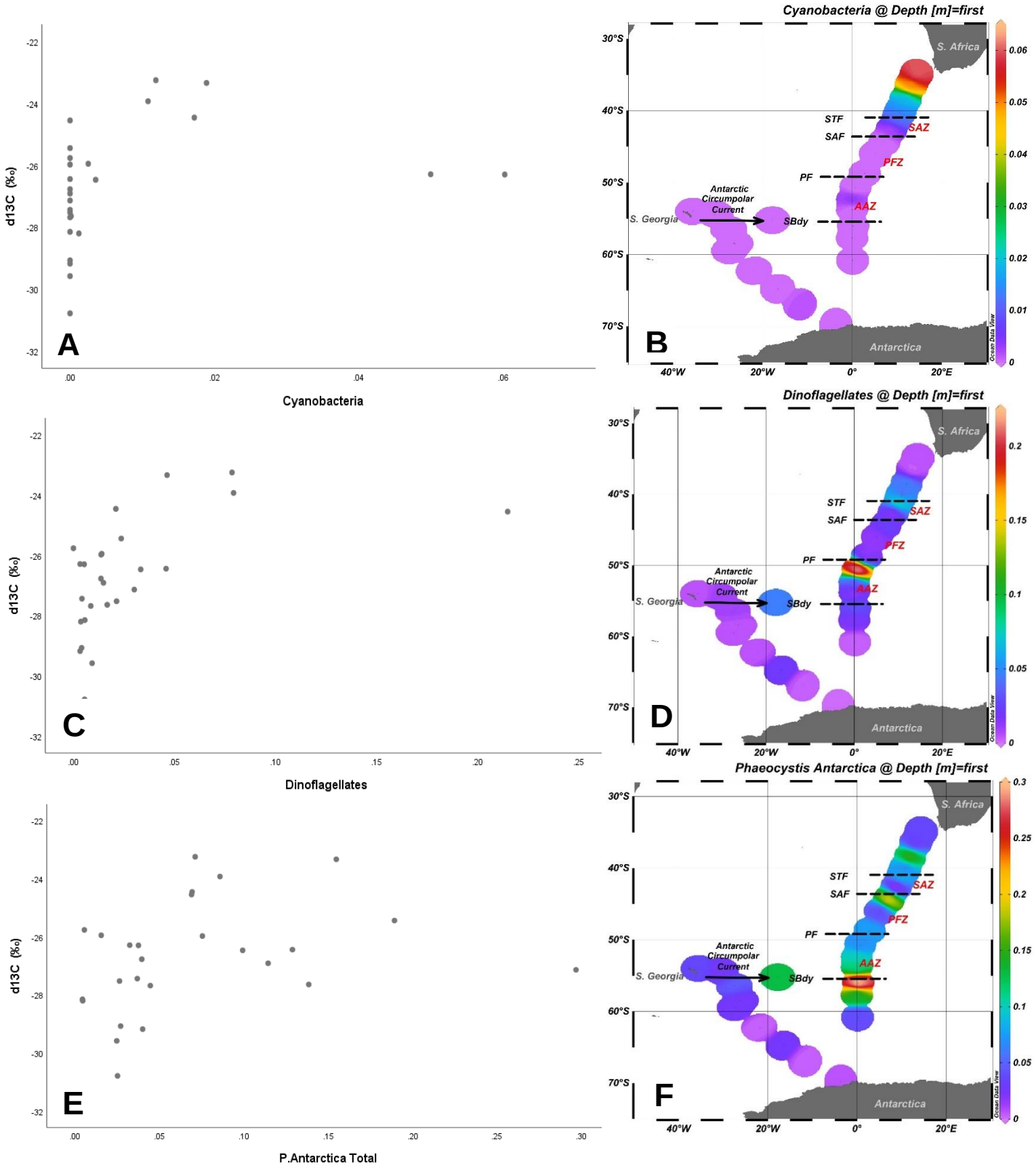

Figure 4.23. Scatterplots (phytoplankton groups's contribution to total chl-a in µg/L represented on the x-axis) of phytoplankton groups showing significant correlation results to $\delta^{13}C_{POC}$ (A, C & E) and their contribution to total chlorophyll-a concentration in the surface water along the transect (B, D & F). P. antarctica is one of the most dominant species found in the surface water during SANAE 56.

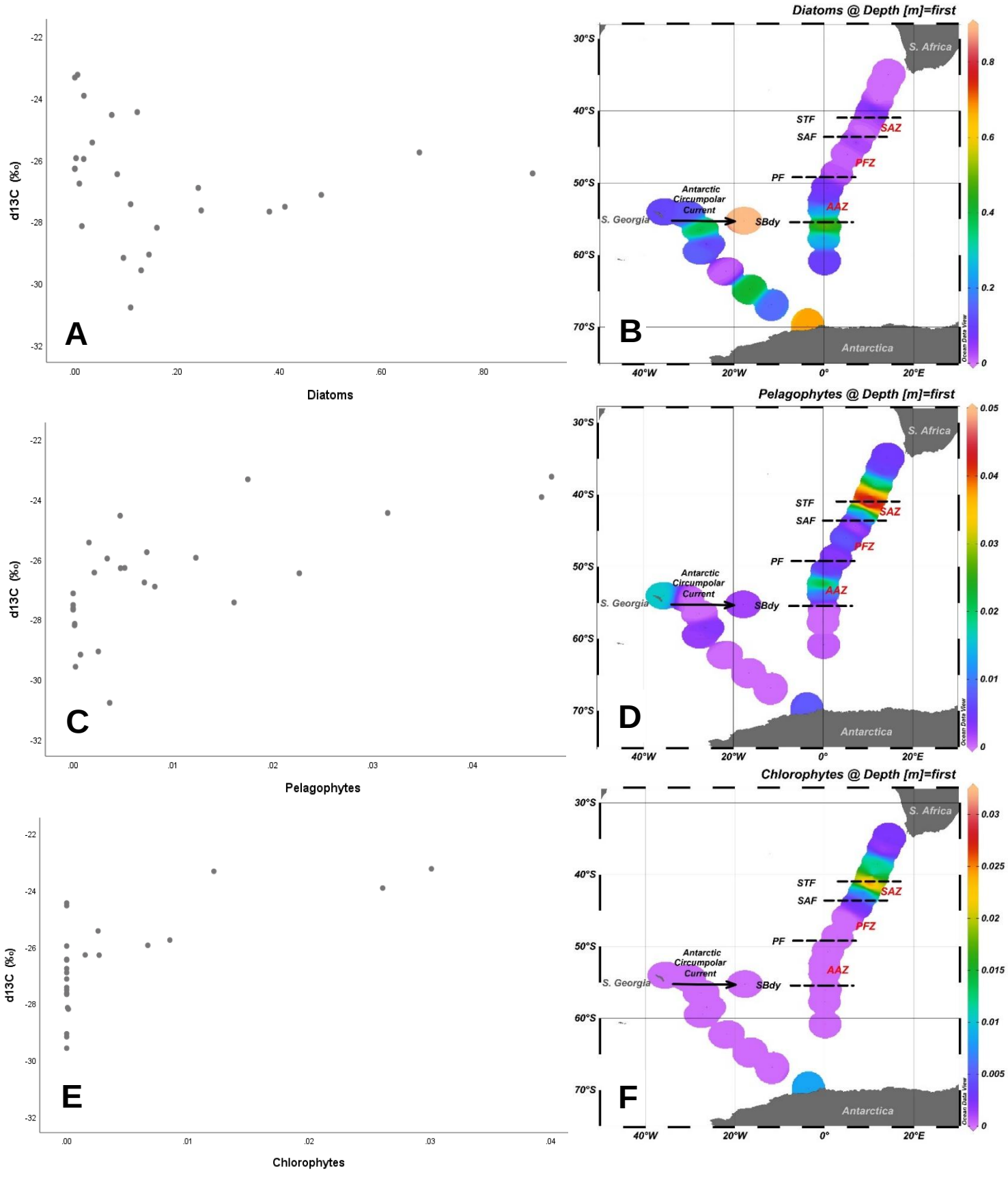

Figure 4.24. Scatterplots (phytoplankton groups's contribution to total chl-a in µg/L represented on the x-axis) of phytoplankton groups showing significant correlation results to $\delta^{13}C_{POC}$ (A, C & E) and their contribution to total chlorophyll-a concentration in the surface water along the transect (B, D & F). Diatoms are one of the three most dominant species found in the surface water during SANAE 56.

Pelagophytes, like cyanobacteria and chlorophytes, only show small contributions to total chl-a in the warmer tropical waters north of the SBdy, with the highest contribution of 0.047 µg/L at 40.25ºS (Figure 4.24-D) and have a positive correlation against $\delta^{13}C_{POC}$ at r = 0.671 and is significant at p = 0.000 (Table 4.9). Thus, it can be argued that with increasing contribution of pelagophytes to the total chl-a, the $\delta^{13}C_{POC}$ increase, thereby decreasing the fractionation (Figure 4.24-C). This could be an indication of higher productivity, although the POC is not the highest at that point, the concentration is still higher than most of the transect (Figure 4.20-B). Chlorophytes show peaks north of the SAF and a small peak at the highest latitude (Figure 4.24-F). There is a positive correlation between chlorophytes and $\delta^{13}C_{POC}$ at r = 0.584 and it is significant at p = 0.002 (Table 4.9), thus $\delta^{13}C_{POC}$ increase with increasing chlorophytes in the upper layer of the SO, decreasing the fractionation (Figure 4.24-E). The only two phytoplankton groups that do not show a significant correlation to $\delta^{13}C_{POC}$ during the 2016-2017 summer are prasinophytes and cryptophytes (Table 4.9). Cryptophytes only show a small contribution of 0.11 µg/L on the South Georgia leg at 27.31ºW and 59.43ºS (Figure C.2-C; Appendix C). Prasinophytes shows the highest contribution in the PFZ with 0.07 µg/L (Figure C.2-A; Appendix C).

Table 4.9. Correlation tests on chlorophyll-a concentration and all phytoplankton groups (µg/L) were investigated during SANAE 56. All the data is tested using a two-tailed correlation. N represents the number of data points used.

			$d13C_{POC}$ (‰)	Chl-a (µg/L)	Cyano-bacteria	Prasino phytes	Dinoflagellates	Cryptophytes	*P.antarctica* Total	Coccolithophores	Pelago phytes	Chloro-phytes	Diatoms
Spearman's rho	$d13C_{POC}$ (‰)	Correlation Coefficient	1.000	.053	.510**	.353	.562**	-.105	.426*	.404*	.671**	.584**	-.431*
		Sig. (2-tailed)	.	.797	.008	.077	.003	.611	.030	.041	.000	.002	.028
		N	26	26	26	26	26	26	26	26	26	26	26

**. Correlation is significant at the 0.01 level (2-tailed).

*. Correlation is significant at the 0.05 level (2-tailed).

4.3.4. Temperature and salinity

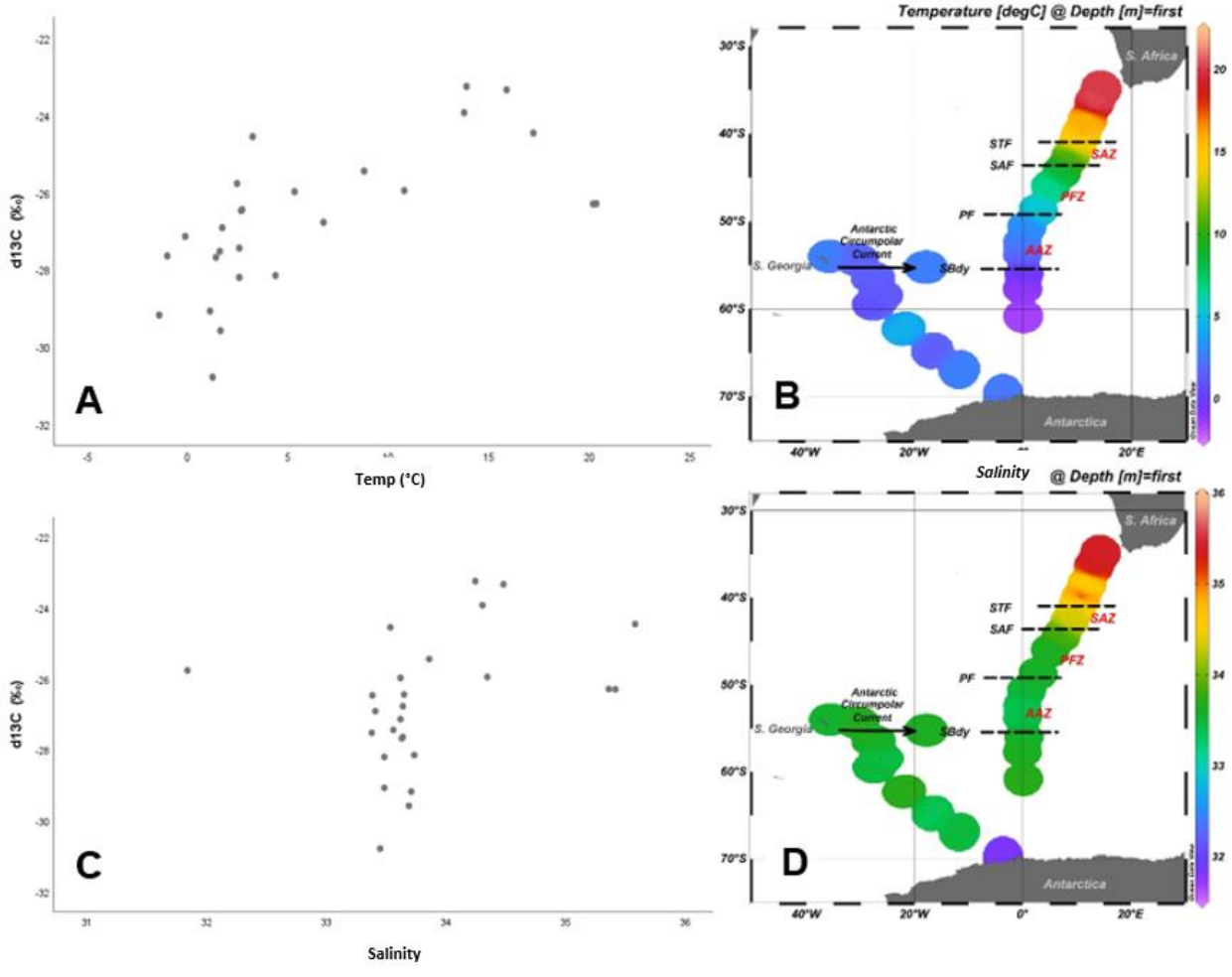

Figure 4.25. Scatterplots for temperature (A) and salinity (C) against $\delta^{13}C_{POC}$ during the SANAE 56 voyage and surface temperature (B) and salinity (D) results obtained.

Just like during the previous summer cruise investigated, temperature shows a positive relationship to $\delta^{13}C_{POC}$ at r = 0.649 and is significant at p = 0.000 (Table 4.10). Surface temperature decrease to the south (Figure 4.25-B) and increase with increasing $\delta^{13}C_{POC}$ (Figure 4.25-A), thus the fractionation decreases. Yet again, the temperature may have a significant correlation to $\delta^{13}C_{POC,}$ but it cannot be the main source of the change in fractionation. Salinity maintains an average value through most of the cruise (33 – 34) as shown in figures 4.25-C&D, and there is no significant correlation towards $\delta^{13}C_{POC}$ at p = 0.077 (Table 4.10).

Table 4.10. Pearson correlation test was done for surface temperature and surface salinity during SANAE 56. All the data is tested using a two-tailed correlation. N represents the number of data points used.

		$d13C_{POC}$ (‰)	Salinity	Temp (ºC)
$d13C_{POC}$ (‰)	Pearson Correlation	1	.353	.649**
	Sig. (2-tailed)		.077	.000
	N	26	26	26

**. Correlation is significant at the 0.01 level (2-tailed).

4.3.5. pCO_2

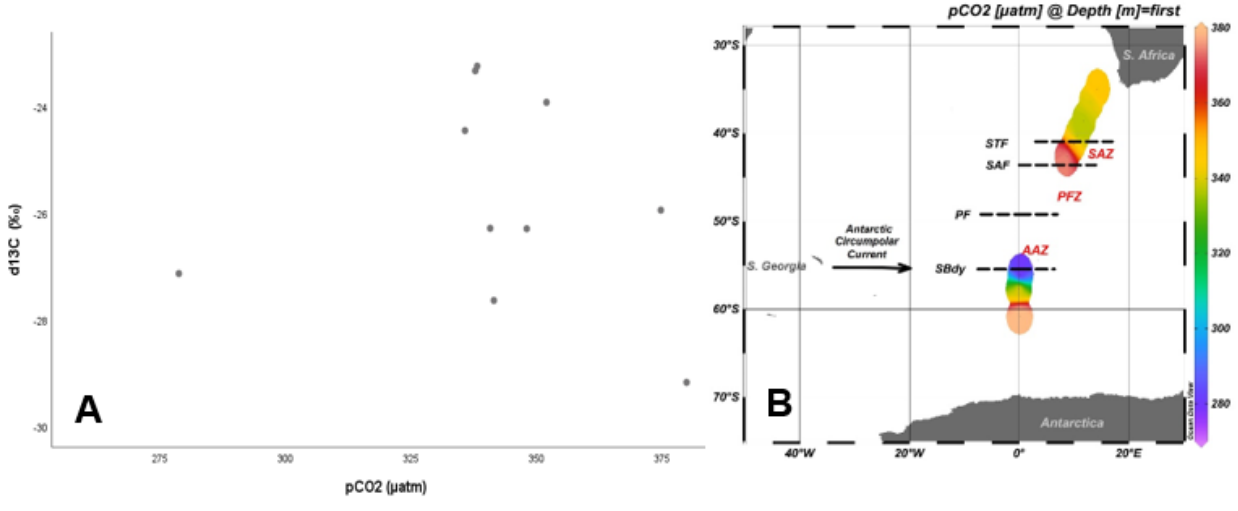

Figure 4.26. Scatterplot of pCO_2 versus $\delta^{13}C_{POC}$ during SANAE 56 (A) and surface pCO_2 concentrations (while measurements were possible) along the cruise track (B).

During this cruise only a few measurements were taken for pCO_2, this may be due to an instrumental malfunction or broken pumps, this reason is unknown (W. Joubert *et al.*, pers. comm.). With the available data, an analysis was done. Figures 4.26-A&B show two peaks; one in the SAZ and the other one very close to Antarctica. There is no significant correlation between pCO_2 and $\delta^{13}C_{POC}$ at r = -0.309 and p = 0.385 (Table C.2; Appendix C), thus it can be said that pCO_2 has little to no effect on the carbon isotopic signature. This will be discussed in detail in chapter 5.

4.4. Winter Cruise 2017

4.4.1. $\delta^{13}C_{POC}$

Underway samples were only taken for leg S during this cruise (Figure 4.27). The results support the model used by (Wong & Sackett, 1978; Rau *et al.*, 1997); $\delta^{13}C_{POC}$ decreases in colder waters. Throughout the transect, the highest $\delta^{13}C_{POC}$ values are north of the PF and decrease to -28‰ in the ice shelf. A slight decrease from -23‰ to -25.5‰ is observed close to South Africa in warmer waters, whereafter it increases until the SAZ is reached. The descriptive statistics for this cruise can be seen in appendix D, table D.1.

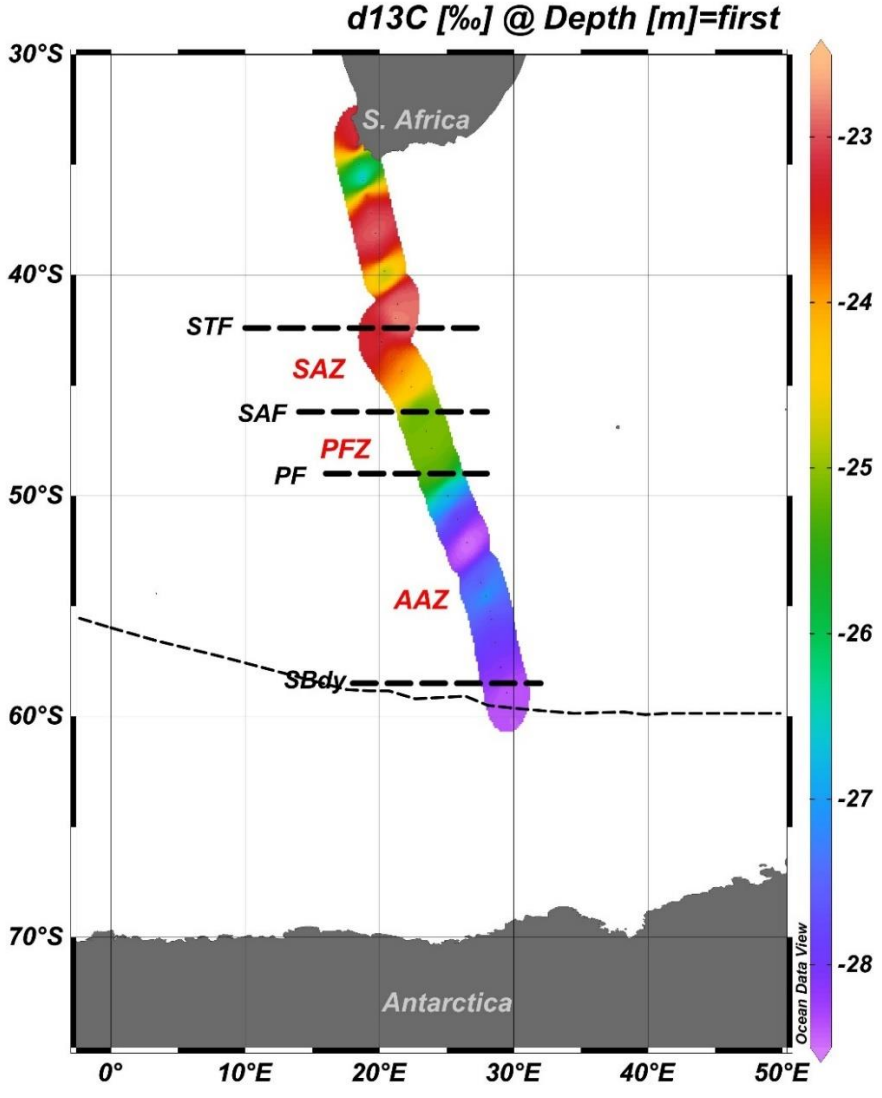

Figure 4.27. Carbon isotopic signature in the euphotic layer of the SO during WC 2017 on leg S. Major waterfronts were crossed (indicated with horizontal dashed lines) all the way South towards the ice shelf.

4.4.2. Macronutrients

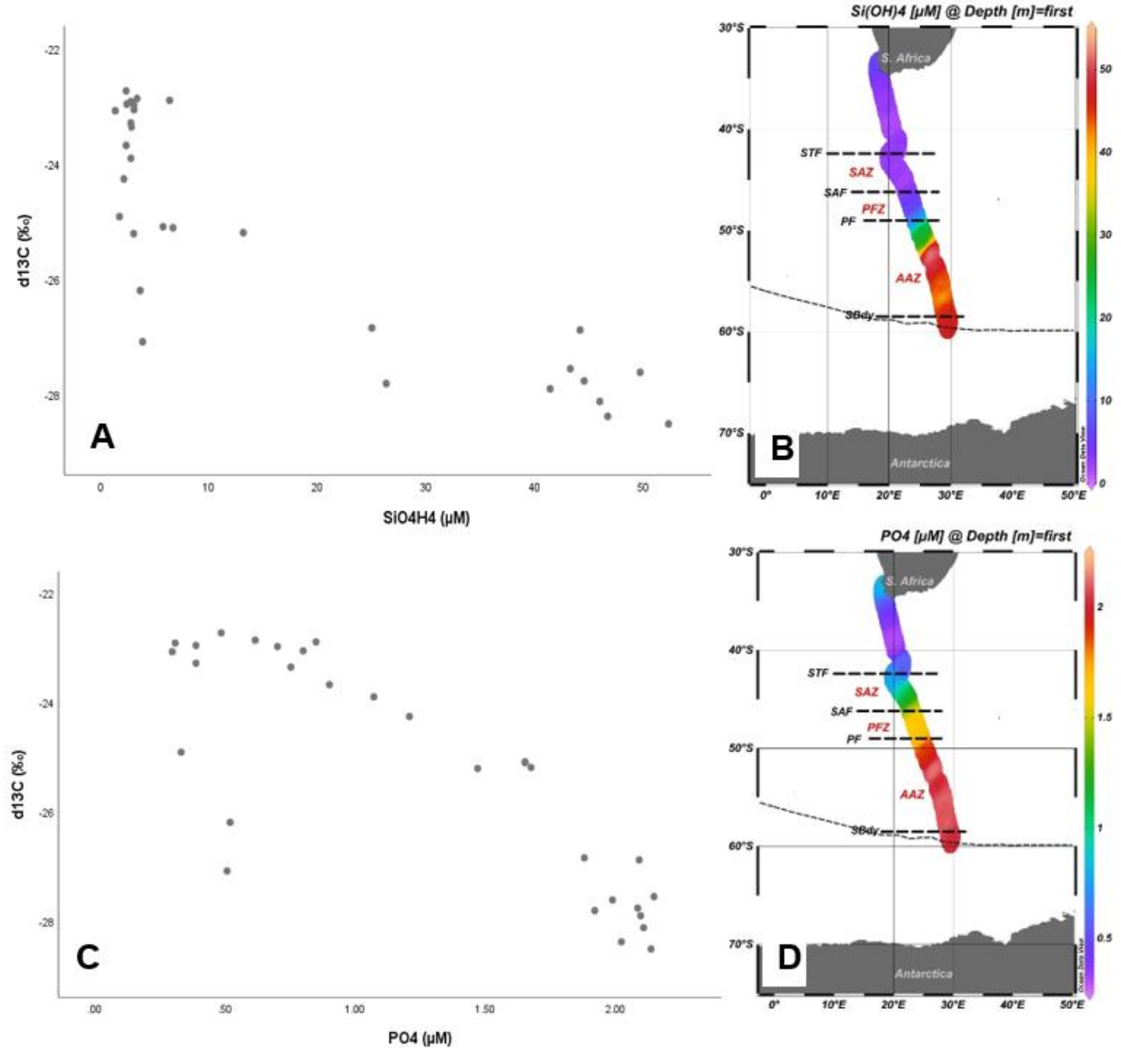

Figure 4.28. $Si(OH)_4$ (A) and PO_4 (C) scatterplots against $\delta^{13}C_{POC}$ to determine if there is a significant correlation during WC 2017. $Si(OH)_4$ concentrations in the surface water during leg S (B) and PO_4 concentrations (D) during the voyage.

Macronutrient concentrations all increase from north to south along the transect (Figure 4.28-B&D and Figure 4.29-B&D) and all have an inverse significant correlation to $\delta^{13}C_{POC}$ (Table 4.11). $Si(OH)_4$ and NO_3 are the most abundant in the surface water. $Si(OH)_4$ is mostly depleted south of the PF and increases from 20 µM to 50 µM in the AAZ (Figure 4.28-B). The $Si(OH)_4$ concentration increases as the $\delta^{13}C_{POC}$ decreases, thus the fractionation increases (Figure 4.28-A) and is significant at $p = 0.000$. PO_4 follows a similar trend than that of $Si(OH)_4$ and only increases in the AAZ at 48.92ºS. It is negatively correlated to $\delta^{13}C_{POC}$ at $r = -0.817$ and is significant at $p = 0.000$ (Table 4.11), as is NO_3 with only a different $r = -0.796$.

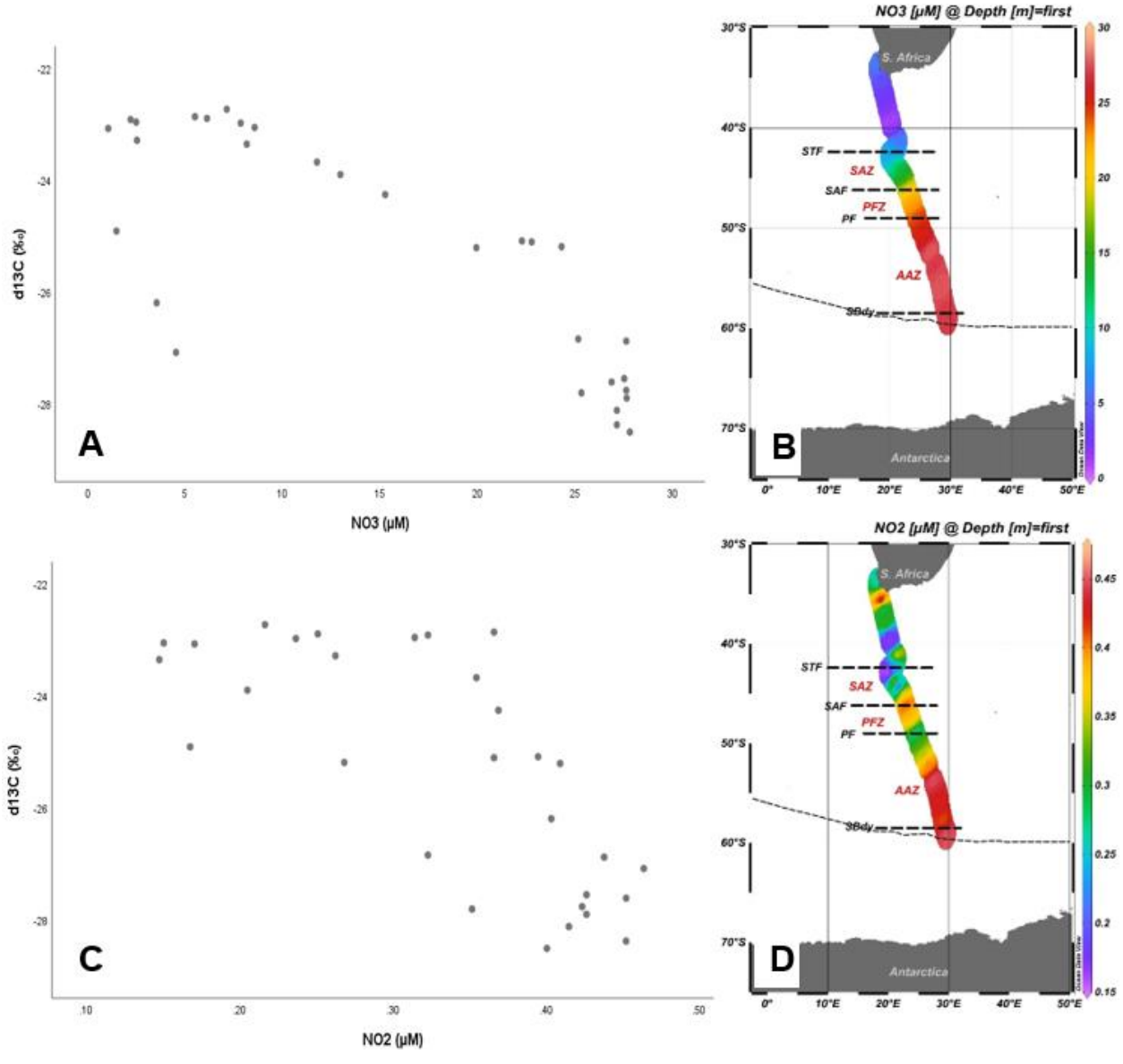

Figure 4.29. NO_3 (A) and NO_2 (C) scatterplots and ODV maps of $Si(OH)_4$ (B) and PO_4 (D) during WC 2017.

NO_2 concentrations vary between 0.3 - 0.4 µM south of the PF, whereafter there is a clear increase to 0.45 µM at the SBdy (Figure 4.29-B). There is a negative relationship between NO_2 and $\delta^{13}C_{POC}$ at r = -0.731 and is significant at p = 0.000 (Table 4.11). Both these concentrations increase with decreasing $\delta^{13}C_{POC,}$ thus increasing the fractionation. This may be due to a depletion in the heavier isotope in phytoplankton as the lighter carbon isotope is subsumed and increased within the phytoplankton.

Table 4.11. Pearson correlation test results for POC and macronutrients during WC 2017. All the data is tested using a two-tailed correlation. N represents the number of data points used.

		$d13C_{POC}$ (‰)	POC (µg/L)	NO_2 (µM)	NO_3 (µM)	$Si(OH)_4$ (µM)	PO_4 (µM)
$d13C_{POC}$ (‰)	Pearson Correlation	1	-.037	-.731**	-.796**	-.858**	-.817**
	Sig. (2-tailed)		.847	.000	.000	.000	.000
	N	30	30	30	30	30	30

**. Correlation is significant at the 0.01 level (2-tailed).

*. Correlation is significant at the 0.05 level (2-tailed).

4.4.3. POC, Chlorophyll-a and phytoplankton groups

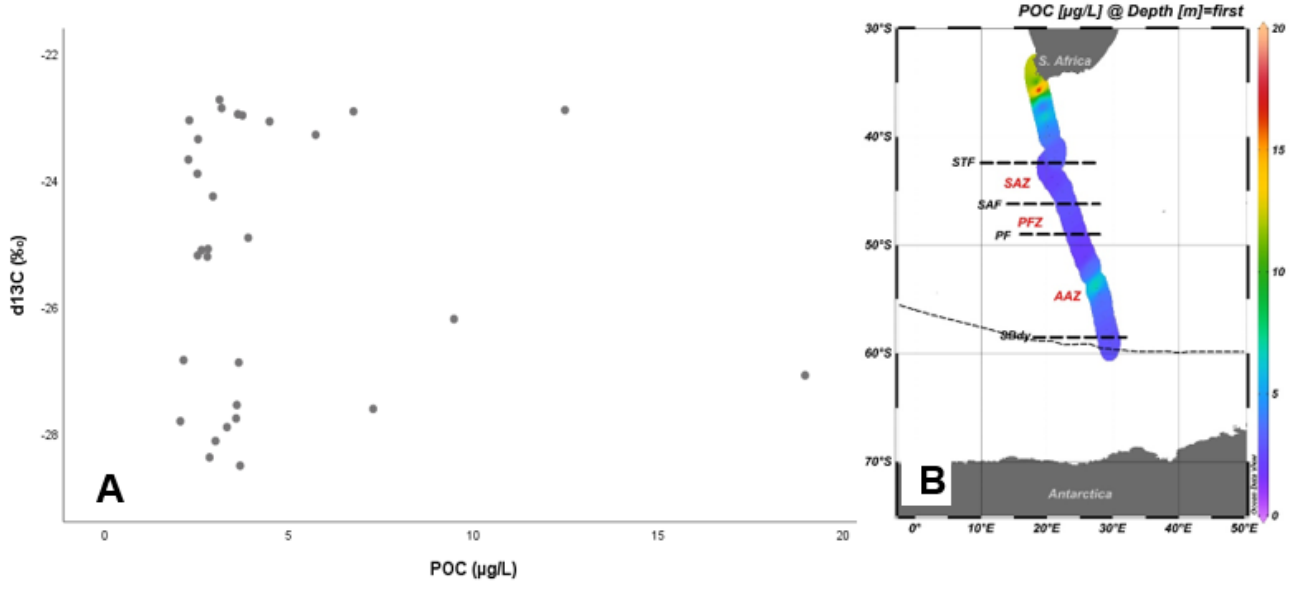

Figure 4.30. Scatterplot of POC versus $\delta^{13}C_{POC}$ along the transect (A) and the surface POC concentrations during the WC 2017 (B).

POC: There is a decrease from 19 µg/L to 2.8 µg/L north to south along the transect (Figure 4.30-B), this could be an indication of decreasing productivity in the winter. There is no significant correlation between POC and $\delta^{13}C_{POC}$ at r = -0.037 and p = 0.847 (Table 4.11). Figure 4.30-A visually support results in table 4.11 with no correlation between POC and $\delta^{13}C_{POC}$.

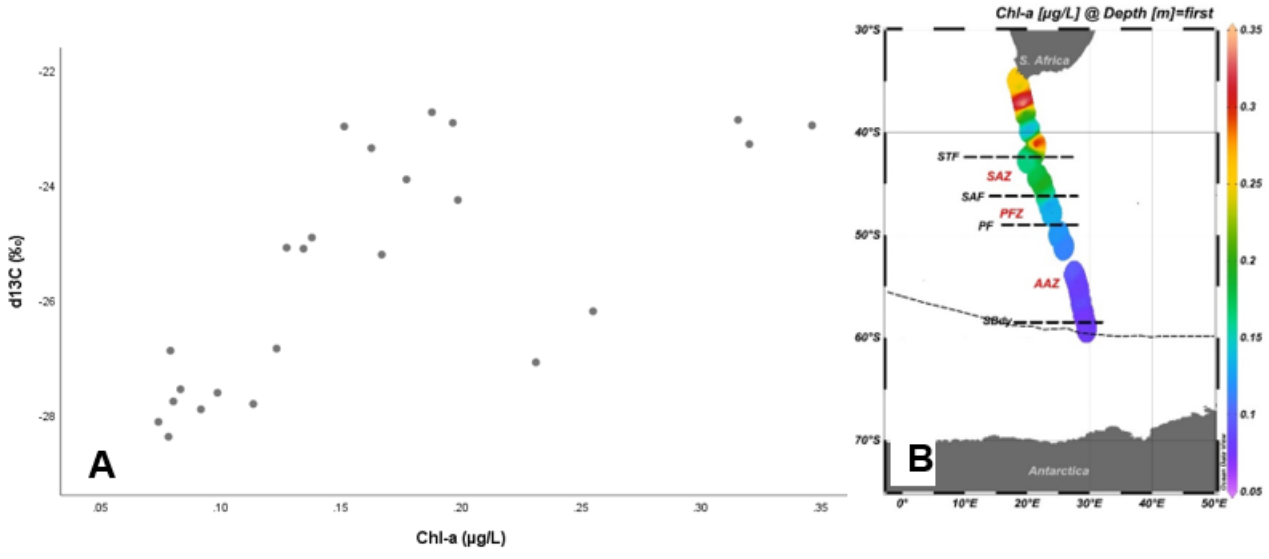

Figure 4.31. Scatterplot for chlorophyll-a concentration against $\delta^{13}C_{POC}$ (A) and surface concentrations for leg S during WC 2017.

Chlorophyll-a: Chl-a concentrations in the surface water during leg S decrease from north to south (Figure 4.31-B). An increase to 0.35 µg/L can be observed at 19.35ºW and 37.20ºS and just north of the STF at 21.35ºW and 41.32ºS from 0.13 µg/L - 0.31 µg/L. Crossing the PF the concentration decreases from 0.12 µg/L - 0.07 µg/L. Decreasing chl-a concentrations results in more negative $\delta^{13}C_{POC}$ values (Figure 4.31-A), showing a positive relationship at r = 0.064 and a significance at p = 0.000 (Table 4.12).

Table 4.12. Pearson correlation test was done for chlorophyll-a concentration and three phytoplankton groups as these groups presented normally distributed datasets. All the data is tested using a two-tailed correlation. N represents the number of data points used.

		$d13C_{POC}$ (‰)	Chl-a (µg/L)	Prasinophytes	*P. antarctica* Total	Pelagophytes
$d13C_{POC}$ (‰)	Pearson Correlation	1	.694**	.707**	.770**	.551**
	Sig. (2-tailed)		.000	.000	.000	.005
	N	30	24	24	24	24

**. Correlation is significant at the 0.01 level (2-tailed).

Phytoplankton community composition: The dominant phytoplankton groups in the surface water during the WC 2017 with the highest contribution to total chl-a are, *P. antarctica* (45%), prasinophytes (19%), diatoms (10%) and cryptophytes (10%) (Figure 4.32). Out of 9 phytoplankton groups, six groups, i.e. prasinophytes, *P. antarctica*, pelagophytes, dinoflagellates, cryptophytes and chlorophytes show to be significantly correlated to $\delta^{13}C_{POC}$ (Table 4.12 & 4.13). Referring to figures 4.33 (B, D & F), a decrease in phytoplankton community distribution from north to south along the transect are observed. *P. antarctica* decreases from 0.08 µg/L

contribution to total chl-a at the South African border to 0.04 µg/L in the ice shelf with three small peaks at 19.05ºE and 36.43ºS to 0.09 µg/L, at 19.70ºE and 38.12ºS to 0.10 µg/L and in the middle of the SAZ at 22.38ºE and 45.07ºS to 0.12 µg/L. Crossing the PF, a gradual decrease is observed until reaching the ice shelf. With an increasing contribution to total chl-a of *P. antarctica* in the surface water along the transect, the $\delta^{13}C_{POC}$ increase, showing a positive relationship (Figure 4.33-A) and a significant correlation (Table 4.12). Prasinophytes show a 19% contribution to the total chl-a in the surface water (Figure 4.32) and decrease from 0.06 µg/L contribution to the total chl-a in the tropical waters to 0.002 µg/L when reaching the SBdy (Figure 4.33-D). There are two small peaks at 19.35ºE and 37.20ºS to 0.079 µg/L and 21.35ºE and 41.32ºS to 0.08 µg/L. A positive relationship between prasinophytes and $\delta^{13}C_{POC}$ can be seen in figure 4.33-C and table 4.13 at r = 0.707. Prasinophytes depict a significant correlation towards $\delta^{13}C_{POC}$ with p = 0.000 (Table 4.12).

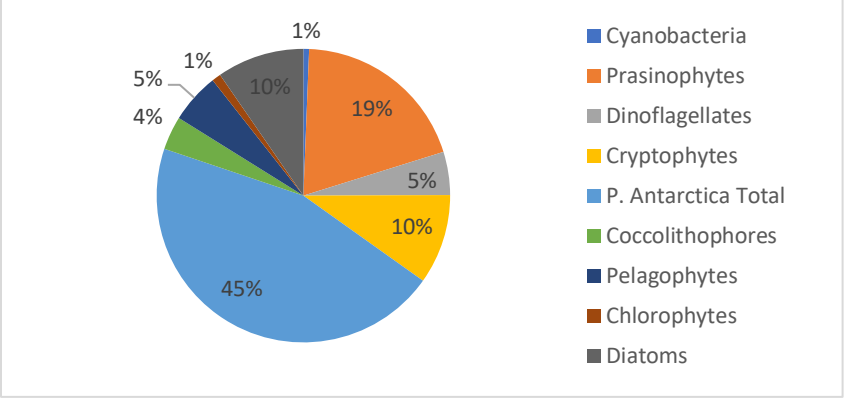

Figure 4.32. Average phytoplankton community composition (%) within the surface water of the SO during WC 2017.

Cryptophytes are almost depleted south of the STF (Figure 4.33-F) with the highest contribution at 19.35ºE and 37.20ºS with 0.054 µg/L and another small peak 21.35ºE and 41.32ºS with 0.045 µg/L to total chl-a. Cryptophytes show a positive relationship with $\delta^{13}C_{POC}$ at r = 0.572 and a significant correlation at p = 0.003 (Table 4.13). Pelagophytes decrease from north to south (Figure D.1-F; Appendix D) and contribute 5% to the surface phytoplankton community. There is a positive relationship between pelagophytes and $\delta^{13}C_{POC}$ at r = 0.551 and a significant correlation at p = 0.005 (Table 4.12). Dinoflagellates also have a 5% contribution towards the total surface phytoplankton community and show a positive relationship to $\delta^{13}C_{POC}$ at r = 0.673 and is significant at p=0.000 (Table 4.13). Chlorophytes only contribute to 1% of the phytoplankton community, although a significant correlation between this group and $\delta^{13}C_{POC}$ is observed at p = 0.000 (Table 4.13). Diatoms (10%), cyanobacteria (5%) and coccolithophores (4%) do not have a significant

correlation with $\delta^{13}C_{POC}$ with p = 0.053, p = 0.452 and p = 0.488, respectively. Coccolithophores (Figure D.2-C; Appendix D) and cyanobacteria (Figure D.2-A; Appendix D) both have positive relationships with $\delta^{13}C_{POC}$ as diatoms have a negative relationship with $\delta^{13}C_{POC}$, thus with increasing diatom contribution along the transect (Figure D.1-D; Appendix D), the $\delta^{13}C_{POC}$ become more negative and increased fractionation will take place.

Table 4.13. Spearman's rho correlation test was done on the remaining six phytoplankton groups during WC 2017. Kurtosis and skewness results can be seen in appendix D. All the data is tested using a two-tailed correlation. N represents the number of data points used.

			$d13C_{POC}$ (‰)	Cyanobacteria	Dinoflagellates	Cryptophytes	Coccolithophores	Chlorophytes	Diatoms
Spearman's rho	$d13C_{POC}$ (‰)	Correlation Coefficient	1.000	.161	.673**	.572**	.149	.748**	-.400
		Sig. (2-tailed)	.	.452	.000	.003	.488	.000	.053
		N	30	24	24	24	24	24	24

**. Correlation is significant at the 0.01 level (2-tailed).

*. Correlation is significant at the 0.05 level (2-tailed).

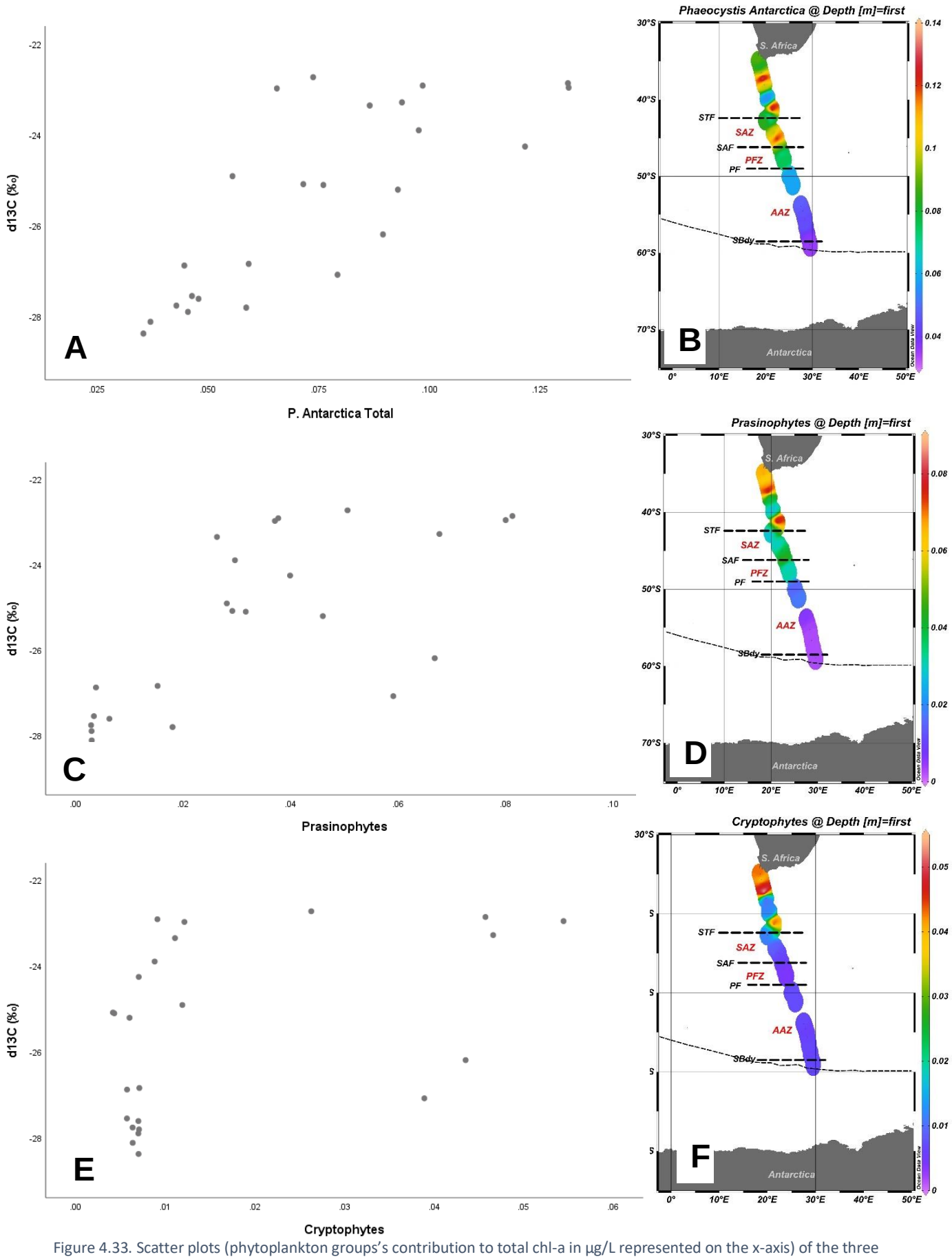

Figure 4.33. Scatter plots (phytoplankton groups's contribution to total chl-a in µg/L represented on the x-axis) of the three dominant phytoplankton groups versus $\delta^{13}C_{POC}$ (A, C & E) and their contribution to total chl-a concentration in the surface water of leg S during WC 2017 with positive significant correlations to $\delta^{13}C_{POC}$ (B, D & F).

4.4.4. Temperature and salinity

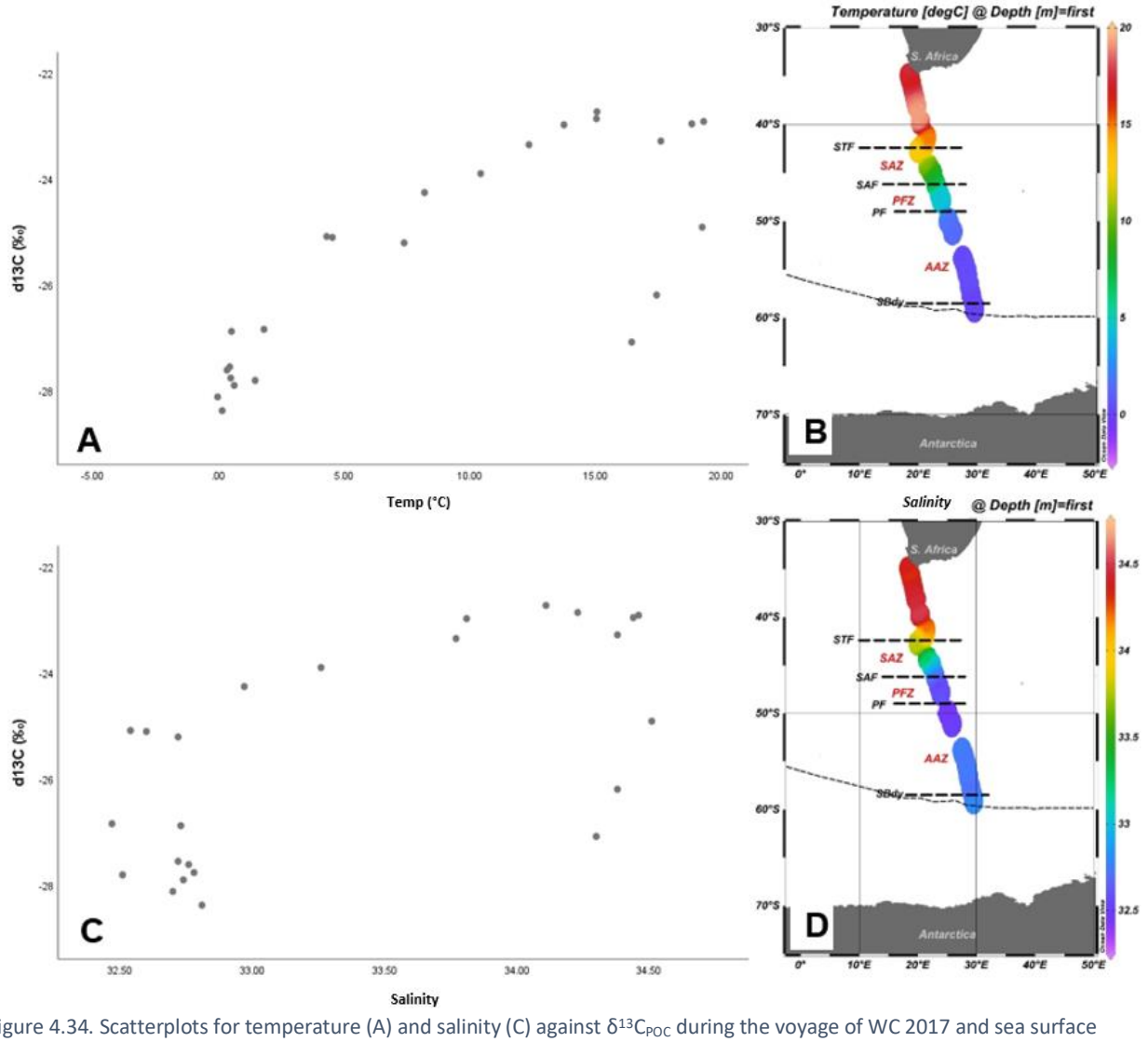

Figure 4.34. Scatterplots for temperature (A) and salinity (C) against $\delta^{13}C_{POC}$ during the voyage of WC 2017 and sea surface distribution of temperature (B) and salinity (D) along the transect.

Temperature and salinity decrease from north to south (Figure 4.34-A&B). With increasing temperature from north to south, $\delta^{13}C_{POC}$ increases (Figure 4.34-A), i.e. becomes less negative indicating a decrease in the fractionation in the water north of the STF. As for the other three cruises, the fractionation is the lowest, i.e. $\delta^{13}C_{POC}$ highest, where the temperature is the highest in the transect, with a significant correlation between temperature and $\delta^{13}C_{POC}$ for SANAE 54 and SANAE 56. During this cruise (WC 2017), temperature shows a significant correlation at $p = 0.000$ (Table 4.14). Salinity depicts a perfect, yet very small decline in the surface water up until the AAZ, where a slight increase can be observed from 32.47 to 32.81 (Figure 4.34-D). There is a positive relationship between salinity and $\delta^{13}C_{POC}$ (Figure 4.34-C) at $r = 0.587$ and there is a significant correlation at $p = 0.003$ (Table 4.14).

Table 4.14. Spearman's rho correlation test for surface temperature and surface salinity against $\delta^{13}C_{POC}$ during WC 2017. All the data is tested using a two-tailed correlation. N represents the number of data points used.

			d13C$_{POC}$ (‰)	Temp (ºC)	Salinity
Spearman's rho	d13C$_{POC}$ (‰)	Correlation Coefficient	1.000	.795**	.587**
		Sig. (2-tailed)	.	.000	.003
		N	30	24	24

**. Correlation is significant at the 0.01 level (2-tailed).

4.4.5. pCO_2

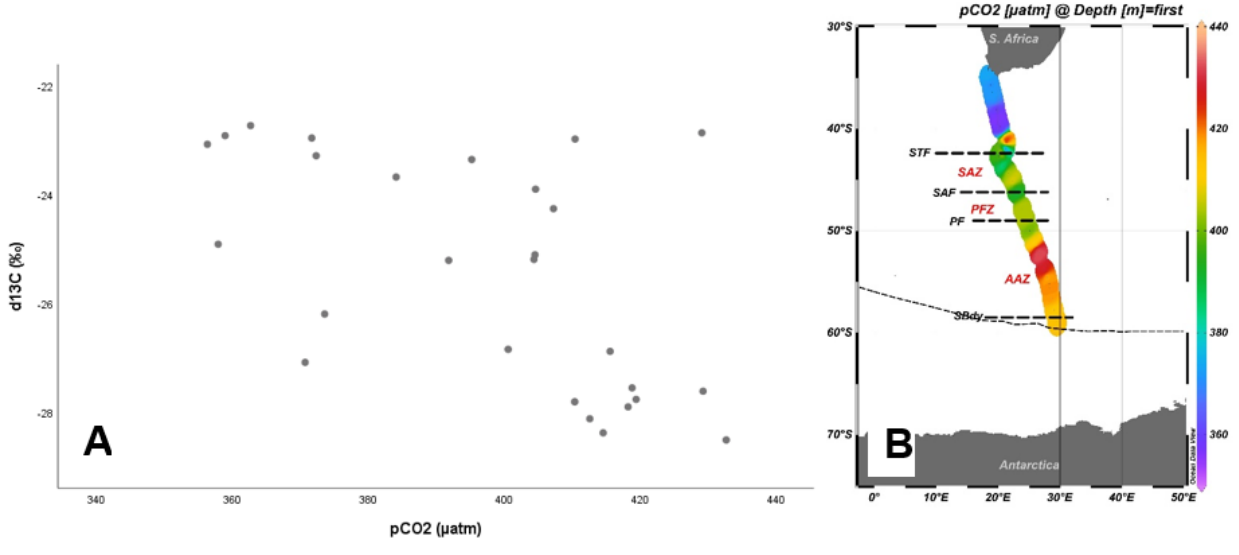

Figure 4.35. Scatterplot of $\delta^{13}C_{POC}$ against pCO_2 during WC 2017 (A) and surface pCO_2 concentrations along the cruise track (B).

A negative relationship between pCO_2 and $\delta^{13}C_{POC}$ is observed in figure 4.35-A and at r = -0.583 (Table 4.15). North of the STF in the subtropical waters, pCO_2 decreases from 374 µatm to 356 µatm whereafter there is a peak at 21.4ºE and 41.3ºS to 429 µatm (Figure 4.35-B). Crossing the STF from north to south, pCO_2 increase to 433 µatm in the AAZ at 26.5ºE and 52.1ºS and decrease to 4158 µatm at the SBdy. There is a significant correlation between pCO_2 and $\delta^{13}C_{POC}$ at p = 0.001 (Table 4.15).

Table 4.15. Spearman's rho correlation test on pCO_2 for values during leg S.

			d13C$_{POC}$ (‰)	pCO_2 (µatm)
Spearman's rho	d13C$_{POC}$ (‰)	Correlation Coefficient	1.000	-.583**
		Sig. (2-tailed)	.	.001
		N	30	27

**. Correlation is significant at the 0.01 level (2-tailed).

5. Discussion

Considering the rapid increase of CO_2 in the atmosphere and continuous climate change, it is important to find new ways to better predict these changes in the future. One of the ways to do this is to use pCO_2 in underlying sediments, although it is not possible to directly measure the pCO_2, but it is possible to measure $\delta^{13}C_{POC}$ in the sediments. Therefore, it is important to investigate what drives the $\delta^{13}C_{POC}$ to potentially find a link.

The main source of carbon isotope fractionation is photosynthesis where living organisms (autotrophs) convert inorganic carbon (CO_2) to organic compounds using the energy from the sun or the energy of inorganic oxidation (Roy-Barman & Jeandel, 2016). Organic carbon produced during photosynthesis is systematically depleted in ^{13}C. According to Roy-Barman & Jeandel (2016), marine organic C has a $\delta^{13}C$ ranging between -18‰ and -30‰. The $\delta^{13}C_{POC}$ values obtained during all four cruises in this study, fall within this range. Several parameters were investigated during summer and winter in the Southern Ocean to investigate what drives the changesin $\delta^{13}C_{POC}$ within this range.

5.1. Atlantic Ocean (SANAE 54 & 56 and WC 2015)

5.1.1. Potential of macronutrients as drivers for $\delta^{13}C_{POC}$ distribution

Phytoplankton, which form the base of the marine food web and play a very important role in the biogeochemical cycles in the SO, have different nutrient requirements. Most macronutrients seem to be depleted in the surface water north of the STF (Figure 4.2-D&H; 4.10-D&H; 4.19-B&D), where others are depleted north of the PF (Figure 4.2-B; 4.18-B). Depletion of nutrients in surface waters occurs due to the uptake by phytoplankton. Silicic acid gradually increases along the Good Hope line with a peak at 59.4ºS (SANAE 54), and another peak is observed close to South Georgia (SANAE 56). $Si(OH)_4$ has a negative relationship with $\delta^{13}C_{POC}$ during summer (SANAE 54 & 56), which indicates lower $\delta^{13}C_{POC}$, i.e. an increase in fractionation, in areas where higher $Si(OH)_4$ concentration is observed. In contrast with that, during WC 2015, $Si(OH)_4$ has a positive relationship with $\delta^{13}C_{POC}$, indicating less negative $\delta^{13}C_{POC}$ concentration, i.e. decrease in fractionation where high $Si(OH)_4$ concentrations are observed. However, $Si(OH)_4$ cannot be directly responsible for the fractionation. Diatoms typically strive in regions characterized by a high concentration of $Si(OH)_4$; which can be confirmed with the results obtained in this study. Consequently, diatom contribution to total chl-a is also strongly correlated in the surface waters along the SANAE 54, WC 2015 and SANAE 56 transects. Hence, $Si(OH)_4$ and diatoms both show a negative relationship with $\delta^{13}C_{POC}$, indicating an increase in fractionation in areas with higher $Si(OH)_4$ and diatom contribution to total chl-a during the summer. It can thus be argued that

diatoms may influence the carbon isotope fractionation process and $Si(OH)_4$ concentrations being indicative of this impact.

Phosphate concentrations in the surface ocean are much lower than those of $Si(OH)_4$ and NO_3. PO_4 peaks can be observed north of the SBdy (WC 2015) and south of the SBdy (SANAE 54 & 56). $\delta^{13}C_{POC}$ and PO_4 show negative relationships in both summer cruises in the Atlantic sector and the only positive relationship is observed in WC 2015. SANAE 54 and WC 2015 show no significant correlation between these two parameters. SANAE 56, however, shows a significant negative relationship towards $\delta^{13}C_{POC}$ (Table 4.8): with increasing PO_4 concentrations along the transect, the $\delta^{13}C_{POC}$ decreases indicating that fractionation increases. It is clear that PO_4 increases with decreasing $\delta^{13}C_{POC}$ for both summer and winter, although there is not enough evidence to confidently state that PO_4 can be a primary driving factor for $\delta^{13}C_{POC.}$

Nitrate concentrations in the Atlantic sector's surface ocean are higher during the austral summer than in the winter and are depleted in lower latitudes near Cape Town. This may be due to smaller phytoplankton groups being present in these regions and utilizing this macronutrient. During SANAE 54 and 56, NO_3 shows a negative relationship and significant correlation with $\delta^{13}C_{POC}$ indicating that the fractionation increases along the transect from north to south. During WC 2015, there was no correlation between NO_3 and $\delta^{13}C_{POC.}$ Nitrite is present in very small concentrations in the surface ocean. During SANAE 54 and WC 2015 (where a peak is observed in the PFZ), there is no significant correlation between $\delta^{13}C_{POC}$ and NO_2, although a significant correlation between NO_2 and $\delta^{13}C_{POC}$ is observed for SANAE 56. NO_3 only show to have a significant correlation to $\delta^{13}C_{POC}$ during the summer in the Atlantic sector of the SO, whereas NO_2 only show significant results during one cruise in the summer in the Atlantic sector of the SO. It can thus be argued that there might be other environmental factors influencing these nutrients, thereby influencing the $\delta^{13}C_{POC}$, therefore it cannot be said to be primary driving factors for $\delta^{13}C_{POC.}$

Macronutrients, therefore, have an effect on the fractionation during the uptake of inorganic carbon through phytoplankton, but the nutrients alone may not control the fractionation. External factors likely influence the nutrients which thereby affect the fractionation.

5.1.2. POC and chlorophyll-a as indicators for $\delta^{13}C_{POC}$ distribution

Primary production is dependent on photosynthesis carried out by autotrophic organisms (Helbling & Villafañe, 2009). For both summer cruises, the total chl-a concentration shows a gradual increase from north to south with the highest concentration close to the ice edge (SANAE 54) and just south of the SBdy (SANAE 56), although a higher concentration is still observed at the ice shelf (Figure 4.21-B). North of the PF, chl-a concentrations are almost depleted, which

correlates with very low macronutrient concentrations for both cruises in this region, except for PO_4 and NO_2 (Figure 4.2-D&F) during SANAE 54. WC 2015 chl-a concentration shows no definite increase from north to south or vice versa, although the highest concentration is observed north of the SAF in the SAZ (Figure 4.12-B).

Distinctive chlorophyll-a and POC spikes at the major fronts cannot be seen for the cruises that took place on the Good Hope line in the Atlantic sector of the SO. For example, SANAE 56 showed elevated chl-a concentrations in the surface water at the SBdy (Figure 4.21-B), although this was only a slight increase. Higher concentrations of diatoms and *P. Antarctica* (Figure 4.24-B and 4.23-F) at the SBdy are observed during SANAE 56, which correspond to elevated $Si(OH)_4$, PO_4 (Figure 4.18-B&D) and NO_3 (Figure 4.19-D) concentrations in the same region. These results agree with literature stipulating that productivity, linked to POC and chl-a, is dependent on nutrient addition along the fronts (Laubscher, Perissinotto & McQuaid, 1993). During the 2015 WC there are only two spikes in POC along the transect: in the subtropical water north of the STF at approximately 38ºS and in the PFZ.

As previously mentioned, phytoplankton are responsible for a large amount of carbon fixation in the carbon cycle, although they can only be held accountable for 0.2% of the total global primary producer biomass (Fielding *et al.*, 1998; Schabhüttl, Hingsamer, Weigelhofer, *et al.*, 2013). Biological fractionation of carbon isotopes is a result of CO_2 fixation through the enzyme RUBISCO during photosynthesis (Freeman & Hayes, 1992). The change in $\delta^{13}C_{POC}$ has been theorised to be due to the variations in the utilization and biochemical differences of CCM's in different phytoplankton groups (Wong & Sackett, 1978; Henley *et al.*, 2012). Thus, an influential factor is the rate of primary productivity. Theoretically, with stronger, faster productivity, more ^{13}C are subsumed by phytoplankton. These higher uptake rates of ^{13}C instead of the usually preferential uptake of ^{12}C, i.e. decrease in fractionation, should lead to an increase in $\delta^{13}C_{POC}$ (Morée *et al.*, 2018). This is however not the case for either SANAE 54, SANAE 56 or WC 2015. Here we use chl-a and POC as biomass indicators that are related to productivity. There is no significant correlation between chl-a or $\delta^{13}C_{POC}$ and between the POC and the $\delta^{13}C_{POC}$ during WC 2015 and SANAE 56. Hence neither chl-a nor POC seem to be suitable indicators of $\delta^{13}C_{POC}$ distribution along the latitudinal transects in those cruises. In contrast, there is a significant correlation between chl-a concentration and $\delta^{13}C_{POC}$ during SANAE 54 (Figure 4.4-A), where the concentrations increase from north to south, while the $\delta^{13}C_{POC}$ decreases, following increased fractionation.

5.1.3. Phytoplankton community composition

Community structure affects the fractionation and consequently $\delta^{13}C_{POC}$. For example, there is a fractionation range of ~12‰ in natural phytoplankton blooms (Hinga *et al.*, 1994; Rau *et al.*, 1996). The results of the $\delta^{13}C_{POC}$ range for this study are 7‰, thus correlates with literature. Higher productivity results from growing phytoplankton population (Hinga *et al.*, 1994; Arrigo *et al.*, 1999; Moore *et al.*, 1999; Moore & Abbot, 2000) and as a result more CO_2 is removed from the atmosphere and blooms of different phytoplankton will provide a constant change in the carbon isotopic signature of the organic carbon in the ecosystem. The dominant phytoplankton groups along the Good Hope transect during these three cruises were *P. antarctica* (SANAE 54&56, WC 2015), diatoms (SANAE 54&56), coccolithophores (SANAE 54 and WC 2015), prasinophytes (WC 2015) and cryptophytes (SANAE 56). During WC 2015, coccolithophores show a positive relationship to $\delta^{13}C_{POC}$; as the contribution to the phytoplankton community increases, the $\delta^{13}C_{POC}$ also increases (less negative values), following from a decrease in fractionation. This may be a result of coccolithophores using carbonate to form their exoskeleton. In coccolithophores, the DIC exists in mutually exchanging intracellular reservoirs and the intracellular process which is responsible for the largest isotopic fractionation is the conversion of inorganic CO_2 to organic matter, thus leading to isotopic implications for carbon pools located elsewhere in the cell; i.e. (in coccolithophores) the calcification (Mitchell, Brody, Holm-Hansen, *et al.*, 1991; McClelland, Bruggeman, Hermoso, *et al.*, 2017). During SANAE 54, coccolithophores' contribution to total chl-a shows to have a negative significant relationship towards $\delta^{13}C_{POC,}$ and it contributes 11% to the total phytoplankton community in the surface water. During SANAE 56, coccolithophores only contribute 8% to the total phytoplankton community in the surface water and show a significant positive relationship towards $\delta^{13}C_{POC}$. This correlation may be a result of the intracellular calcification that has an isotopic effect (McClelland *et al.*, 2017). The different directions of significant relationships of coccolithophores towards $\delta^{13}C_{POC}$ seen in the summer cruises, may be a result of the different amounts of datapoints during this cruise, it can also be contributed to the utilization of a wider range of carbon sources than other phytoplankton groups. Due to the different results, it cannot be said that coccolithophores are in fact one of the driving factors of $\delta^{13}C_{POC}$. Diatoms are the most dominant group during SANAE 54 and SANAE 56. Per Fischer (1991) diatoms can assimilate carbon rapidly as a result of larger cell sizes, thus more carbon content per cell and higher growth rates which then lead to increased carbon demand as to other phytoplankton groups and this should lead to a decrease in fractionation with higher $\delta^{13}C_{POC}$ values. The above-mentioned statement was contradicted by a study done by Tuerena *et al.* (2019) where a 3‰ fractionation increase was observed in larger phytoplankton. This can be confirmed by results found in this study for both SANAE 54 and SANAE 56 as there is a significant negative relationship between diatoms and $\delta^{13}C_{POC}$, possibly because the fractionation increases

leading to lower, more negative $\delta^{13}C_{POC}$ with higher diatoms contribution. The significant correlation between diatoms and $\delta^{13}C_{POC}$ does not necessarily mean that diatoms are a driving or sole factor for the fractionation. Wong *et al.* (1978) stated that with decreasing temperature the fractionation process of diatoms change with 0.36‰ per ºC and $Si(OH)_4$ trends along the Good Hope line also suggest that it may influence the diatoms, thus the fractionation can, for instance, be controlled by temperature.

P. antarctica was one of the dominant groups along the transect during all three cruises, with the highest contribution to the total chl-a concentrations during WC 2015 with 37%. For both SANAE 54 and SANAE 56, the contribution to total chl-a seem to be very low on the South Georgia leg, with a peak at the SBdy (SANAE 56) and a peak at approximately 50ºS, south of the PF on the South Georgia leg back to South Africa (SANAE 54). The highest contribution of *P. antarctica* during WC 2015 is north of the SAF in the subtropical waters. The total *P. antarctica* contribution during these cruises is very low because it occurs more abundantly in deeply mixed waters (Alderkamp, Kulk, Buma, *et al.*, 2012). The results show no constant trend between *P. Antarctica* and $\delta^{13}C_{POC}$ although there is a significant positive relationship during SANAE 56, where $\delta^{13}C_{POC}$ values increase, indicating decreasing in fractionation, with a higher contribution of *P. Antarctica* along the transect and. This positive relationship is also observed during WC 2015 (Figure 4.14-D) although there is no significant correlation. Due to the non-uniform results shown by phytoplankton groups during different seasons, it can be argued that although fractionation could be specific to one phytoplankton group, the overall process can be controlled by interacting factors such as temperature, nutrient availability and the cell size of phytoplankton.

5.1.4. Temperature, salinity and pCO_2

During the summer months, the temperature has a positive relationship to $\delta^{13}C_{POC}$, as the temperature increase from south to north, the $\delta^{13}C_{POC}$ becomes less negative, resulting in a decrease in fractionation. Temperature does have a significant correlation with $\delta^{13}C_{POC}$, although temperature most likely influences a large variety of cellular functions. It is not realistic to expect one a simple mechanism to be completely responsible for the fractionation effect observed in these results. During the WC 2015, temperature shows a non-significant, negative relationship towards $\delta^{13}C_{POC}$ as the $\delta^{13}C_{POC}$ values decrease with increasing fractionation. Salinity shows positive relationships towards $\delta^{13}C_{POC}$ during SANAE 54 and SANAE 56, thus with increasing surface salinity, the fractionation decreases. During WC 2015, there is no correlation between salinity and $\delta^{13}C_{POC.}$ Here, salinity was used as a parameter for water masses, therefore if a relationship was found, then the distribution of $\delta^{13}C_{POC}$ would be as a result of physical mixing of

water masses, it is thus not the case and it can be said that the distribution is caused by not only physical factors, but biological factors as well.

The dramatic change in [$CO_{2(aq)}$] and its isotopic signature can directly affect the sensitivity of $\delta^{13}C_{POC}$. The Suess effect can be described as the phenomenon where the $\delta^{13}C_{DIC}$ decreases due to the invasion of anthropogenic CO_2 which is enriched in the lighter carbon isotope, ^{12}C (Keeling, 1979). The anthropogenic CO_2 invasion into the world's oceans has led to a decrease in $\delta^{13}C_{DIC}$. An increase in seawater pCO_2 correlates with increasing DIC at higher temperatures, and an increase in pCO_2 (assuming an equilibrium climate sensitivity) in warmer waters, would increase the fractionation by approximately 1.8‰ for cells > 10 µm (Tuerena *et al.*, 2019). Thereby it can be argued that temperature affects the pCO_2, which affects the cell size of phytoplankton, which can influence the fractionation during the photosynthetic uptake of carbon. All three cruises show a non-significant negative relationship between pCO_2 and $\delta^{13}C_{POC,}$ thus with increasing pCO_2 concentration in the surface water, the fractionation may increase, but the results are not significant. The pCO_2 concentrations increase with decreasing temperatures along the transect, with the highest pCO_2 concentration just south of the SBdy in the proximity of the ice during the WC 2015. SANAE 54 shows three pCO_2 peaks along the Good Hope line and SANAE 56 shows a peak in the SAZ, then again south of the SBdy along the transect.

The pCO_2 was chosen to be one of the prime parameters to measure against $\delta^{13}C_{POC}$ to improve the understanding of the pCO_2 – fractionation relationship. pCO_2 needs to be reconstructed over past glacial-interglacial cycles to improve understanding of past climatic conditions, knowledge that is used for future climate predictions. It is not possible to measure the pCO_2 directly in marine sediments. Therefore, a prediction was made that the carbon isotopic signature will significantly correlate to pCO_2 and can be used to reconstruct the pCO_2 in marine sedimentary archives. However, the results obtained for the cruises that took place along the Good Hope line in the Southern Atlantic Ocean show no significant correlation between pCO_2 and $\delta^{13}C_{POC.}$

5.2. Indian Ocean (WC 2017)

5.2.1. Potential of macronutrients as drivers for $\delta^{13}C_{POC}$ distribution

A different transect was done during WC 2017 than those of the previous three cruises. The ship departed in Cape Town (Atlantic Ocean) and steamed to the Atlantic Indian Ocean at 30ºE. PO_4 and NO_3 seem to be almost depleted in the subtropical waters south of the STF and begin to increase at approximately 40ºS, where $Si(OH)_4$ only begins to increase when the PF is crossed at 49.3ºS. Maximum concentrations of all four nutrients can be seen south of the PF to the ice shelf. These increased nutrient concentrations correlate with low biomass south of the PF, thereby the nutrients are not being utilized by phytoplankton in this region. This weak depletion of nutrients in the surface water may result from less biological uptake because of the slower growth rate in the winter, alternatively; trace element limitation. A slower growth rate in the winter period is most likely the result of colder temperature and light limitation, which may be the result of depleted iron in the surface ocean. All four nutrients have a significant negative relationship with $\delta^{13}C_{POC}$. As the nutrient concentrations increase from north to south, the $\delta^{13}C_{POC}$ decreases, indicating that the fractionation increases, which contradicts the above-mentioned slower growth rate.

5.2.2. POC and chlorophyll-a as indicators for $\delta^{13}C_{POC}$ distribution

During the winter months, lower chlorophyll-a concentrations were found, compared to the summer. POC and Chl-a can be used as an indication of biomass and phytoplankton abundance. Chl-a shows a significant positive relationship with $\delta^{13}C_{POC}$. As chl-a decreases from north to south, $\delta^{13}C_{POC}$ decreases indicating that fractionation increases. The three-dominant phytoplankton groups along the transect are *P. antarctica*, prasinophytes and cryptophytes which all have similar trends along the transect as chl-a and all show positive significant correlations to $\delta^{13}C_{POC}$. These three dominant groups decrease from north to south with increased fractionation taking place. Diatoms are the most abundant phytoplankton group present south of the PF. It can thus be speculated that the trend in POC and chl-a affect the phytoplankton community distribution along the transect which affects the nutrient distribution along the transect and eventually the $\delta^{13}C_{POC}$.

5.2.3. Temperature, salinity and pCO_2

Temperature and salinity relationships for WC 2017 follow the same trend as the previous cruises with decreasing temperature and salinity from north to south. During this cruise, both temperature and salinity were significantly correlated to $\delta^{13}C_{POC}$, which indicates that both can be a driving factor for $\delta^{13}C_{POC}$, although it has previously discussed (section 5.1.4) that temperature alone may not be a primary indicator for the isotopic signature. The temperature influences several physical-

and biological cycles within the ocean that has an influence on the fractionation during photosynthesis.

pCO_2 within the Indian sector of the SO shows some expected results as it has a significant correlation with $\delta^{13}C_{POC}$. Increasing pCO_2 is due to higher atmospheric carbon dioxide concentrations as well as changes in dissolution (Hauck, 2012). The highest concentration can be observed in the middle of the AAZ. The influence here may be attributed to water temperature (Hauck *et al.*, 2015). With increasing pCO_2 concentrations along the transect, the fractionation increases and no other parameter during this cruise, except for diatoms show a similar negative relationship with $\delta^{13}C_{POC}$ along the transect. This wintertime correlation in the Indian Southern Ocean contrasts the findings along the Good Hope line in the Southern Atlantic Ocean that showed no significant correlation between pCO_2 and $\delta^{13}C_{POC.}$

6. Conclusion

There are several physical- and chemical parameters that may have an influence on the fractionation of particulate organic carbon by marine phytoplankton in the SO. Certain environmental- and biological factors may also affect the parameters focused on in this study. From South Africa towards Antarctica along the Good Hope line as well as in the Indian sector, during winter and summer, several environmental factors played a role in determining $\delta^{13}C_{POC}$.

The results correlate with global trends that macronutrient concentrations in the surface water, increase from north to south in the SO. Macronutrients ($Si(OH)_4$ and NO_3) were significantly negatively correlated with $\delta^{13}C_{POC,}$ although this correlation may not be explained by the macronutrients alone. Macronutrients, however, have a direct effect on the distribution and abundance of certain phytoplankton groups, therefore affecting the total phytoplankton community structure within the SO and these changes in community structure may be the reason for changes in $\delta^{13}C_{POC.}$ Temperature that was significantly positively correlated with $\delta^{13}C_{POC}$ may also either directly impact fractionation and/or indirectly influence the phytoplankton community composition. Salinity shows to have no effect on the $\delta^{13}C_{POC,}$ except during WC 2017, where the salinity increased with increasing $\delta^{13}C_{POC,}$ following decreasing fractionation.

Phytoplankton groups are likely responsible for the variation of $\delta^{13}C_{POC}$ values observed. Biological factors, such as the type of RUBISCO enzyme, CCM's, cell size, growth rate and composition play a role in how the different phytoplankton groups take up carbon during photosynthesis, therefore resulting in different fractionation processes. During the summer months in the Atlantic SO, cyanobacteria and diatoms show to have a positive and negative, respectively, relationship with $\delta^{13}C_{POC}$. The diatom chl-a concentration increases from north to south as the $\delta^{13}C_{POC}$ decreases, a result of increased fractionation; while decreased fractionation results in increasing $\delta^{13}C_{POC}$ values in the subtropical waters where cyanobacteria concentrations are higher. Yet again, the results obtained, show that phytoplankton groups do influence the fractionation, however, the exact extent of these influences is not known and requires more research.

Previous research showed an increase in dissolved CO_2 concentrations with a decrease in temperature. This is due to greater solubility of CO_2 in colder water, thereby increasing the pCO_2 in the surface ocean. The pCO_2 results obtained in this study correspond to previous studies where the $\delta^{13}C_{POC}$ is lower in high CO_2 environments, i.e. in colder waters of the high latitudes, likely as a result of increased fractionation in phytoplankton. Although from these results we cannot state that pCO_2 is a direct driving factor of the carbon isotopic signature, as other physical factors are influencing these results. Past CO_2 concentrations can be used to understand past

climatic conditions. It is important to study these conditions as it can result in predicting future changes. The fractionation of stable carbon isotopes can be used to estimate these CO_2 concentrations and play an important role in identifying and modelling changes in the global carbon cycle. It is important to study the wide range of biological factors, to find out what the main driving factor of $\delta^{13}C_{POC}$ would be. This study showed a wide range of factors that are significantly correlated with $\delta^{13}C_{POC}$ and can influence the fractionation.

7. Recommendations

To improve the results and the understanding of this study, my recommendations would firstly be to focus only on one region in the Southern Ocean, or at least to compare two different seasons in different sections, if that is required. Data should be taken specifically for this study to avoid results obtained during WC 2015 and SANAE 2017, where a complete picture of potential driving factors cannot be seen due to a lack of data at certain points. Secondly, I would recommend to also bring factors such as cell size and biological activity into consideration as the cell size of phytoplankton plays a huge role in their ability to take up carbon as well as their fractionation ability. I would also recommend to include incubation studies done on the Good Hope line and in the Indian sector of the Southern Ocean because it would be interesting to see what happens in a controlled environment, as it is difficult to see precise results in such a complex environment with so many role-playing factors as seen in the ocean. Furthermore, it will be beneficial to investigate different relationships (not just linear relationships) between the factors used in this study and the $\delta^{13}C_{POC}$ and also the effect they might have on eachother, thereby affecting the $\delta^{13}C_{POC}$. Lastly I would recommend to study the distribution of the $\delta^{13}C_{POC}$ in the core top sediments and compare it to the modern day upper ocean distrubiiton on these parameters.

Bibliography

Alderkamp, A.C., Kulk, G., Buma, A.G.J., Visser, R.J.W., Van Dijken, G.L., Mills, M.M. & Arrigo, K.R. 2012. The effect of iron limitation on the photophysiology of phaeocystis antarctica (prymnesiophyceae) and fragilariopsis cylindrus (bacillariophyceae) under dynamic irradiance. *Journal of Phycology*. 48(1):45–59.

Allègre, C. 2008. *Isotope Geology*. First edition. Cambridge: Cambridge University Press.

Andrews, J., Brimblecombe, P., Jickells, T.D., Liss, P. & Reid, B. 2004. *An Introduction to Environmental*. 2nd editon. Malden: Blakwell Publishers.

Arrigo, K.R. & van Dijken, G.L. 2015. Continued increases in Arctic Ocean primary production. *Progress in Oceanography*. 136:60–70.

Arrigo, K.R., Robinson, D.H., Worthen, D.L., Dunbar, R.B., DiTullio, G.R., VanWoert, M. & Lizotte, M.P. 1999. Phytoplankton community structure and the drawdown of nutrients and CO_2 in the Southern Ocean. *Science*. 283(5400):365–367.

Bathmann, U., Scharek, R., Klaas, C., Dubischar, C. & Smetacek, V. 1996. Spring development of phytoplankton biomass and composition in major water masses of the Atlantic sector of the Southern Ocean. *Deep-Sea Research Part II*. 44(1-2):51-67.

Boller, A.J., Thomas, P.J., Cavanaugh, C.M. & Scott, K.M. 2011. Low stable carbon isotope fractionation by coccolithophore RubisCO. *Geochimica et Cosmochimica Acta*. 75(22):7200–7207.

Boschker, H.T.S., Kromkamp, J.C. & Middelburg, J.J. 2005. Biomarker and carbon isotopic constraints on bacterial and algal community structure and functioning in a turbid, tidal estuary. *Limnology and Oceanography*. 50(1):70–80.

Bousquet, P., Peylin, P. & Ciais, P. 2000. Regional Changes in Carbon Dioxide Fluxes of Land and Oceans Since 1980. 290(November):1342–1346.

Burkhardt, S., Riebesell, U. & Zondervan, I. 1999. Stable carbon isotope fractionation by marine phytoplankton in response to daylength, growth rate, and CO_2 availability. *Marine Ecology Progress Series*. 184:31–41.

Caldeira, K. & Duffy, P.B. 2000. The Role of the Southern Ocean in Uptake and Storage of Anthropogenic Carbon Dioxide. 287(January):620–622.

Cermeno, P., Dutkiewicz, S., Harris, R.P., Follows, M., Schofield, O. & Falkowski, P.G. 2008. The role of nutricline depth in regulating the ocean carbon cycle. *Proceedings of the National Academy of Sciences*. 105(51):20344–20349.

Church, M., Hutchins, D. & Ducklow, H. 1990. Limitation of bacterial growth by dissolved organic matter in the subarctic Pacific. *Marine Ecology Progress Series*. 62(1–2):47–54.

Clarke, A. & Leakey, R.J.G. 1996. The seasonal cycle of phytoplankton, macronutrients, and the microbial community in a nearshore Antarctic marine ecosystem. *Limnology and Oceanography*. 41(6):1281–1294.

Coale, K.H., Johnson, K.S., Chavez, F.P., Buesseler, K.O., Barber, R.T., Brzezinski, M.A., Cochlan, W.P., Millero, F.J., *et al*. 2004. Southern Ocean Iron Enrichment Experiment: Carbon Cycling in High- and Low-Si Waters. *Science*. 304(April):408–414.

Condie, K.. 2016. *Earth as an Evolving planetary system*. Third Edition. Academic Press.

Cooper, T., Filmer, D., Wishnick, M. & Lane, M. 1969. The active species of "CO_2"" utilized by Ribulose diphosphate carboxylase". *Journal of Biological Chemistry*. 244(4):1080–1083.

CSIRO. 2002. Australian Antarctic magazine. *In deep Australian research in the Southern Ocean*. [Online]. Available: https://www.antarctica.gov.au/magazine/issue-4-spring-2002/feature2/the-southern-oceans-global-reach/ [2018, August 2].

Davis, S.J. & Caldeira, K. 2010. Consumption-based accounting of CO_2 emissions. *PNAS. 107(12)*:5687-5692.

Deppeler, S.L. & Davidson, A.T. 2017. Southern Ocean Phytoplankton in a Changing Climate. *Frontiers in Marine Science.* 4(February):1-40.

Doney, S.C., Lindsay, K. & Moore, J.K. 2003. Global Ocean Carbon Cycle Modeling in M.J.R. Fasham (eds). *Ocean Biogeochemsitry*. Berlin: Springer. 217–238.

Duckiow, H.W., Steinberg, D.K. & Buesseler, K.O. 2001. Upper Ocean Carbon Export and the Biological Pump. *Oceanography.* 14(4):56008–56016.

Egan, K.E., Rickaby, R.E.M., Leng, M.J., Hendry, K.R., Hermoso, M., Sloane, H.J., Bostock, H. & Halliday, A.N. 2012. Diatom silicon isotopes as a proxy for silicic acid utilisation: A Southern Ocean core top calibration. *Geochimica et Cosmochimica Acta*. 96:174–192.

Endo, H., Ogata, H. & Suzuki, K. 2018. Contrasting biogeography and diversity patterns between diatoms and haptophytes in the central Pacific Ocean. 8:1–13.

Eynaud, F., Giraudeau, J., Pichon, J-J. & Pudsey, C.J. 1999. Sea-surface distribution of coccolithophores, diatoms, silicoflagellates and dinoflagellates in the South Atlantic Ocean during the late austral summer 1995. *Deep Sea Research Part I: Oceanographic Research Papers*. 46(3):451–482.

Field, A. 2009. *Discovering statistics using SPSS*. Third ed. London: SAGE Publications Ltd.

Fielding, A.S., Turpin, D.H., Guy, R.D., Calvert, S.E., Crawford, D.W. & Harrison, P.J. 1998. Influence of the carbon concentrating mechanism on carbon stable isotope discrimination by the marine diatom Thalassiosira pseudonana. *Canadian Journal of Botany*. 76(6):1098–1103.

Finkel, Z. V., Beardall, J., Flynn, K.J., Quigg, A., Rees, T.A. V. & Raven, J.A. 2010. Phytoplankton in a changing world: Cell size and elemental stoichiometry. *Journal of Plankton Research*. 32(1):119–137.

Fischer, G. 1991. Stable carbon isotope ratios of plankton carbon and sinking organic matter from the Atlantic sector of the Southern Ocean. *Marine Chemistry*. 35(1–4):581–596.

Fontugne, M.R. 1981. Organic carbon isotopie fractionation by tnarine plankton in the tetnperature range -1 to 31ºC. *Oceanologica Acta.* 4(1):85-90.

Fontugne, M., Descolas-Gros, C. & de Billy, G. 1991. The dynamics of CO_2 fixation in the Southern Ocean as indicated by carboxylase activities and organic carbon isotopic ratios. *Marine Chemistry*. 35(1–4):371–380.

Freeman, H. & Hayes, J.M. 1992. Fractionation of carbon isotopes by phytoplankton and estimates of ancient CO_2 levels. *Glob. Biogeochem. Cycles*. 6(2):185–198.

Fritz, P. & Buchardt, B. 1980. Environmental isotopes as environmental and climatological indicators in P. Fritz & J.C. Fontes (eds.). *Handbook of Environmental Isotope Geochemistry.* 1st ed. Amsterdam: Elsevier.

Fry, B. 1996. 13C/12C fractionation by marine diatoms. *Marine Ecology Progress Series*. 134(1–3):283–294.

Fry, B. & Wainright, S.C. 1991. Diatom sources of ^{13}C-rich carbon in marine food webs. *Marine Ecology Progress Series*. 76(2):149–157.

García-Robledo, E., Corzo, A. & Papaspyrou, S. 2014. A fast and direct spectrophotometric method for the sequential determination of nitrate and nitrite at low concentrations in small volumes. *Marine Chemistry*. 162(3):30–36.

Gillott, M.A. & Gibbs, S.P. 1980. The cryptomonad nucleomorph: its ultrastructure and evolutionary significance. *Journal of Phycology*. 16(4):558–568.

Graham, R.M. 2013. Marine Geology The Location and Variability of Southern Ocean Fronts. Published doctoral dissertation. Stockholm.

Graham, R.M., Boer, A.M. De, Heywood, K.J., Chapman, M.R. & Stevens, D.P. 2012. Southern Ocean fronts: Controlled by wind or topography? *Journal of Geophysical Research.* 117:1–14.

Grasshof, K., Kremling, K. & Ehrhard, M. 1983. *Methods of seawater Analysis*. Weinheim: Wiley-VCH.

Hansell, D.A. & Carlson, C.A. 2015. *Biogeochemistry of marine dissolved organic matter*. Second edition. Miami: Elsevier.

Hauck, J. 2012. Processes in the Southern Ocean carbon cycle: Dissolution of carbonate sediments and inter-annual variability of carbon fluxes. Published doctoral dissertation. Universität Breman.

Hauck, J., Völker, C., Laufkötter, C., Vogt, M., Aumont, O., Bopp, L., Buitenhuis, E.T., Doney, S.C., *et al*. 2015. On the Southern Ocean CO_2 uptake and the role of the biological carbon pump in the 21st century. *Global Biogeochemical Cycles*. 29:1451–1470.

Hayes, J.M. 1993. Factors controlling ^{13}C contents of sedimentary organic compounds: Principles and evidence. *Marine Geology*. 113(1-2):111-125.

Helbling, E.W. & Villafañe, V.E. 2009. Phytoplankton and primary production. *Fisheries and aquaculture*. 5:206–226.

Henley, S.F., Annett, A.L., Ganeshram, R.S., Carson, D.S., Weston, K., Crosta, X., Tait, A., Dougans, J., *et al*. 2012. Factors influencing the stable carbon isotopic composition of suspended and sinking organic matter in the coastal Antarctic sea ice environment. *Biogeosciences*. 9(3):1137–1157.

Henson, S.A., Cole, H.S., Hopkins, J., Martin, A.P. & Yool, A. 2018. Detection of climate change-driven trends in phytoplankton phenology. *Global Change Biology*. 24(1):e101–e111.

Hibberd, D.J., Greenwood, A.D. & Griffiths, H.B. 1971. Observations on the ultrastructure of the flagella and periplast in the Cryptophyceae. *British Phycological Journal*. 6(1):61–72.

Hinga, K.R., Arthur, M.A., Pilson, M.E.Q. & Whitaker, D. 1994. Carbon isotope fractionation by marine phytoplankton in culture: The effects of CO_2 concentration, pH, temperature, and species. *Global Biogeochemical Cycles*. 8(1):91–102.

Hoefs, J. 2009. *Stable Isotope Geochemistry*. 6th ed. Berlin Heidelberg: Springer.

Hoins, M., Eberlein, T., Van de Waal, D.B., Sluijs, A., Reichart, G.J. & Rost, B. 2016. CO_2-dependent carbon isotope fractionation in dinoflagellates relates to their inorganic carbon fluxes. *Journal of Experimental Marine Biology and Ecology*. 481:9–14.

Huang, G., Chen, F., Kuang, Y., He, H. & Qin, A. 2016. Current Techniques of Growing Algae Using Flue Gas from Exhaust Gas Industry: a Review. *Applied Biochemistry and Biotechnology*. 178(6):1220–1238.

Keeling, C.D. 1979. The Suess effect: 13Carbon-14Carbon interrelations. *Environment International*. 2(4–6):229–300.

Landschützer, P., Gruber, N., Haumann, F.A., Rödenbeck, C., Bakker, D.C.E., Heuven, S. Van, Hoppema, M., Metzl, N., *et al*. 2015. Ocean carbon sink. *Science*. 349(6253):1221–1224.

Laubscher, R.K., Perissinotto, R. & McQuaid, C.D. 1993. Phytoplankton production and biomass at frontal zones in the Atlantic sector of the Southern Ocean. *Polar Biology*. 13(7):471–481.

Laws, E.A. & Bidigare, R.R. & Popp, BN. 1997. Effect of Growth Rate and CO_2 Concentration on Carbon Isotopic Fractionation by the Marine Diatom Phaeodactylum tricornutum. *Limnology and Oceanography*. 42(7):1552–1560.

Laws, E.A., Popp, B.N., Bidigare, R.R., Kennicutt, M.C. & Macko, S.A. 1995. Dependence of phytoplankton carbon isotopic composition on growth rate and $[CO_{2(aq)}]$: Theoretical considerations and experimental results. *Geochimica et Cosmochimica Acta*. 59(6):1131–1138.

Leeuwe, M.A. Van, Visser, R.J.W. & Stefels, J. 2014. The Pigment Composition Of Phaeocystis Antarctica (Haptophyceae) Under Various Conditions Of Light, Temperature, Salinity, And Iron. *J. Phycol.* 50:1070–1080.

Lourey, M.J., Trull, T.W. & Tilbrook, B. 2004. Sensitivity of δ13C of Southern Ocean suspended and sinking organic matter to temperature, nutrient utilization, and atmospheric CO2. *Deep-Sea Research Part I: Oceanographic Research Papers*. 51(2):281–305.

Mahowald, N.M., Baker, A.R., Bergametti, G., Brooks, N., Duce, R.A., Jickells, T.D., Kubilay, N., Prospero, J.M., *et al*. 2005. Atmospheric global dust cycle and iron inputs to the ocean. *Global Biogeochemical Cycles*. 19(4).

McClelland, H.L.O., Bruggeman, J., Hermoso, M. & Rickaby, R.E.M. 2017. The origin of carbon isotope vital effects in coccolith calcite. *Nature communications*. 8:14511.

Mitchell, B., Brody, E., Holm-Hansen, O., McClain, C. & Bishop, J. 1991. Light limitation of phytoplankton biomass and macronutrient utililization in the Southern Ocean. *Limnology and Oceanography.* 36(8):1662–1677.

Monteiro, F.M., Bach, L.T., Brownlee, C., Bown, P., Rickaby, R.E.M., Poulton, A.J., Tyrrell, T., Beaufort, L., et al. 2016. Why marine phytoplankton calcify. *Science Advances*. 2(7):1-14.

Monteiro, P., Ansorge, I., Fietz, S., Thomalla, S., Swart, S., Roychoudhury, R., Mtshali, T., Fawcett, S., *et al*. 2015. *Winter 2015 Cruise Report* SA Agulhas II. [Cape Town].

Mook, W.G., Bommerson, J.C. & Staverman, W.H. 1974. Carbon isotope fractionation between dissolved bicarbonate and gaseous carbon dioxide. *Earth and Planetary science letters*. 22(2):169–176.

Moore, J.K. & Abbot, M.R. 2000. Phytoplankton chlorophyll distributions and primary production in the Southern Ocean mean chlorophyll concentrations remained quite Phytoplankton blooms where chlorophyll concentration exceeded at midlatitudes. *Journal of Geophysical Research.* 105(C12):709-722.

Moore, J.K., Abbott, M.R. & Richman, J.G. 1999. Location and dynamics of the Antarctic Polar Front from satellite sea surface temperature data. *Journal of Geophysical Research.* 104(C2):3059–3073.

Morée, A.L., Schwinger, J. & Heinze, C. 2018. Southern Ocean controls of the vertical marine δ13C gradient-a modelling study. *Biogeosciences*. 15(23):7205–7223.

Moroney, J. V. & Ynalvez, R.A. 2007. Proposed Carbon Dioxide Concentrating Mechanism in Chlamydomonas reinhardtii . *Eukaryotic Cell*. 6(8):1251–1259.

O'Leary, M.H., Madhavan, S. & Paneth, P. 1992. Physical and chemical basis of carbon isotope fractionation in plants. *Plant, Cell & Environment*. 15(9):1099–1104.

Palinska, K.A. & Surosz, W. 2014. Taxonomy of cyanobacteria: a contribution to consensus approach. *Hydrobiologia*. 740(1):1–11.

Park, R. & Epstein, S. 1960. Carbon isotope fractionation during photosynthesis. *Geochim. et cosmochim. acta*. 21.

Passow, U. & Carlson, C.A. 2012. The biological pump in a high CO_2 world. *Marine Ecology Progress Series.* 470(2):249–271.

Pienaar, Z. 2017. Stable carbon isotope fractionation by marine phytoplankton in the Southern Ocean. Stellenbosch University.

Pierrot, D., Neill, C., Sullivan, K., Castle, R., Wanninkhof, R., Lüger, H., Johannessen, T., Olsen, A., et al. 2009. Recommendations for autonomous underway pCO2 measuring systems and data-reduction routines. *Deep-Sea Research Part II: Topical Studies in Oceanography*. 56(8–10):512–522.

Pollard, R.T., Salter, I., Sanders, R.J., Lucas, M.I., Moore, C.M., Mills, R.A., Statham, P.J., Allen, J.T., *et al*. 2009. Southern Ocean deep-water carbon export enhanced by natural iron fertilization. *Nature*. 457(7229):577–580.

Popp, B.N., Trull, T., Kenig, F., Wakeham, S.G., Rust, T.M., Tilbrook, B., Griffiths, B., Wright, S.W., et al. 1999. Controls on the carbon isotopic composition of Southern Ocean phytoplankton. *Glob. Biogeochem. Cycles*. 13(4):827–843.

Price, G.D. & Badger, M.R. 1989. Isolation and characterization of high CO_2-requiring-mutants of the cyanobacterium Synechococcus PCC7942. *Plant Physiol.* 91:514–525.

Puerta, M.V.S., Bachvaroff, T.R. & Delwiche, C.F. 2005. The complete plastid genome sequence of the haptophyte Emiliania huxleyi: A comparison to other plastid genomes. *DNA Research*. 12(2):151–156.

Rau, G.H., Riebesell, U. & Wolf-Gladrow, D. 1996. A model of photosynthetic 13C fractionation by marine phytoplankton based on diffusive molecular CO_2 uptake. *Marine Ecology Progress Series*. 133(1–3):275–285.

Rau, G.H., Riebesell, U. & Wolf-Gladrow, D. 1997. $CO_{2(aq)}$-dependent photosynthetic 13C fractionation in the ocean: A model versus measurements. *Global Biogeochemical Cycles*. 11(2):267–278.

Raven, J., Johnston, A.M. & Turpin, D.H. 1993. Influence of changes in CO2 concentration and temperature on marine phytoplankton 13C/12C ratios: an analysis of possible mechanisms. *Global and Planetary Change*. 8(1–2):1–112.

Raven, J., Cockell, C. & De La Rocha, C. 2008. The evolution of inorganic carbon concentrating mechanisms in photosynthesis. *Philosophical Transactions of the Royal Society B: Biological Sciences*. 363(1504):2641–2650.

Repeta, D. & Eglinton, T. *Marine Organic Geochemistry*. [Online]. 2005. Available: https://ocw.mit.edu [2018, August 11].

Roy-Barman, M. & Jeandel, C. 2016. *Marine Geochemistry Ocean Circulation, Carbon Cycle and Climate Change*. First edition. New York: Oxford University Press.

Russel, J.. 2006. The Southern Hemisphere Westerlies in a Warming World : Propping Open the Door. *Journal of Climate*. 19:6382–6390.

Sabine, C.L., Feely, R.A., Gruber, N., Key, R.M., Bullister, J.L., Wanninkhof, R., Wong, C.S., Wallace, D.W.R., et al. 2004. The oceanic sink for anthropogenc CO_2. 1–18.

Sarmiento, J.L. & Gruber, N. 2004. Carbon Cycle, CO_2, and Climate. *Ocean Biogeochemical Dynamics.* Princeton: Princeton University Press. 392-460.

Sarnthein, M., Winn, K., Duplessy, J. & Fontugne, M.R. 1988. Global variations of surface ocean productivity in low and mid latitudes: Influence on CO_2 reservoirs of the deep ocean and atmosphere during the last 21,000 years. *Paleoceanography and Paleoclimatology*. 3(3):361–399.

Sathyendranath, S., Platt, T., Brewin, R.J.W. & Jackson, T. 2019. Primary Production Distribution. *Encyclopedia of Ocean Sciences*. (January, 1):635–640.

Schabhüttl, S., Hingsamer, P., Weigelhofer, G., Hein, T., Weigert, A. & Striebel, M. 2013. Temperature and species richness effects in phytoplankton communities. *Oecologia*. 171(2):527–536.

Schlitzer, R. 2016. [Online], Available: http://odv.awi.de. [2019, February 3].

Schlüter, L., Henriksen, P., Nielsen, T.G. & Jakobsen, H.H. 2011. Phytoplankton composition and biomass across the southern Indian Ocean. *Deep Sea Research Part I: Oceanographic Research Papers*. 58(5):546–556.

Schoemann, V., Becquevort, S., Stefels, J. & Lancelot, C. 2005. Phaeocystis blooms in the global ocean and their controlling mechanisms : a review. *Journal of Sea Research.* 53(1-2):43–66.

Scholes, B., Scholes, M. & Lucas, M. 2015. *Climate Change*. Johannesburg: Wits University Press.

Scott, K.M., Harmer, T.L., Henn-Sax, M., Longo, D.L., Frame, C.H. & Cavanaugh, C.M. 2007. Kinetic Isotope Effect and Biochemical Characterization of Form IA RubisCO from the Marine Cyanobacterium Prochlorococcus marinus MIT9313. *Limnology and Oceanography.* 52(5):2199–2204.

Sharkey, T.D. & Berry, J.A. 1985. Carbon isotope fractionation of algae as influenced by an inducible CO_2 concentrating mechanism in W.J. Lucas & J.A. Berry (eds). *Inorganic carbon uptake by aquatic photosynthetic organisms*. America: American Society of Plant Physiologists. 389–401.

Simon, N., Cras, A.-L., Foulon, E. & Lemée, R. 2009. Diversity and evolution of marine phytoplankton. *Comptes rendus biologies*. 332(2–3):159–170.

Smetacek, V., Klaas, C., Strass, V.H., Assmy, P., Montresor, M., Cisewski, B., Savoye, N., Webb, A., *et al*. 2012. Deep carbon export from a Southern Ocean iron-fertilized diatom bloom. *Nature.*487:313-319.

Soppa, M.A., Völker, C. & Bracher, A. 2016. Diatom Phenology in the Southern Ocean: Mean Patterns, Trends and the Role of Climate Oscillations. *Remote Sensing*. 8(420):1–17.

Swart, S., Chang, N., Fauchereau, N, et al. 2012. Southern Ocean Seasonal Cycle Experiment 2012: Seasonal scale climate and carbon cycle links. *S Afr J Sci. 2012* [Electronic], 108:3–5. Available: http:// dx.doi.org/10.4102/sajs. v108i3/4.1089 [2019, March 6]

Tabita, F.R., Satagopan, S., Hanson, T.E., Kreel, N.E. & Scott, S.S. 2008. Distinct form I, II, III, and IV Rubisco proteins from the three kingdoms of life provide clues about Rubisco evolution and structure/function relationships. *Journal of Experimental Botany*. 59(7):1515–1524.

Takahashi, T., Olafsson, J., Goddard, J.G., Chipman, D.W. & Sutherland, S.C. 1993. Seasonal variation of CO_2 and nutrients in the high-latitude surface oceans: A comparative study. *Global Biogeochemical Cycles*. 7(4):843–878.

Takahashi, T., Sweeney, C., Hales, B., Chipman, D.W., Newberger, T., Goddard, J.G., Iannuzzi, R.A. & Sutherland, S.C. 2012. The changing carbon cycle in the Southern Ocean. *Oceanography*. 25(3):26–37.

Tiwari, M., Singh, A.. & Sinha, D. 2015. Stable isotopes: Tools for understanding past climatic conditions and their applications in chemostratigraphy. *Chemostratigraphy*. 65–92.

Tréguer, P.J. 2014. The Southern Ocean silica cycle. *Comptes Rendus - Geoscience*. 346(11–12):279–286.

Tuerena, R.E., Ganeshram, R.S., Humphreys, M.P., Browning, T.J., Bouman, H. & Piotrowski, A.P. 2019. Isotopic fractionation of carbon during uptake by phytoplankton across the South Atlantic subtropical convergence. *Biogeosciences Discussions*. 2(May):1–29.

Tynan, C.T. 1998. Ecological importance of the southern boundary of the Antarctic Circumpolar Current. *Nature*. 392(16 April):708–710.

Vichi, M. 2017. *Winter 2017 Cruise Report* SA Agulhas II Voyage 25: *Final Report*. [Cape Town]: UCT.

Viljoen, J.. 2016. Phytoplankton Pigment Analysis and CHEMTAX determination of phytoplankton community structure in the Southern Ocean. Stellenbosch University.

Viljoen, J.J., Weir, I., Fietz, S., Cloete, R. & Loock, J. 2019. Links Between the Phytoplankton Community Composition and Trace Metal Distribution in Summer Surface Waters of the Atlantic Southern Ocean. *Frontiers in Marine Sciences*. 6(June):1–17.

Wada, E., Terazaki, M., Kabaya, Y. & Nemoto, T. 1986. 15N and 13C abundances in the Antarctic Ocean with emphasis on biogeochemical structure of food web. *Mitsubishi-Kasei Institute of Life Sciences*. II(40):400–402.

Watson, A.J., Bakker, D.C.E., Ridgwell, A.J., Boyd, P.W. & Law, C.S. 2000. Effect of iron supply on Southern Ocean CO_2 uptake and implications for glacial atmospheric CO_2. *Letters of Nature*. 407(October):730–33. [Online], Available: www.nature.com.

Weir, I.J. 2018. Phytoplankton variability in the Atlantic and Indian sectors of the Southern Ocean: a biogeochemical approach. Stellenbosch University.

White, W. 2015. *Geochemistry*. First ed. Oxford: John Wiley & Sons Ltd.

Wolf-Gladrow, D.A., Riebesell, U., Burkhardt, S. & Buma, J. 1999. Direct effects of CO_2 concentration on growth and isotopic composition of marine plankton. *Tellus B: Chemical and Physical Meteorology*. 51(2):461–476.

Wong, W.W. & Sackett, W.M. 1978. Fractionation of stable carbon isotopes by marine phytoplankton. *Geochimica et Cosmochimica Acta*. 42(12):1809–1815.

Appendix A – SANAE 54

Table A.1. Descriptive analysis done on SPSS to determine the skewness and kurtosis for all parameters in SANAE 54. For a moderately normally distributed dataset, the skewness statistic should be between -1 and 1 (Section 3.1.3) and kurtosis statistic should be between -1 and 3.

Descriptive Statistics

	N	Minimum	Maximum	Mean	Std. Deviation	Skewness		Kurtosis	
	Statistic	Statistic	Statistic	Statistic	Statistic	Statistic	Std. Error	Statistic	Std. Error
$d13C_{POC}$ (‰)	47	-30.818487749929600	-20.025241691842897	-25.577268415110737	1.969128144743010	.209	.347	.974	.681
POC (µg/L)	47	5.314966716852260	241.242987761321980	81.050402531621880	59.954668557740190	.721	.347	.490	.681
NO_2 (µM)	27	.002528349846614	.381380075667661	.167975360835834	.091589767283253	.326	.448	.006	.872
NO_3 (µM)	27	.336694177200219	25.842699407673074	15.044590776730300	6.888893578935530	-.423	.448	-.559	.872
$Si(OH)_4$ (µM)	27	.585714285714286	83.571428571428570	24.908201058201062	26.162274525254620	.627	.448	-.976	.872
PO_4 (µM)	27	.063219074486345	2.339105755994769	1.220926883351967	.577286082871670	.159	.448	-.538	.872
Chl-a (µg/L)	30	.0303	.5704	.175237	.1209115	1.352	.427	2.424	.833
Cyanobacteria	30	.000000000000000	.010777229443193	.000828921503853	.002319778308247	3.540	.427	12.988	.833
Prasinophytes	30	.000000000000000	.023143051192165	.003078994297600	.006365076702419	1.936	.427	2.665	.833
Dinoflagellates	30	.000000000000000	.013279242441059	.004161239524767	.004600946827468	.484	.427	-1.322	.833
Cryptophytes	30	.000000000000000	.016169100999833	.001289565007638	.003388515726040	3.467	.427	13.132	.833
P. antarctica Total	45	.000000000000000	.092397140339017	.017226098597490	.020022402347327	1.540	.354	3.140	.695
Coccolithophores	30	.000000000000000	.195608884096146	.018543097297273	.036251176406804	4.274	.427	20.860	.833
Pelagophytes	30	.000000000000000	.008031528443099	.001379238819937	.001802651965481	2.082	.427	5.396	.833
Chlorophytes	30	.000000000000000	.000834772537929	.000049072446200	.000160036065143	4.519	.427	21.636	.833
Diatoms	30	.010894848033786	.318648636341095	.120067388440172	.092460915785455	.854	.427	-.452	.833
pCO_2 (µatm)	36	279.9683962	397.5868136	351.076269042	29.9976698369	-.759	.393	.175	.768
Temperature (ºC)	36	-1.561926667	19.797106670	3.62643532414	5.083247748556	1.882	.393	4.052	.768
Salinity	36	33.11793667	35.45360000	33.8387792592	.42655592350	2.498	.393	8.058	.768

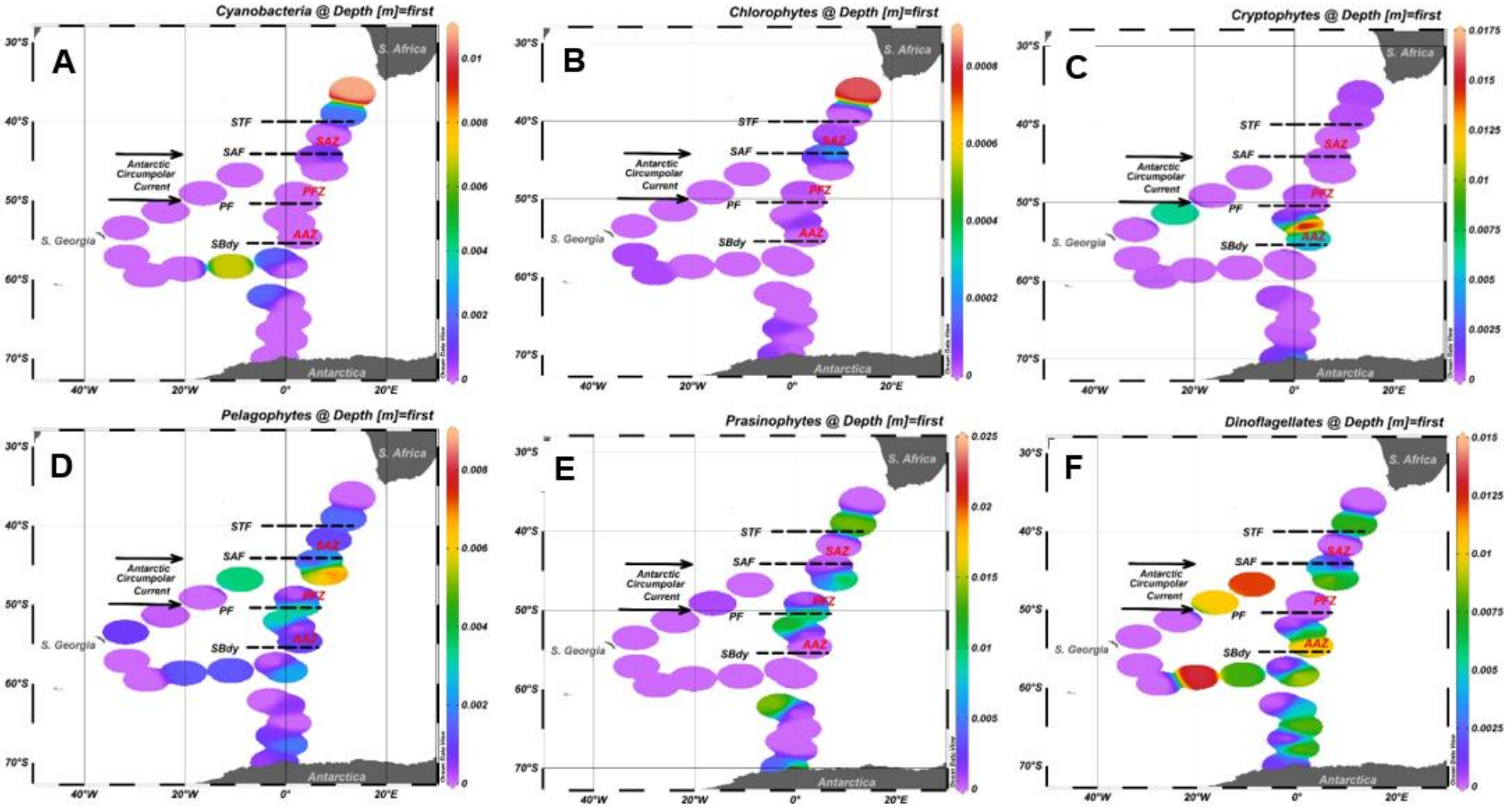

Figure A.1. Six phytoplankton groups within the surface ocean that does not have a significant correlation with $\delta^{13}C_{POC}$ during SANAE 54. Cyanobacteria (A), chlorophytes (B) and cryptophytes (C) are almost depleted along the transect expect for a small peak close to SA for cyanobacteria and chlorophytes and in the AAZ for cryptophytes. Pelagophytes (D), prasinophytes€ and dinoflagellates show more contributions, although small, along the transect. Dinoflagellates (F) show peaks on the South Georgia leg.

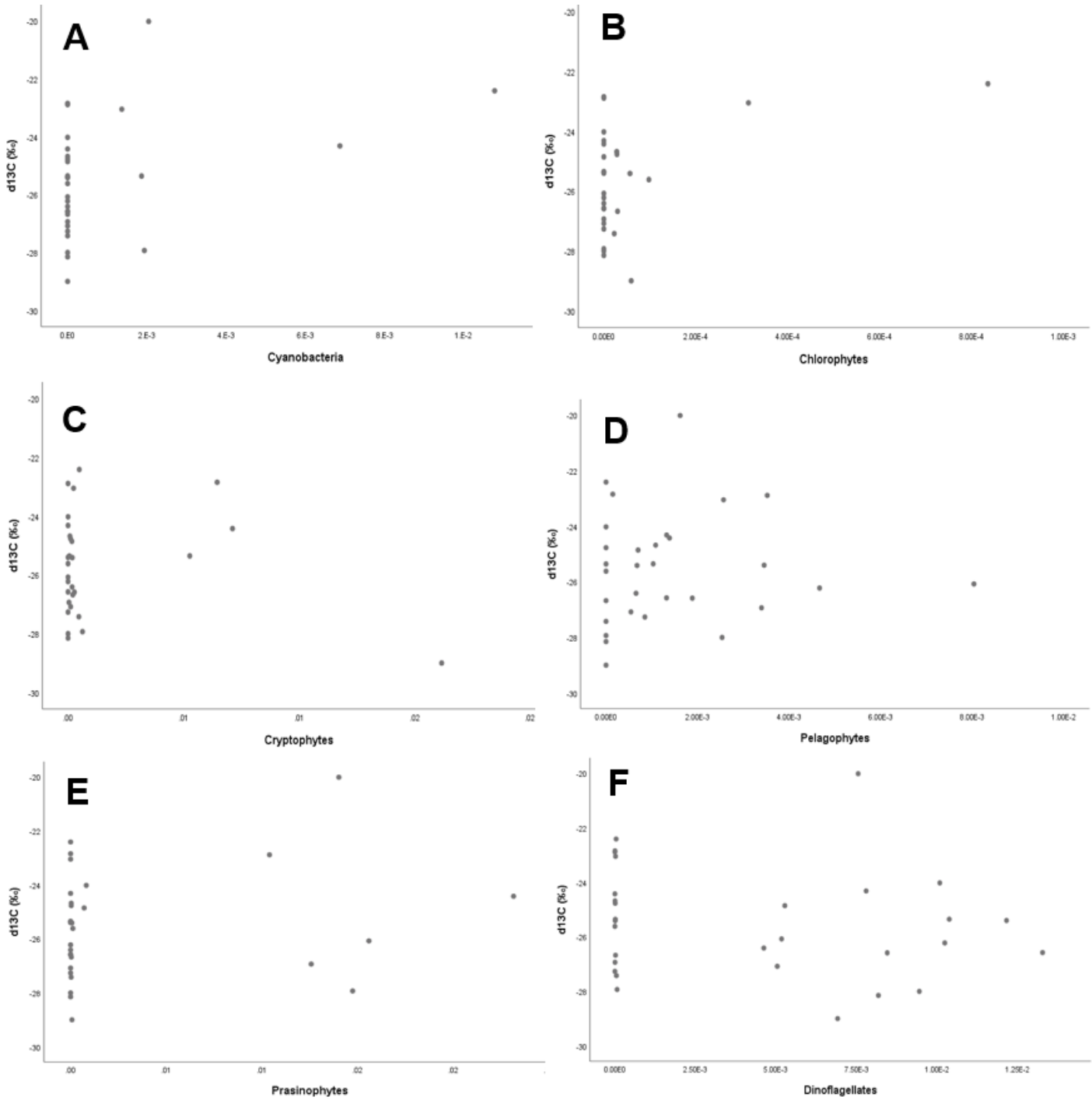

Figure A.2. Scatterplots of phytoplankton groups (phytoplankton groups's contribution to total chl-a in µg/L represented on the x-axis); cyanobacteria (A), chlorophytes (B), cryptophytes (C), pelagophytes (D), prasinophytes (E) and dinoflagellates (F) showing no significant correlation towards $\delta^{13}C_{POC}$ during the SANAE 54 voyage.

Appendix B – WC 2015

Table B.1. Descriptive statistics for data obtained during Winter Cruise 2015. Skewness- and kurtosis statistics were used to determine whether the data are normally distributed or not.

Descriptive Statistics

	N	Minimum	Maximum	Mean	Std. Deviation	Skewness		Kurtosis	
	Statistic	Statistic	Statistic	Statistic	Statistic	Statistic	Std. Error	Statistic	Std. Error
$d13C_{POC}$ (‰)	8	-27.450148139455500	-22.521372106727980	-25.404025430528560	1.453722030799201	1.011	.752	1.902	1.481
POC (µg/L)	8	52.271759605322170	101.63788608162655 0	68.759112909254000	16.320697444825186	1.262	.752	1.522	1.481
NO_3 (µM)	8	1.59600000000000	26.36800000000000	6.426206900983101	8.366352374682771	2.474	.752	6.266	1.481
NO_2 (µM)	8	.0167794	.3519337	.190971438	.1097303178	-.039	.752	-.269	1.481
$Si(OH)_4$ (µM)	8	1.10	57.60	9.0450	19.65587	2.808	.752	7.910	1.481
PO_4 (µM)	8	.107039	1.795985	.79066000	.579162937	.591	.752	-.621	1.481
Chl-a (µg/L)	5	.0765	.1387	.108000	.0256279	-.189	.913	-1.896	2.000
Cyanobacteria	5	.000000000000000	.001655651256443	.000786465359852	.000601909994262	.302	.913	1.113	2.000
Prasinophytes	5	.021567219868303	.070671483874321	.053615022078157	.019593407171212	-1.401	.913	1.973	2.000
Dinoflagellates	5	.000032085488784	.002973477588967	.001596486374911	.001443017832068	-.377	.913	-3.095	2.000
Cryptophytes	5	.000000000000000	.005874036811293	.002470662980341	.002332093113041	.602	.913	-.234	2.000
P. antarctica Total	5	.021441683173180	.052126724272967	.040046804212034	.012630155796992	-.658	.913	-.196	2.000
Coccolithophores	5	.000000000000000	.007640074472875	.003919778647833	.003173572383182	-.243	.913	-2.012	2.000
Pelagophytes	5	.000000000000000	.001857738127001	.000620139611420	.000759478723642	1.349	.913	1.925	2.000
Chlorophytes	5	.000000000000000	.004450814798475	.001265861582943	.001957451214094	1.470	.913	1.429	2.000
Diatoms	5	.000742292671931	.011987851932645	.003678778314498	.004695100006573	2.118	.913	4.582	2.000
pCO_2 (µatm)	8	347.7221388	407.3953099	367.254162125	20.1112578149	1.255	.752	1.270	1.481
Temperature (ºC)	8	-.776233333	16.750000000	10.52240333338	5.942932227919	-1.094	.752	.505	1.481
Salinity	8	33.69092667	35.59532500	34.5969618750	.66786479583	.025	.752	-1.211	1.481

Table B.2. Spearman's rho correlation test (left) between the carbon isotopic signature and particulate organic carbon, and Pearson correlation test (right) done between the carbon isotopic signature and cyanobacteria and P. antarctica during WC 2015.

			$d13C_{POC}$ (‰)	POC (µg/L)
Spearman's rho	$d13C_{POC}$ (‰)	Correlation Coefficient	1.000	-.024
		Sig. (2-tailed)	.	.955
		N	8	8

		$d13C_{POC}$ (‰)	Cyanobacteria	*P. antarctica* Total
$d13C_{POC}$ (‰)	Pearson Correlation	1	-.300	.396
	Sig. (2-tailed)		.624	.510
	N	8	5	5

Table B.3. Spearman's rho correlation done between the carbon isotopic signature and chlorophyll-a concentrations and the remaining 8 phytoplankton species in the upper layer of the SO during WC 2015.

			$d13C_{POC}$ (‰)	Chl-a (µg/L)	Prasinophytes	Dinoflagellates	Cryptophytes	Coccolitho-phores	Pelagophytes	Chlorophytes	Diatoms
Spearman's rho	$d13C_{POC}$ (‰)	Correlation Coefficient	1.000	-.400	-.700	.100	.200	-.100	-.359	-.224	.100
		Sig. (2-tailed)	.	.505	.188	.873	.747	.873	.553	.718	.873
		N	8	5	5	5	5	5	5	5	5

*. Correlation is significant at the 0.05 level (2-tailed).

**. Correlation is significant at the 0.01 level (2-tailed).

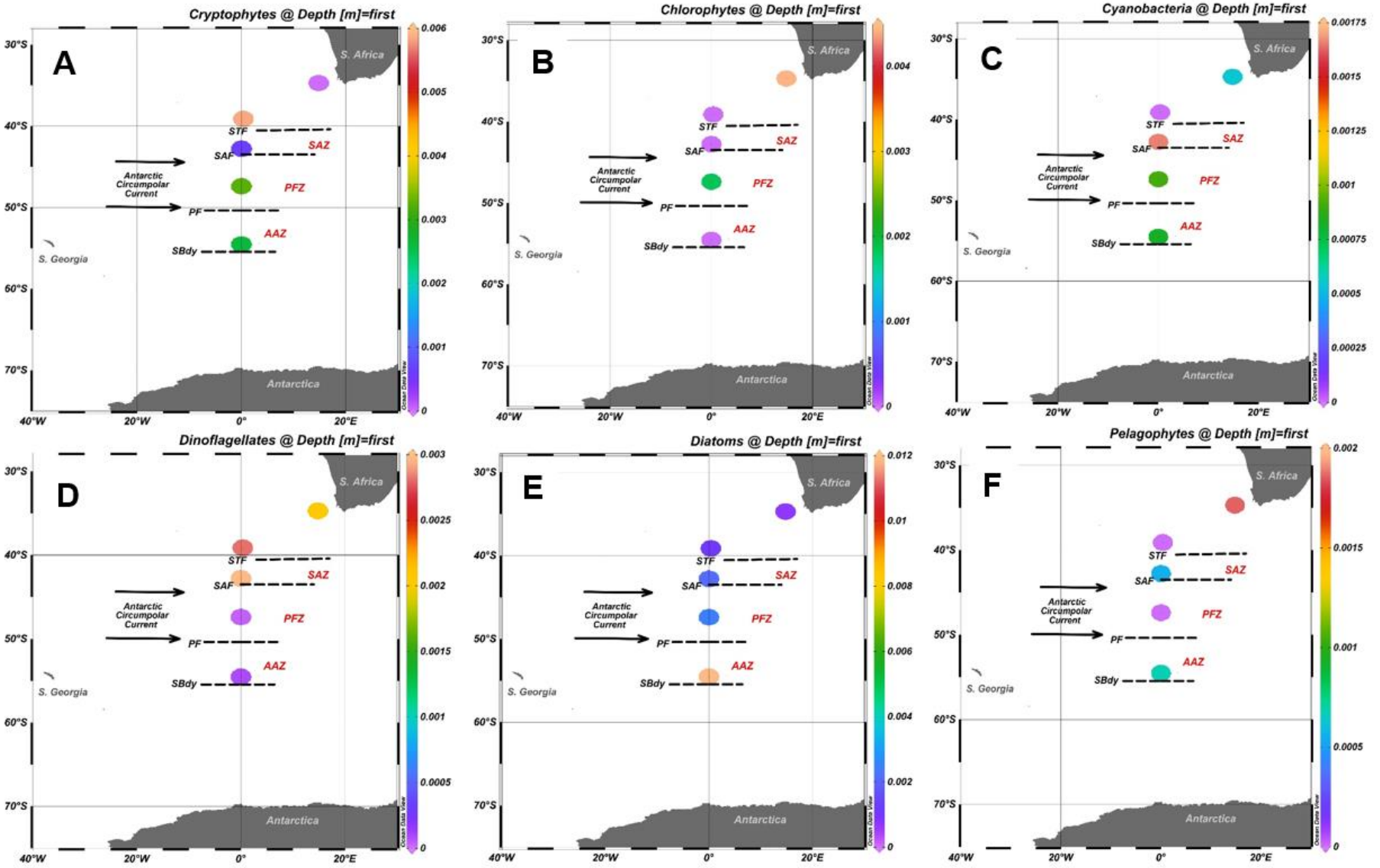

Figure B.1. Cryptophytes (A), chlorophytes (B), cyanobacteria (C), dinoflagellates (D), diatoms (E) and pelagophytes (F) distribution in the surface water of the SO during WC 2015 crossing all major fronts.

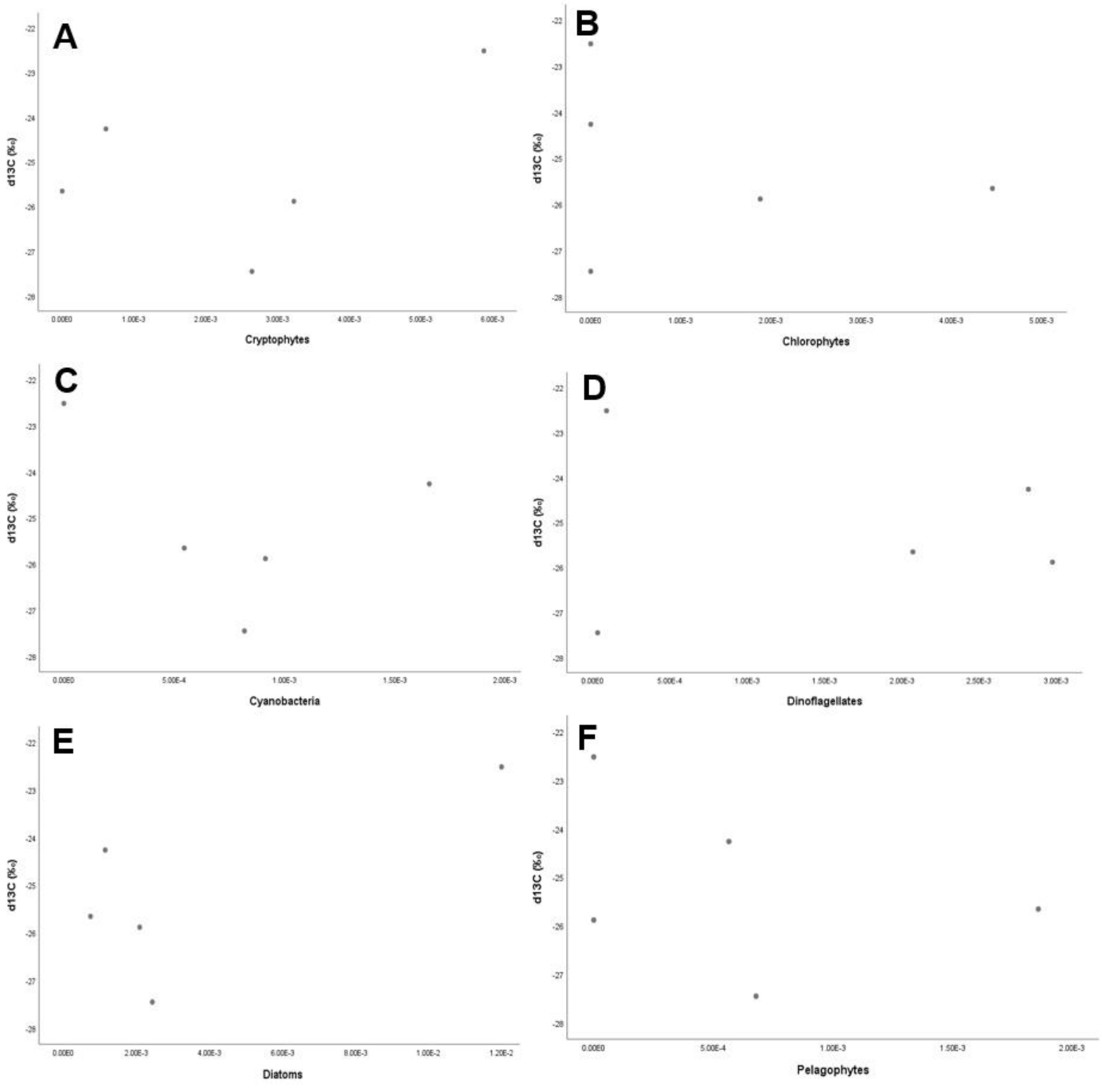

Figure B.2. Scatterplots (phytoplankton groups's contribution to total chl-a in µg/L represented on the x-axis) for phytoplankton groups; cryptophytes (A), clorophytes (B), cyanobacteria (C), dinoflagellates (D), diatoms (E) and pelagophytes (F) in the surface water of the SO during WC 2015 which show no significant correlation towards $\delta^{13}C_{POC}$.

Appendix C – SANAE 56

Table C.1. Descriptive statistics done on all parameters for SANAE 56.

Descriptive Statistics

	N	Minimum	Maximum	Mean	Std. Deviation	Skewness		Kurtosis	
	Statistic	Statistic	Statistic	Statistic	Statistic	Statistic	Std. Error	Statistic	Std. Error
d13C$_{POC}$ (‰)	26	-30.782159075907590	-23.250628382838283	-26.700642544639077	1.885565374021405	-.027	.456	-.152	.887
POC (µg/L)	24	8.02	23.08	15.2933	3.84446	-.078	.472	-.228	.918
Chl-a (µg/L)	26	.0308	1.1230	.400427	.3062035	1.245	.456	.881	.887
Cyanobacteria	26	.000000000000000	.060195134952665	.006783220121668	.015300132692106	2.786	.456	7.443	.887
Prasinophytes	26	.000000000000000	.080175109207631	.029656450994690	.026678870725473	.594	.456	-1.042	.887
Dinoflagellates	26	.000000000000000	.214734464883804	.027671244425270	.043692098388905	3.469	.456	13.937	.887
Cryptophytes	26	.000000000000000	.904982328414917	.047432911483786	.176981932275205	4.917	.456	24.649	.887
P.antarctica Total	26	.004459756426514	.296688705682755	.071434906898783	.067375481834016	1.781	.456	3.870	.887
Coccolithophores	26	.000000000000000	.174244821071625	.032232191637517	.043408697405444	1.716	.456	3.258	.887
Pelagophytes	26	.000000000000000	.047894157469273	.009487650610167	.013646271699886	1.948	.456	3.172	.887
Chlorophytes	26	.000000000000000	.030117528513074	.003484034197195	.007883695757416	2.697	.456	6.790	.887
Diatoms	26	.000000000000000	.896495103836060	.171575078158639	.226812560267115	1.919	.456	3.564	.887
pCO_2 (µatm)	10	278.66937306465700	379.87761514998397	342.707253827994800	27.331154394386015	-1.211	.687	3.402	1.334
Temp (ºC)	26	-1.430000000000000	20.330000000000000	6.128846153846153	6.688267833705869	1.017	.456	-.287	.887
Salinity	26	31.840000000000000	35.580000000000000	33.848269230769220	.757592162456412	.434	.456	2.320	.887
$Si(OH)_4$ (µM)	26	.563981042654028	50.635897435897434	21.622154296140206	18.581662130914616	.162	.456	-1.679	.887
PO_4 (µM)	26	.000000000000000	2.535211267605634	1.137170549655987	.692282603879353	-.147	.456	-.693	.887
NO_3 (µM)	26	-3.632352941176470	30.219330855018590	13.996508827993445	10.432401409220962	-.313	.456	-1.208	.887
NO_2 (µM)	26	-.132352941176471	.426470588235294	.107414177676403	.143494837906500	.674	.456	-.155	.887

Table C.2. Pearson correlation test done for POC results obtained during SANAE 56 (a) and spearman's rho correlation for pCO_2 results obtained during SANAE 56 in the surface water of the SO (b) which show no correlation between carbon isotopic fractionation and these parameters.

		$d13C_{POC}$ (‰)	POC (µg/L)
$d13C_{POC}$ (‰)	Pearson Correlation	1	.328
	Sig. (2-tailed)		.118
	N	26	24

			$d13C_{POC}$ (‰)	pCO_2 (µatm)
Spearman's rho	$d13C_{POC}$ (‰)	Correlation Coefficient	1.000	-.309
		Sig. (2-tailed)	.	.385
		N	26	10

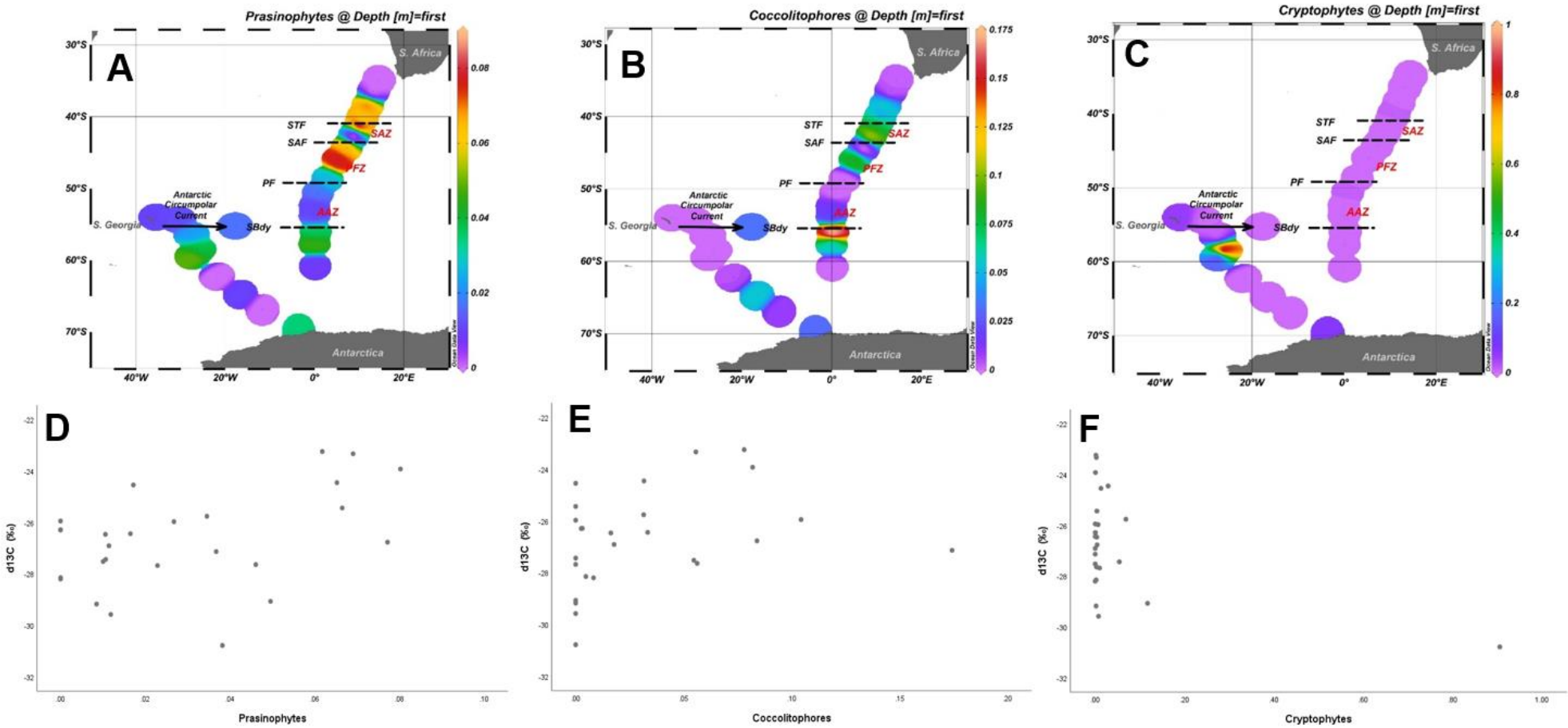

Figure C.1. Phytoplankton (Prasinophytes (A), coccolithophores (B), cryptophytes (C)) distribution along the Good Hope line in the Atlantic surface ocean during the SANAE 56 summer cruise. Scatterplots (phytoplankton groups's contribution to total chl-a in µg/L represented on the x-axis) of the same phytoplankton groups (D, E, F) towards $\delta^{13}C_{POC}$.

Appendix D – WC 2017

Table D.1. Descriptive statistics done on the results obtained from the Indian Ocean surface water during WC 2017.

Descriptive Statistics

	N	Minimum	Maximum	Mean	Std. Deviation	Skewness		Kurtosis	
	Statistic	Statistic	Statistic	Statistic	Statistic	Statistic	Std. Error	Statistic	Std. Error
$d13C_{POC}$ (‰)	30	-28.504650673400672	-22.734488117288798	-25.269959978296940	2.070852537251358	-.214	.427	-1.595	.833
POC (µg/L)	30	2.051093873760806	18.967807260299770	4.455058357159956	3.579316398869275	2.923	.427	9.431	.833
NO_2 (µM)	30	.147758988671811	.463799047775406	.331732610956055	.099830881378990	-.543	.427	-1.011	.833
NO_3 (µM)	30	1.053717925608333	27.809813013333330	15.340722264892037	10.414307032227473	-.027	.427	-1.795	.833
$Si(OH)_4$ (µM)	30	1.352877342844445	52.327280472222230	16.499947669131856	19.116897702220122	.899	.427	-1.053	.833
PO_4 (µM)	30	.297496138525323	2.146939273229819	1.234794732135599	.700415724497652	.038	.427	-1.726	.833
Chl-a (µg/L)	24	.0741	.3463	.163883	.0805741	.955	.472	.107	.918
Cyanobacteria	24	.000000000000000	.005783403757960	.001022796163549	.001623278032525	1.720	.472	2.179	.918
Prasinophytes	24	.002860319800675	.081228822469712	.032050837782057	.025360044708590	.511	.472	-.755	.918
Dinoflagellates	24	.001991037745029	.017239833250642	.007797474187101	.005458239707047	.509	.472	-1.481	.918
Cryptophytes	24	.004169683437795	.054441362619401	.016231755590222	.016274682934946	1.408	.472	.357	.918
P. antarctica Total	24	.035486938431860	.131387716159225	.074281792098191	.028700689485412	.558	.472	-.520	.918
Coccolithophores	24	.000000000000000	.020905880257488	.006063731370281	.005714497343232	1.130	.472	.623	.918
Pelagophytes	24	.000000000000000	.023362930864096	.009047316081706	.006937910800955	.638	.472	-.512	.918
Chlorophytes	24	.000000000000000	.005036337301136	.001625628190444	.001844682057734	.520	.472	-1.365	.918
Diatoms	24	.002569032367319	.044358503073454	.015762003449103	.008690511877969	1.619	.472	4.161	.918
Temperature (ºC)	24	-.03	19.28	8.5621	7.47656	.170	.472	-1.717	.918
Salinity	24	32.47	34.51	33.3625	.78891	.382	.472	-1.750	.918
pCO_2 (µatm)	27	356.40108102694400	432.66377194441200	397.354898077267140	23.839109918859204	-.414	.448	-1.122	.872

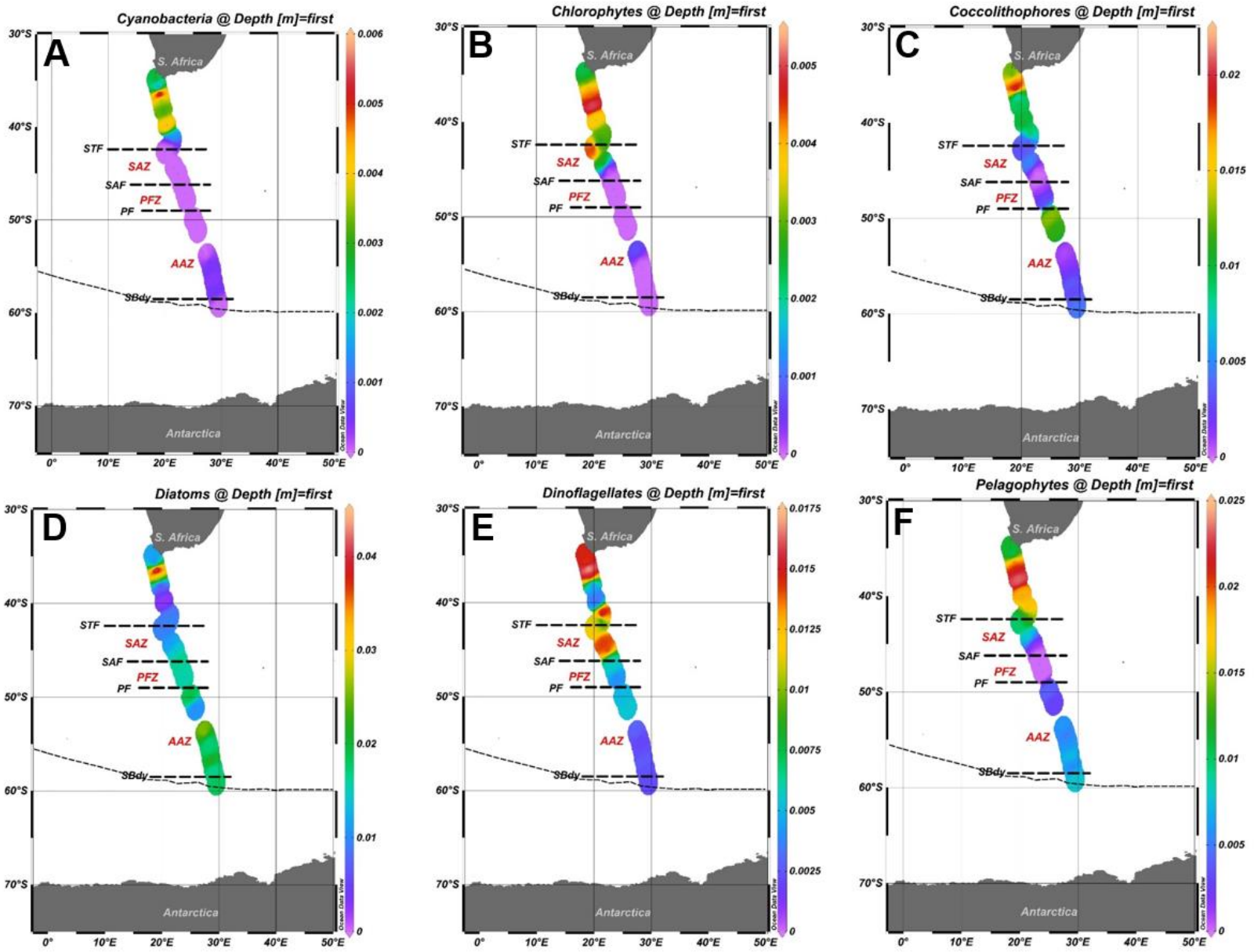

Figure D.1. Cyanobacteria (A), chlorophytes (B), coccolithophores (C), diatoms (D), dinoflagellates (E) and pelagophytes (F) distribution in the surface water of the SO during WC 2017 crossing all major fronts.

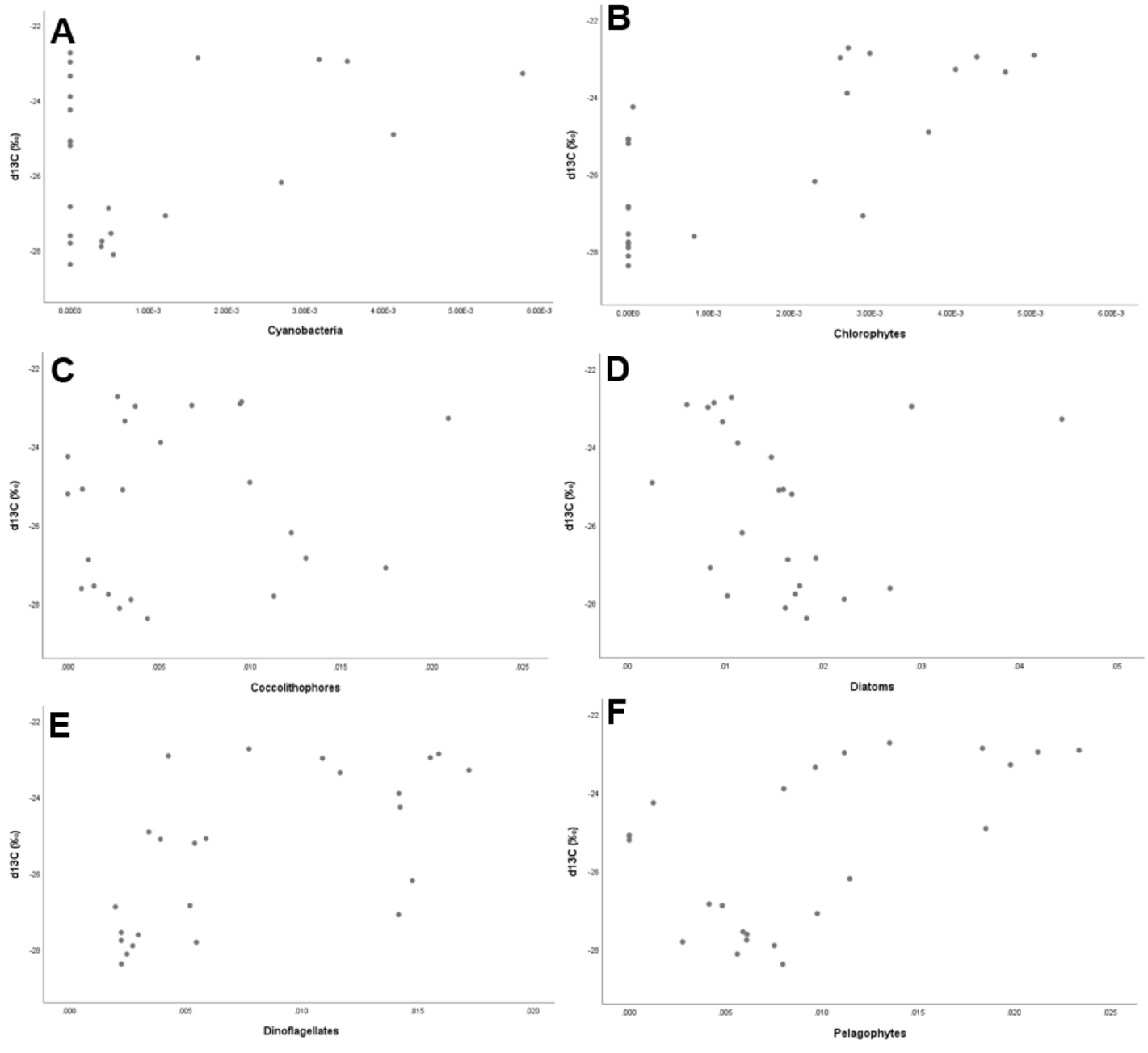

Figure D.2. Scatterplots (phytoplankton groups's contribution to total chl-a in µg/L represented on the x-axis) for phytoplankton groups; cyanobacteria (A), chlorophytes (B), coccolithophores (C), diatoms (D), dinoflagellates (E) and pelagophytes (F) in the surface water of the SO during WC 2017 which show correlations with $\delta 13C_{POC}$.